Block Polymer Membranes for Selective Separations

A THESIS
SUBMITTED TO THE FACULTY OF THE GRADUATE SCHOOL
OF THE UNIVERSITY OF MINNESOTA
BY

William A. Phillip

IN PARTIAL FULFILLMENT OF THE REQUIREMENTS
FOR THE DEGREEE OF
DOCTOR OF PHILOSOPHY

Adviser: Professor Edward L. Cussler

June 2009

Acknowledgements

For me, writing a document over 5 pages long is a clear indication that massive amounts of help and encouragement were given to me along the way. I would feel remiss if I did not take a moment to thank everyone who was there along the way.

First, thank you to my adviser Professor E. L. Cussler whose guidance helped me develop into the engineer and researcher that I am today. The patience you showed as I slowly learned will remain with me. Your constant enthusiasm reminded me that in the end, this really is fun. Also, thank you to Professor Marc Hillmyer who provided me with his time and valuable insights. Thank you to his students Liang Chen, Mark Amendt, Marc Rodwogin and Javid Rzayev who synthesized all of the polymers used to fabricate the membranes in this work. I think keeping the number of polymers I synthesize at 0 was best for everyone. Thank you to Eddie Martono and Brandon O'Neill for all of the help making gas diffusion and ultrafiltration measurements and giving me someone to talk with in the lab.

Most importantly, I would like to thank my family for giving me the opportunity to pursue a PhD. To my parents, Liz McCool and Lou Phillip, thank you for the trips to the park, the bedtime stories, the Boy Scout trips and the love throughout the years. To Chas and Katie thank you for putting up with my crap and reminding me what is truly important. Friends like you would be hard to find, siblings like you are one in a million. Now go take a shower you smell! To Matt and Jenny, thanks for visiting MN every once in a while. Good luck you crazy kids! To Uncle Len for trying to warn me how hard the last few months would be, too bad I didn't believe you. To Aunt Aggie and Aunt Clare for the trips to Werts and the jokes through the years, thank you.

Finally, thank you to all my friends. In particular, thank you to ZThompsco Inc. and the Tuesday Lunch Club. College football Saturdays, the Bad News Beers, Champagne Brunch and TMN were largely responsible for keeping me partially sane during this process. Thank you to the TANK guys. Keeping me down to earth during my time at ND turned out to be a valuable life skill and I owe that to you guys.

It has been a great experience and I wouldn't trade it for the world.

Scientific Progress Goes "Boink"?

Dedication

For Pop Pop Joe and Grandpop Louie who taught me the value of hard work and a kind heart…

Abstract

Polymeric membranes are used for many separations. Some act as selective filters, separating viruses and other undesirable solutes from drinking water. Others perform chemical separations, separating air to make an atmosphere which extends fruit shelf-life. The ability of a membrane to perform a separation is determined by its chemistry and microstructure.

Block polymers are macromolecules composed of two or more chemically incompatible polymers (blocks) covalently bonded together. Depending upon the relative amounts of each block, the polymer forms different ordered structures 5-50 nm in scale. This control over the constituent polymers and microstructure will be used to produce membranes with different transport properties. Ammonia selective membranes which retain selectivity in mixed gas systems are made from poly(cycloocetene-b-styrene sulfonate). Using poly(styrene-b-lactide) as a template, ultrafiltration membranes with a monodisperse pore size distribution are formed.

Table of Contents

List of Tables

List of Figures

Chapter 1: Introduction

1.1 Introduction to Membrane Science

Membrane mediated separations are used to refine a variety of feed streams. Examples are membranes being used to separate the components of a bulk gas mixture into another bulk gas, called gas permeation; a liquid mixture into a gas phase, known as pervaporation; and a liquid feed into a purified liquid stream, called osmosis, dialysis and filtration.[1, 2] To accomplish this large number of documented separations, an equally diverse number of membranes are used. These membranes differ in both their chemical and physical structure. Non-porous solid membranes separate gas mixtures, microporous solid membranes remove colloidal particles from solution, and supported liquid membranes extract one metal ion from mixed salts. [1, 2] This work will focus on porous and dense polymeric membranes.

In general, the membrane processes consist of two bulk phases divided by a third phase, the membrane. The two bulk phases in the membrane process are mixtures of several components. The goal is to deplete one phase of a component while enriching the other thereby producing a purified product. This goal is achieved by selectively controlling the mass transfer of the mixture components across the membrane. The movement of a species across a membrane is caused by a driving force which may arise due to any combination of gradients in chemical, electrical and mechanical potentials. The flux of species i, j_i, across the membrane is proportional to this driving force, expressed as a partial pressure or concentration difference.

$$j_i = \frac{P_i}{\ell}\left(\Delta p_i \text{ or } \Delta c_i\right) \tag{1.1}$$

The proportionality constant that relates the flux to the driving force is called the membrane permeance, $\frac{P_i}{\ell}$. The permeance is the quotient of the permeability of species i P_i, an intrinsic material property, and the effective membrane thickness ℓ.

Permeance and selectivity are two variables crucial to determining the viability of a membrane process. [1-4] Selectivity, a measure of a membrane's ability to separate two components *i* and *j*, can be defined in several ways. A common definition is

$$\alpha_{ij} = \frac{c_i^{II} \big/ c_j^{II}}{c_i^{I} \big/ c_j^{I}} \tag{1.2}$$

where α_{ij} is the selectivity, and c_i is the concentration. The subscripts *i* and *j* refer to the two components, and the superscripts *I* and *II* refer to the feed and permeate phases, respectively. In situations where the permeate concentrations are negligible relative to the feed concentrations, the selectivity is equal to the ratio of the component permeabilities.

$$\alpha_{ij} = \frac{P_i}{P_j} \tag{1.3}$$

Membranes with high permeances and selectivities are desired for economic process design. A high selectivity can be realized by the clever selection of membrane material. Once the material is selected, the permeabilities of the different components are fixed. In

order to achieve the high permeances desired, the effective membrane thickness should be as thin as possible.

Loeb and Sourirajan were the first to develop a membrane formation technique which provided the ability to produce thin membranes. [1, 2, 5, 6] They used a method, now known as phase inversion, to make anisotropic membranes with a thin selective layer, which carried out the desired separation and was supported by a thicker microporous support (Figure 1.1). In order to produce this structure, a polymer is dissolved in a solvent. After this solution is cast onto a non-woven backing layer, the solvent is allowed to partially evaporate before the web is plunged into a non-solvent bath. The evaporation step allows the selective skin to form, and the microporous support structure is created when the web is exposed to the non-solvent. This method has been refined to allow control of the thin selective layer properties. Longer evaporation times prior to immersion in the non-solvent bath result in a dense selective layer suitable for gas separation membranes. Short evaporation times lead to membranes with a porous selective layer which can be used as filtration media. Additives to the initial casting solution have also been explored further enhancing control of the selective layer properties.

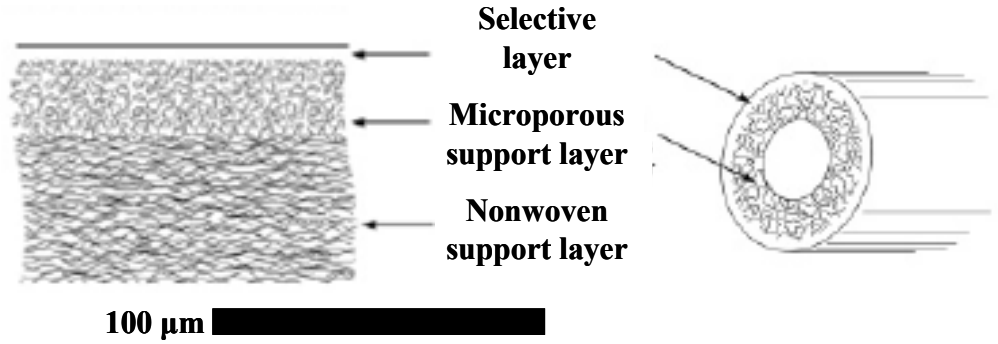

Figure 1.1: The Structure of a Membrane Made Using the Loeb-Sourirajan Method.[7] The thin selective layer which performs the separation and the underlying microporous support are made of the same polymer.

The phase inversion technique is not without its flaws. The structure formed in the Loeb-Sourirajan method results in the selective and support layers being made from the same polymer. The chosen polymer must perform the separation as well as be sufficiently mechanically robust to provide support. This limits the number of polymers that can be used, especially because of the high cost of the more specialized polymers synthesized. These factors are driving the trend in commercial seprations toward composite membranes.[7]

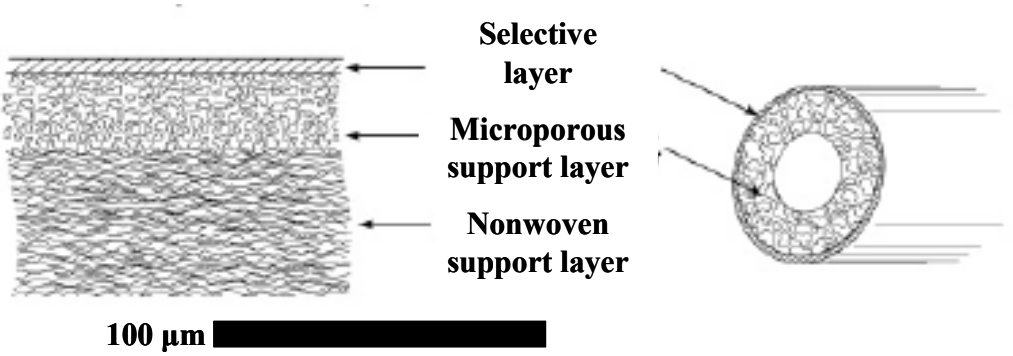

Figure 1.2: The Structure of a Composite Membrane.[7] The thin selective layer and the underlying support are made of different materials allowing for more economical membrane design.

Composite membranes are made using a robust, inexpensive microporous membrane as a mechanical support.[1, 2, 7] A thin (0.5 to 1.0 μm) selective layer deposited onto this support allows the separation and support functions to be separated (Figure 1.2). Because these two functions are separated, they can be independently optimized. An additional benefit of composites is their lower cost: smaller amounts of the expensive selective polymer are needed because none is wasted forming a support layer.

We can make more quantitative estimates of this effect. New tailor made polymers with good separation capabilities often cost as much as $1000/kg-$10000/kg to produce. A membrane made using the Loeb-Sourirajan technique uses on the order of 50 grams of polymer to make 1 m^2 of membrane, so the materials for such a membrane cost in the $\$50/m^2$-$500/m^2$ range. Composite membranes have selective layers only 0.5 μm thick, so less than one gram of polymer is need to produce a square meter of membrane. The material cost for composite membranes, capable of the same separation as a Loeb-Sourirajan membrane, is a more affordable $\$10/m^2$.[7] The microporous support used in composite membranes can be made from low-cost materials and does not contribute significantly to the overall costs.

The development of new membrane formation methods and a more complete understanding of the transport phenomena across membranes have helped to drive the increased use of membrane based separations. The increased use of these techniques has also resulted in the identification of additional shortcomings of membrane systems. Problems have been identified in all aspects of the membrane process. Poor selection of operating conditions can lead to concentration polarization and fouling; dilute impurities

in the feed stream can slowly poison the membrane (i.e., membrane conditioning); and the membrane structure can contain inherent flaws such as the wide distribution of pore sizes.[1, 2, 8] These shortcomings present serious and real hurdles that must be addressed if membrane systems are to continue improving.

1.2 Block Polymers

Significant advances in the characterization of materials at the nanoscale and the macroscale properties they effect have occurred in the past 30 years. The ability to characterize nanoscale materials has not only led to a deeper understanding of how these materials function, but also has driven development of new types of zeolites and block polymers. This thesis focuses on the use of block polymers in membrane science. Specifically, membranes templated by the self-assembly of block polymers will be used to address membrane conditioning in gas permeation systems and narrow distribution of pore sizes in ultrafiltration modules.

Block polymers consist of chemically distinct polymers attached end to end through a covalent bond.[9-11] If unfavorable enthalpic interactions exist between the polymer segments, called blocks, a phase separation will occur. Due to the shared covalent bonds this phase separation does not occur on the macroscale, but on the nanoscale. This nanoscale separation results in different spontaneous geometries. Among the factors influencing the structures that form are the number of blocks in the polymer, the sequence and relative amounts of these blocks and the magnitude of the interaction energies between the blocks. Greater mechanical stability and increased chemical

functionality are two benefits of adding more blocks to the polymer chain; these gains are at the expense of more complex synthesis schemes. The work discussed here will focus on the simplest case of diblock copolymers, those that contain only two distinct segments. While more complex block polymers now being synthesized may find future applications in membrane science, the diblock copolymers are selected as a starting point here.

A large amount of theoretical and experimental research into block copolymers gives a strong foundation for our attempts to make membranes from these materials. The feature of this prior work we want to focus on is the most commonly observed structures. At the top of Figure 1.3 is a schematic representation of a generic copolymer, which contains two polymers, block A (represented by blue) and block B (shown in red). Below this are the nanostructures that form as the volume fraction of block A is increased. As small amounts of polymer A are added to a continuous phase of polymer B, polymer A will transition through a body centered cubic spherical phase, a hexagonally packed cylindrical phase, a bicontinuous gyroid phase, and a lamellar phase. Addition of still more polymer A after the lamellar phase has been formed results in A becoming the majority phase, while B assumes the same geometries in reverse order.

.

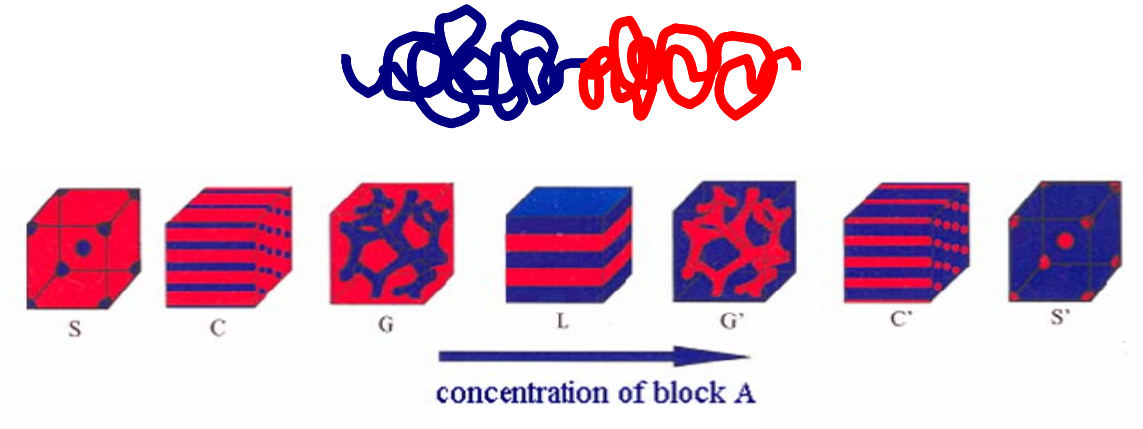

Figure 1.3: Representations of Commonly Observed Copolymer Structures. The proposed membranes in this work will focus on structures with continuous domains which span the membrane thickness. Cylindrical (C) and gyroid (G) structures meet this requirement.

Along with experimentally identifying what nanostructures can form, theoretical work explains why these particular structures form and which polymer properties control the self-assembly. The phase diagram produced from theory and an experimentally generated diagram are shown in Figure 1.4. The agreement between the theory and experiment is good. Both parts of the figure plot χN vs f_A where χN is the product of the polymer-polymer Flory-Huggins interaction parameter χ and the overall degree of polymerization N, and f_A is the volume fraction of block A in the copolymer. These phase diagrams help guide our selection of copolymers and of the size and concentration of blocks.

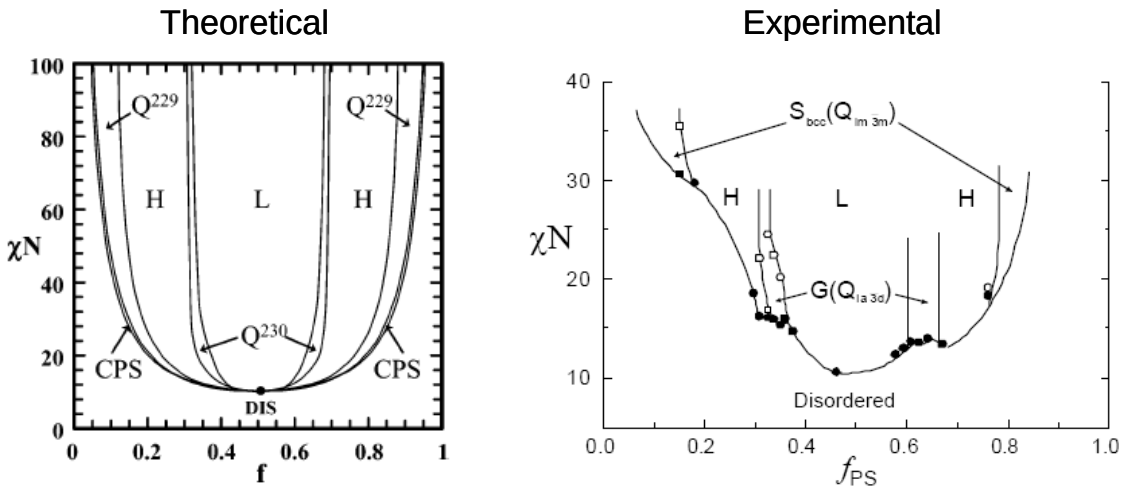

Figure 1.4: Polymer-Polymer Phase Portraits.

Because the goal of this research is to use the microstructures formed by block copolymers to develop membranes, we are attracted to the cylindrical and bicontinuous microstructures, because they contain domains that can span the thickness of a thin polymer film. Along with control of the microstructure, the copolymer chemistry can be varied to address particular issues.

1.3 Developing Ammonia Selective Membranes

We begin with our efforts to make ammonia selective membranes from crosslinked sulfonated copolymers. Ammonia is one the most important commodity chemicals, the key to modern agriculture.[12] It has been the basis for the "green revolution" that increased productivity of farming and has provided enough food for the burgeoning world population. Now, however, the increasing world wealth and

population have caused a dramatic increase in food prices and a subsequent increase in ammonia demand.

At present, ammonia is largely manufactured by the Haber process, which has been carefully optimized for 100 years.[13] The process burns natural gas in air to produce a mixture of hydrogen, nitrogen and carbon dioxide. After the carbon dioxide is removed, the nitrogen and hydrogen are fed to the Haber process reactor. The Haber process reactor combines nitrogen and hydrogen over an iron catalyst at 150 atm to generate the ammonia product. While the equilibrium of this reaction would give an 85 percent conversion at room temperature, the kinetics are so slow that the normal operating temperature is 400 ˚C. Efforts to improve the catalyst, based on metals like ruthenium, have been successful, but practical operating conditions only give a conversion on the order of 20 percent.

This incomplete conversion means that the mixture of gases produced must be separated, and the nitrogen and hydrogen recycled. This difficult recycle requires cooling the gases from 400 ˚C to around 10 ˚C. The ammonia can then be dissolved in water and the remaining gases dried and then recycled. Alternatively, the ammonia can be condensed as a liquid, although this liquid dissolves large amounts of nitrogen and hydrogen. In either case, argon, which has entered with the air used to make the nitrogen, tends to accumulate in the nitrogen-hydrogen recycle. About 10 percent of this recycle must be purged to remove the accumulated argon.

We seek to develop a membrane which facilitates the separation of the mixed gases produced by the Haber process. The membrane should be highly selective for

ammonia vs. hydrogen and nitrogen. Ideally, the membrane would also be permeable to argon and operate at the same high temperature and pressure currently used in the reactor. We begin to meet this challenge by seeking a membrane highly selective for ammonia at modest temperatures (25 ˚C). Such a membrane may find immediate application in existing ammonia plants.

The goal of developing a membrane which is highly selective for ammonia over nitrogen and hydrogen requires finding a material with high ammonia permeability and low nitrogen and hydrogen permeabilities. Being able to select the proper material relies on understanding the factors that influence polymeric membrane permeabilities. These dependencies can be understood by using the solution-diffusion model, the commonly used description of gas permeation.[3, 7, 14] The model pictures a solute which first must dissolve in the membrane material and then diffuse across the membrane down a concentration gradient in order to reach the permeate side. This two-step process gives rise to the variables that affect the membrane permeability, the diffusion coefficient D_i and the gas-membrane partition coefficient H_i. The permeability of species *i* is written as the product of these two variables.

$$P_i = D_i H_i \tag{1.4}$$

The diffusion coefficient is a measure of the mobility of the gas molecules in the membrane material, while the partition coefficient is an indication of the concentration of gas molecules dissolved in the membrane.

Combining the definitions of membrane selectivity and permeability put forth in Equations (1.3) and (1.4), respectively, gives the following expression for the selectivity of a membrane in a gas permeation system.

$$\alpha_{ij} = \left(\frac{D_i}{D_j}\right)\left(\frac{H_i}{H_j}\right) \tag{1.5}$$

The ratio of the two diffusion coefficients, called the mobility selectivity, gives an indication of the rate at which individual gas molecules move through the membrane. The sorption selectivity, the ratio of the partition coefficients, gives a measure of the relative concentration of the components in the membrane material. This concentration increases with the solubility of the component; therefore, the sorption selectivity is proportional to the relative solubility of the components.[1, 7]

In polymeric materials, diffusion coefficients decrease as the molecular size increases. The larger particles interact with more polymer units than small molecules, so the mobility selectivity always favors the permeation of small molecules.[1, 7] Seeking an ammonia selective membrane based on a mobility selectivity has little promise because the collision diameter of ammonia (2.90 Å) is between that of nitrogen (3.80 Å) and hydrogen (2.83 Å).

Developing a membrane based on sorption selectivity has more potential. The partition coefficient between the gas and polymer phases is a measure of the relative energy of a gas particle in the two phases. Because H_i will usually increase with a solute's condensability, sorption selectivity favors the permeation of more condensable components. Another way to increase the solubility of a gas in the polymer phase, and

hence the partition coefficient, is to incorporate functional groups into the polymer chains which have specific interactions with the diffusing solute. A good deal of research has been done working to this end with the ammonia, hydrogen, and nitrogen system. Membranes made from polymers containing thiocyanate, sulfonate and persulfonic acid groups have been shown to have significantly higher ammonia permeabilities than nitrogen and hydrogen permeabilities.[15-24] IR data suggests that these increased permeabilities in the thiocyanate system may result from hydrogen bonding between NH_3 and the SCN^- and $NH4^+$ ions.[15, 24] Work with persulfonic acid membranes (Nafion) is not as conclusive.[20] At low temperatures, the flux varies with the ammonia concentration difference but at higher temperatures, increases less. However, at room temperature, the temperature of this study, the mechanism for previously synthesized membranes is that of solution-diffusion. This model will be used to interpret and understand our results.

The majority of the prior work that looked into this system used pure gas experiments to imply a membrane selectivity. When the system is studied using mixed gas feeds which accurately represent the reactor effluent of the Haber process, the permeabilities of hydrogen and nitrogen are similar to the ammonia permeability. Another way to state this is while the ideal selectivity (i.e., that based on pure gases) is high, the actual selectivity (i.e., based on gas mixtures) is low. Such a loss of selectivity has compromised other potential processes, especially the separation of carbon dioxide and methane.[7, 25]

This loss of selectivity is believed to occur because the membrane swells in the more permeable component, which in our case is ammonia.[26, 27] Thus the hydrogen and

nitrogen are not really faced with the membrane itself but rather with an ammonia swollen polymer. Sensibly, many have tried to crosslink the membranes so that they retain their structure and hence their selectivity at high pressures.[25, 28] These results have been only modestly successful.[29-32]

In this work, we try to retain high ammonia selectivity using a block copolymer templated membrane which contains two interpenetrating nanoscopic domains. One phase has a high ideal selectivity for ammonia; the other is impermeable to all of the gases involved. Our hope is that the impermeable phase will provide a rigid framework which prevents the permeable phase from swelling and in turn losing its high ideal selectivity. We are especially attracted to a bicontinuous network phase because it requires no special alignment.[33] We focus on a polymer consisting of a polycyclooctene or polydicyclopentadiene phase, expected to be impermeable; and a sulfonated polystyrene phase, expected to show high selectivity for ammonia. High ammonia permeabilites are known across films of perfluoronated sulfonic acid (Nafion) and of polyvinylammonium thiocyanate. We hope that, unlike these earlier efforts, our membrane retains its structure and its selectivity at high ammonia concentrations.

1.4 Developing Ultrafiltration Membranes

Recent reports of water availability and quality assert that water purification systems are poised for rapid growth in the next decade.[34-36] Lack of adequate water supplies is the number one cause of early childhood death. Some areas lack an adequate supply of water due to arid conditions, while others have a supply tainted by industrial

chemicals still others are simply burdened by growing populations. Regardless of the reasons for an area's diminished supply, it is clear that more efficient water purification and reuse will be needed in the future.

The desire for pure water affects all of the world's population. Government officials want to provide clean potable water to their citizens. Pharmaceutical companies require high purity water to ensure that their drugs are safe. Chemical companies want to conserve water by cleansing it sufficiently to recycle it in absorption and rinsing processes. More and more individuals are taking an interest in water purity, as witnessed by the success of bottled water and home purification systems.

Membranes offer a flexible, commercially attractive means for purifying water. An indication of membranes growth in popularity is the large installations currently providing drinking water in cities like Minneapolis and Tampa. The contaminants which different locations encounter are different and vary seasonally within a single municipality. Figure 1.5 shows the wide range of membrane systems currently available to deal with this variability. Along with the types of membranes, the chart includes a scale indicating the size range over which the membrane operates and some representative materials in this size range. The figure implies that a key characteristic to consider when selecting a membrane method is the size of the particle to be removed. The size of the particles removed is crucial because most of the methods rely, in part, on a sieving mechanism to purify the feed. Simply put, when a given pore is smaller than the contaminant particle, the particle cannot pass through the pore. This mechanism is the chief cause of the separation for particles larger than 0.5 μm. For smaller particles,

electrostatic and van der Waals forces affect the separation. Salt ions and small molecules are removed using reverse osmosis membranes, in which small pores do not exist but species are transported by the solution-diffusion mechanism.

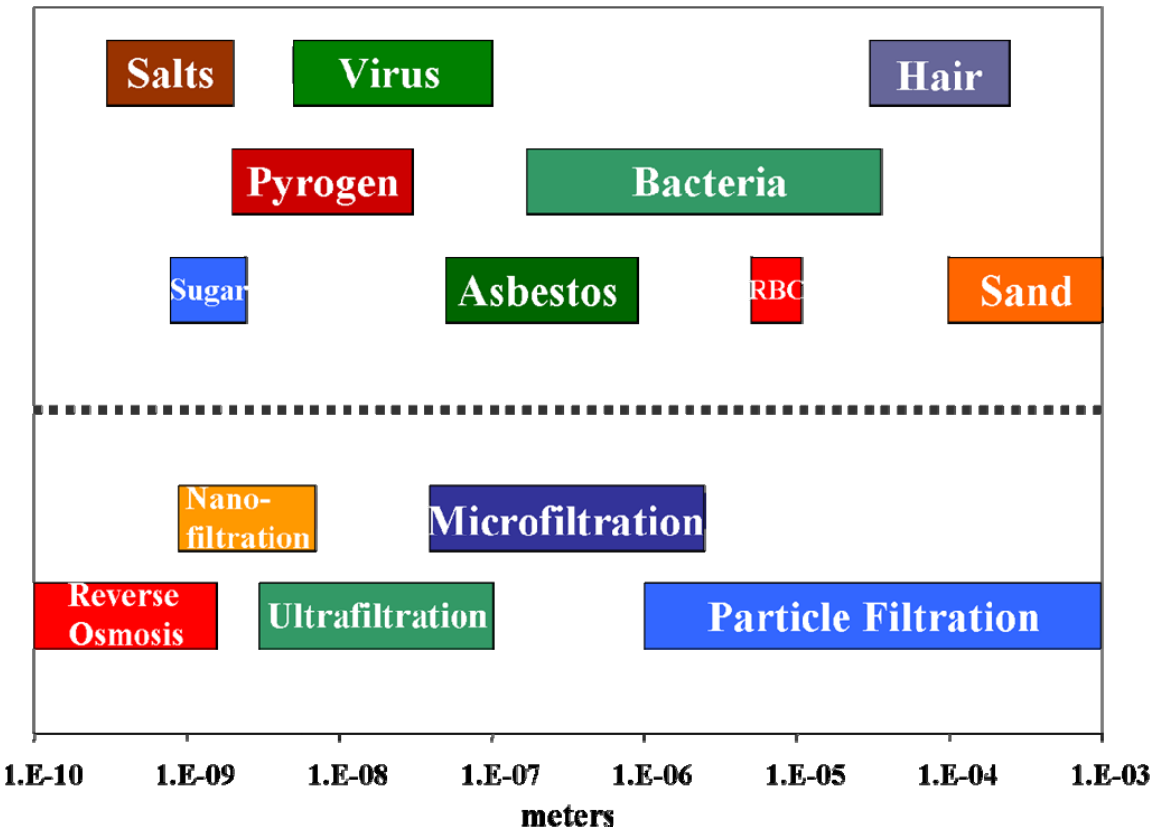

Figure 1.5: The Filtration Spectrum. Particle size determines which membrane method should be used for water purification. Some representative contaminants are shown.

Table 1.1 provides a detailed summary of these different methods. The table lists the process, characteristics of the retained components, the operating pressure, the system geometry and a few example applications. The table demonstrates that as the membrane

pores become smaller, the characteristic size of the retained particles also gets smaller and the pressure gradient needed gets larger, as expected.

Table 1.1: Summary of Membrane Processes for Water Purification.

Process	**Components Retained**	**Operating Pressure**	**Operating Geometry**	**Applictions**
Particle Filtration	Suspended particles greater than 1.0 microns	<25 psig	Dead End	Bulk particle removal, prefiltration, waste treatment
Microfiltration	Small suspended particles greater than 0.1 microns	25-50 psig	Dead End/ Cross Flow	High volume removal of suspended solids as pretreatment for UF processes
Ultrafiltration	Organics with MW > 1000, Bacteria and pyrogens	25-100 psig	Dead End/ Cross Flow	Pretreatment for ion exchange columns, Beverage clarification
Nanofiltration	Organics with MW > 300, Divalent ions	135-230 psig	Cross Flow	Water hardness removal, Dye desalting
Reverse Osmosis	Organics with MW > 150, Monovalent and divalent ions	200-1000 psig	Cross Flow	Bottled water production, desalinization of sea water, ultrapure water production

Column 4 in Table 1.1, which gives process geometry, requires more discussion. There are two configurations for filtration systems, with a crossover from one to the other in the 0.1 to 1 micron range. The first configuration, dead-end filtration, is used when the particles are larger than 0.1 microns this includes sand, human hair and red blood cells. This process, in its most basic form, is like straining cooked pasta with a colander.

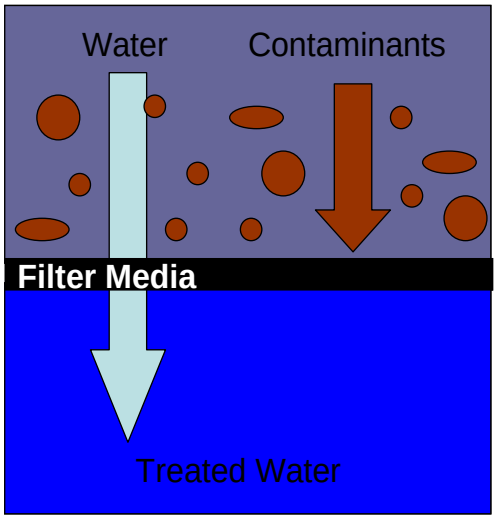

Figure 1.6: Dead-end Filtration. All of the water fed permeates the membrane while retained contaminants build up on the membrane surface.

Figure 1.6 shows a simplified schematic of dead end filtration. A stream containing the contaminated water is fed to the filter media, which passes the water, increasing its purity while retaining the unwanted contaminants. The filters in dead-end filtration can be screens made of plastic or metal, bags constructed of non-woven media, and depth filters of cellulose, cotton or synthetic yarn. These different filters must be backwashed or replaced after a single use, because dead-end filtration collects the unwanted material on the filter surface. Ultrafiltration through particle filtration are the processes which can take advantage of dead-end filtration.

Though ultrafiltration can operate in a dead end geometry, it is usually more effective to operate in the second configuration, cross flow filtration. In cross flow filtration, a pressurized feed of contaminated water is fed parallel to the membrane. The pressure forces the water across the membrane, forming a purified stream called the "permeate". The rest of the water that does not pass through the filter, called the

"retentate", carries away the retained contaminants from the membrane surface. Figure 1.7 provides a picture of this process.

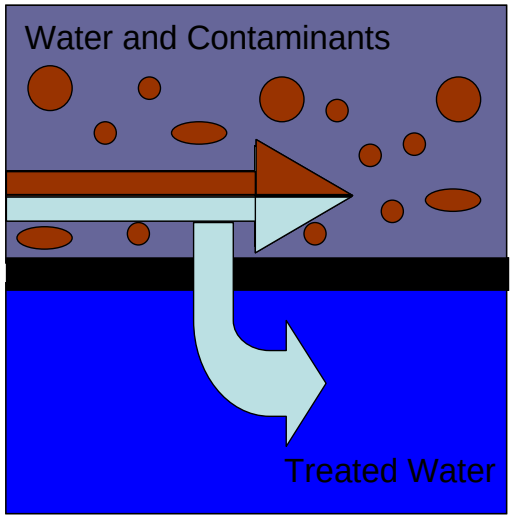

Figure 1.7: Cross Flow Filtration. A fraction of the water fed permeates the membrane while the remaining fraction sweeps contaminants away from the membrane surface.

In order to make either of these filtration processes economically attractive, the membranes must be able to operate for long periods of time. If RO, NF, or UF membranes were to operate in a dead end geometry, the particles would blind the membrane so rapidly that a significant amount of time would be spent trying to clean the membrane surface of contaminant. Even if the times for cleanings were not significant, other factors make cross flow filtration a necessity for RO, NF and UF. First, filters that operate above 0.1 microns are made from strong, cheap materials like bags of non-woven polypropylene, but filters that operate under 0.1 microns are made from a 0.5 micron layer of selective polymer coated onto a 50 micron microporous support. Backwashing

these membranes can damage the 0.5 micron polymer layer. Discarding the membranes after one use is not a viable option because these membranes are expensive.

Another advantage of cross flow is the reduction of concentration polarization. This phenomenon has an adverse effect on the membrane performance and permeate quality. During steady state operation of a cross flow filtration system, the selective rejection of particles by the membrane increases the solute concentration at the membrane surface. The concentration at this interface will drive a diffusive flux back to the bulk liquid. This diffusive flux of solute back to the bulk is balanced by the convective flux of solute through the membrane. Under certain circumstances, the concentration at the membrane surface can exceed the solubility of the solute, causing precipitation and increased resistance. This is not uncommon in ultrafiltration of protein solutions.

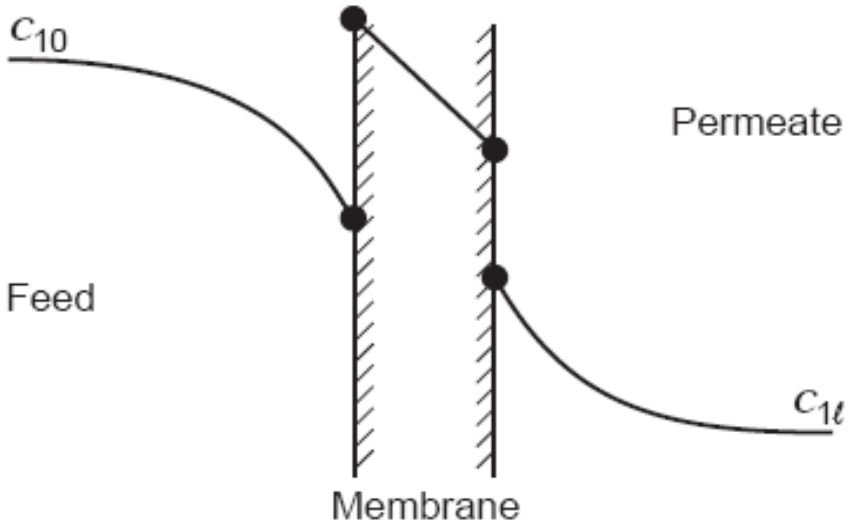

Figure 1.8: Three Mass Transfer Resistances in Series for a Membrane Process.[3] Intelligent design of membrane separations requires minimizing the overall resistance to mass transfer which is the sum of three parts: the feed side, membrane and permeate side resistances.

We can make these ideas more quantitative by considering the resistances to mass transfer present. The water must first go from the bulk to the membrane surface, go across the membrane, and finally move from the membrane surface to the bulk permeate. Therefore, we have a resistance to flow equal to

$$\begin{bmatrix}\text{Flow}\\ \text{Resistance}\end{bmatrix}=\begin{bmatrix}\text{Feed}\\ \text{Resistance}\end{bmatrix}+\begin{bmatrix}\text{Membrane}\\ \text{Resistance}\end{bmatrix}+\begin{bmatrix}\text{Permeate}\\ \text{Resistance}\end{bmatrix} \tag{1.6}$$

or in terms of an overall mass transfer coefficient K

$$\frac{1}{K}=\frac{1}{k_{feed}}+\frac{\ell}{P}+\frac{1}{k_{permeate}} \tag{1.7}$$

where k_{feed} and $k_{permeate}$ are the mass transfer coefficients in the phases shown; ℓ is the membrane thickness; and P is the membrane permeability. In cross flow filtration, the

permeate resistance is usually small compared to the feed and membrane resistances, which are both significant. As concentration polarization and fouling develop, there is a significant increase in the resistance to mass transfer from the feed side, thus decreasing the overall mass transfer coefficient.

The discussion above also implies that the membrane and feed resistances must be improved simultaneously. For example in a system in which $\frac{1}{k_{feed}}$ and $\frac{\ell}{P}$ are equal, we make a 1000 time improvement to $\frac{\ell}{P}$, we observe only a two fold improvement in the process performance. We will continue with a focus on the membranes used in ultrafiltration processes while we recognize the importance of work being done to decrease concentration polarization and fouling through the use of static mixers. The self cleaning nature of cross flow filtration will be improved by the addition of optimally designed static mixers. Because the contaminants are continuously being carried away in the concentrate, leaving the surface free to reject particles from the influent.

Current ultrafiltration modules are operated using membranes made by the Loeb-Sourirajan method previously described.[5] The resulting structure, shown in the left panel of Figure 1.9, is a tangled network of polymer fibers that resembles cooked spaghetti. Because the size and packing of the fibers can be altered by changing the process conditions, the flux can be adjusted without much difficulty. This allows the high fluxes needed to process large volumes of water to be realized. The difficulty phase inversion membranes face is the wide distribution of pore sizes, making a sharp molecular weight cut off difficult to be achieved. The left panel of Figure 1.9 clearly demonstrates that no

single pore dimension can be defined. Instead the convention is to define a nominal pore size based on a technique such as the bubble point test.[1, 8]

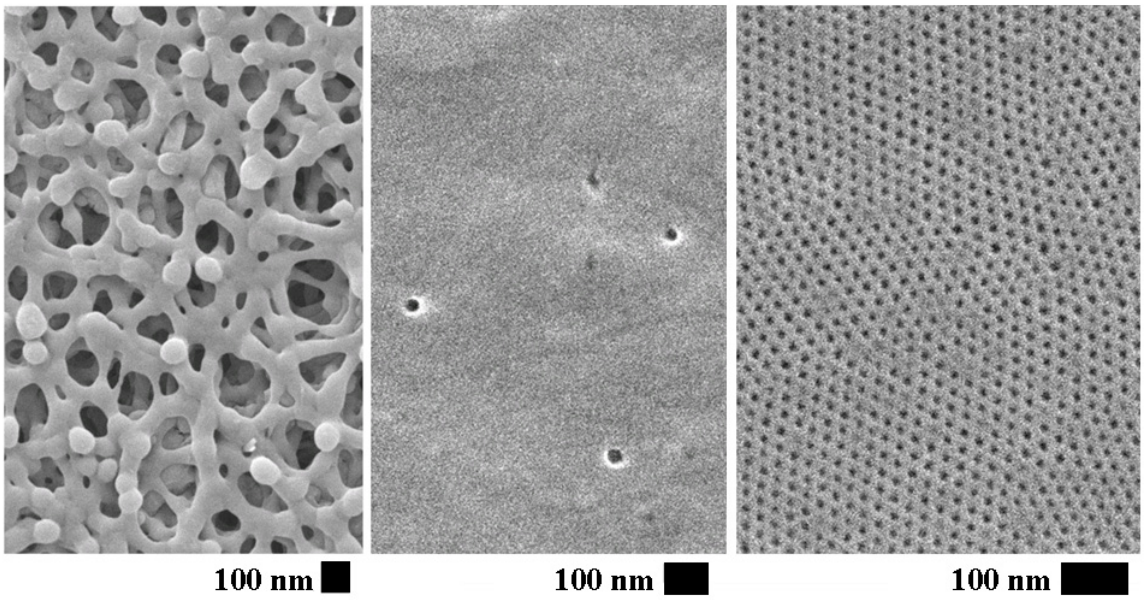

Figure 1.9: Three Size Selective Membranes. That on the left is a conventional ultrafiltration membrane formed by phase inversion, and that in the center is a track-etched polycarbonate film. The membrane on the right is that made here.

An alternative membrane strucuture with a well defined pore geometry is shown in the central panel of Figure 1.9.[37, 38] These "track-etched" membranes begin with a thin, pore-free polycarbonate film. The film is exposed to ionizing radiation, which weakens regions of the film. The weakened regions are then degraded with a caustic solution, resulting in small near-cylindrical pores like those in the figure. Because the pores are nearly mono-dispersed, the membrane has a very sharp molecular weight cut-off. Unfortunately, the random nature of the radiation used during production restricts the membranes to very small void fractions to avoid overlapping pores. Phase inversion membranes have typical void fractions around 0.3; track etched membranes have void

fractions around 0.01. This means that for membranes with equivalent pore sizes, a track etched membrane will have a dramatically lower flux than a phase inversion membrane.

The image on the right of Figure 1.9 is characteristic of recent efforts by several groups to make filtration membranes, using the self-assembly properties of block copolymers, which offer both high flux and a sharp molecular weight cut-off.[33, 39-41] The contrast between this panel and the other two panels is dramatic. The right panel shows a membrane with a void fraction comparable to a conventional ultrafiltration membrane but with a pore geometry similar to track etched membranes. These materials have the potential to greatly improve ultrafiltration membranes.

In order to take advantage of block copolymers as a template for ultrafiltration membranes, the copolymer must exhibit several properties. First, it must spontaneously form a structure containing domains which span the membrane thickness. This requirement suggests using a cylindrical or bicontinuous network morphology. Using the cylindrical structure requires the cylinders are aligned perpendicular to the surface of the thin films; bicontinuous networks are attractive because no such alignment is needed. Finally, the polymer must contain one block that can be selectively etched while leaving the surrounding continuum intact, thus creating a thin polymer film with a percolating porous structure.[42-44] The work presented here will use both a cylinder forming copolymer and a bicontinuous network geometry to form ultrafiltration membranes.

Pores in the bicontinuous network structure are isotropic and run in all directions. Thus there are no concerns related to aligning the structure, unlike the cylindrical geometry. For this reason, we address thin films made using a network structure first. To

form the bicontinuous network, the "doubly reactive" block polymer polynorbornenylethylstyrene-polylactide is used as a structural template during the metathesis-induced crosslinking of dicyclopentadiene.[4533] After subsequent etching of the polylactide component with dilute base, the tough polydicyclopentadiene membrane remaining has an isotropic nanoporous structure. Such a membrane has narrowly-dispersed pore sizes and so should give high selectivity. Additionally, the membrane's pores are closely packed and so should be capable of high flux. This work explores the details of the membrane geometry by measuring the diffusion of a variety of gases and flow of water at various values of pH and ionic strength. We demonstrate membrane selectivity through transport studies with a series of polyethylene oxides and a mixture of dextrans.

The alignment of the cylinders is a formidable barrier to making ultrafiltration membranes from copolymer templates. The difficulty of aligning cylinders is not a problem unique to making membranes, but is also faced by those attempting to make high density storage media, organic solar cells and cheap biological sensors. Those working on the issue use a varierty of techniques. Because summaries of these techniques are published in detailed review articles, only a short overview is given in this thesis.[46-67]

Ideally, a system could be selected such that the cylinders spontaneously form perpendicular to the thin dimension. Some systems have been identified which do show this equilibrium behavior: thin films of poly(styrene-b-lactide) annealed at 205 ºC for 24 hours[68] as well as poly(styrene-b-ethylene oxide) films exposed to a saturated benzene atmosphere do form perpendicular cylinders.[69] However the cylinders formed often do

not go all the way through the membranes. The "cylinders" are not so much pores as pits.

Alternatively, an external force is required to drive the formation of perpendicular cylinders that span the membrane thickness. Shear forces, electrical and magnetic fields, pre-patterned surfaces and concentration or thermal gradients are all examples of forces which have been applied successfully. The selected method should be effective, safe, and inexpensive. Electric field alignment requires the use of kilovolt fields which combined with organic vapors is a fire hazard, few facilities have magnets large enough to generate the fields needed to drive alignment, and pre-patterned surfaces are expensive.

This led use to study the use of shear forces and concentration gradients to induce alignment. Shear forces by themselves were first used to align cylinders of polylactide in a poly(styrene-b-dimethylacrylamide-b-lactide) sample. This technique results in monoliths which, while too thick to be of practical interest, provide a useful tool for exploring the internal pore architecture. Small angle X-ray scattering (SAXS) and scanning electron microscopy (SEM) provide information about bulk averages and snapshots regarding the porous structure. This information can be used to infer transport properties such as gas diffusion coefficients and water flow rates. Our experiments will make a comparison between experimentally obtained diffusion coefficients and flow rates and those predicted using information from SAXS and SEM. Making this comparison allows us to explore dead-end pores, tortuosity and branched pores, morphological characteristics which influence the transport of solutes but which may not be accounted for by SAXS and SEM.

Controlled solvent evaporation after shear is the other alignment technique we will use. Many of the alignment techniques that involve the use of an external force require the polymer to be cast onto a silicon wafer. This is suitable for making storage media but introduces a difficult processing step for membrane formation. The thin fragile film must be floated off the wafer and then picked up on a porous support. Ideally the thin selective layer could be coated directly onto the support, thereby combining alignment and coating in a single step. Researchers have been able to use a phase inversion technique to make a copolymer film with a 500 nm self-assembled selective layer. Because the support layer in this membrane is also made from the copolymer we believe it does not have much practical interest. We combine the existing knowledge related to making composite membranes with research being done into controlled evaporation alignment to produce a single step process for making filtration membranes with a thin block copolymer self-assembled selective layer.

1.5 Reference

(1) Baker, R. W. In Membrane technology and applications; J. Wiley: Chichester ; New York, 2004; , pp 538.

(2) Ho, W. S. W.; Sirkar, K. K. In Membrane handbook; Kluwer Academic Pub.: Boston, 2001; , pp 954.

(3) Cussler, E. L. In Diffusion, mass transfer in fluid systems; Cambridge University Press: New York, 2009; , pp 654.

(4) Bird, R. B.; Stewart, W. E.; Lightfoot, E. N. In Transport phenomena; J. Wiley: New York, 2002; , pp 895.

(5) Loeb, S.; Sourirajan, S. Patent Application Country: Application: US; Patent Country: US; Priority Application Country: US Patent 3133132, 1964.

(6) Loeb, S.; Sourirajan, S.; Weaver, D. E. Patent Application Country: Application: US; Patent Country: US; Priority Application Country: US Patent 3133137, 1964.

(7) Baker, R. W.; Lokhandwala, K. Ind Eng Chem Res 2008, 47, 2109-2121.

(8) Zeman, L. J.; Zydney, A. L. In Microfiltration and ultrafiltration : principles and applications; M. Dekker: New York, 1996; , pp 618.

(9) Bates, F. S. Science (Washington, D.C., 1883-) 1991, 251, 898-905.

(10) Bates, F. S.; Fredrickson, G. H. Annu. Rev. Phys. Chem. 1990, 41, 525-557.

(11) Hamley, I. W. Dev.Block Copolym.Sci.Technol.; Developments in Block Copolymer Science and Technology 2004, 1-29.

(12) Anonymous In Kirk-Othmer encyclopedia of chemical technology; Kirk, R. E. (. E., Othmer, D. F. (. F., Eds.; Encyclopedia of chemical technology; Wiley: New York, 2000; .

(13) Rafiqul, I.; Weber, C.; Lehmann, B.; Voss, A. Energy (Amsterdam, Neth.) 2005, 30, 2487-2504.

(14) Freeman, B. D. Macromolecules 1999, 32, 375-380.

(15) Bhown, A.; Cussler, E. L. J. Am. Chem. Soc. 1991, 113, 742-749.

(16) Pez, G. P.; Carlin, R. T.; Laciak, D. V.; Sorensen, J. C. United States Patent 4761164, 1988.

(17) Pez, G. P.; Laciak, D. V. Patent Application Country: Application: US; Patent Country: US Patent 4762535, 1988.

(18) Laciak, D. V.; Quinn, R.; Pez, G. P.; Appleby, J. B.; Puri, P. S. Separation Science and Technology 1990, 25, 1295.

(19) Laciak, D. V.; Pez, G. P. Patent Application Country: Application: US; Patent Country: US Patent 4758250, 1988.

(20) He, Y.; Cussler, E. L. J. Membr. Sci. 1992, 68, 43-52.

(21) Sakai, T.; Takenaka, H.; Wakabayashi, N.; Kawami, Y.; Torikai, E. J. Electrochem. Soc. 1985, 132, 1328-1332.

(22) Sakai, T.; Takenaka, H.; Torikai, E. J. Electrochem. Soc. 1986, 133, 88-92.

(23) Bikson, B.; Nelson, J. K.; Perrin, J. E. Patent Application Country: Application: US; Patent Country: US Patent 5009678, 1991.

(24) Timashev, S. F.; Vorobiev, A. V.; Kirichenko, V. I.; Popkov, Y. M.; Volkov, V. I.; Shifrina, R. R.; Lyapunov, A. Y.; Bondarenko, A. G.; Bobrova, L. P. Journal of Membrane Science 1991, 59, 117-131.

(25) Koros, W. J.; Coleman, M. R.; Walker, D. R. B. Annu.Rev.Mater.Sci. 1992, 22, 47-89.

(26) Visser, T.; Masetto, N.; Wessling, M. J. Membr. Sci. 2007, 306, 16-28.

(27) Visser, T.; Wessling, M. Macromolecules 2007, 40, 4992-5000.

(28) Staudt-Bickel, C.; Koros, W. J. J. Membr. Sci. 1999, 155, 145-154.

(29) Zhang, Y.; Musselman, I. H.; Ferraris, J. P.; Balkus, K. J. J. Membr. Sci. 2008, 313, 170-181.

(30) Taniguchi, I.; Duan, S.; Kazama, S.; Fujioka, Y. J. Membr. Sci. 2008, 322, 277-280.

(31) Hanioka, S.; Maruyama, T.; Sotani, T.; Teramoto, M.; Matsuyama, H.; Nakashima, K.; Hanaki, M.; Kubota, F.; Goto, M. J. Membr. Sci. 2008, 314, 1-4.

(32) Zhao, H.; Cao, Y.; Ding, X.; Zhou, M.; Liu, J.; Yuan, Q. J. Membr. Sci. 2008, 320, 179-184.

(33) Phillip, W. A.; Amendt, M.; O'Neill, B.; Chen, L.; Hillmyer, M. A.; Cussler, E. L. ACS Applied Materials & Interfaces 2009, 1, 472-480.

(34) Shannon, M. A.; Bohn, P. W.; Elimelech, M.; Georgiadis, J. G.; Marinas, B. J.; Mayes, A. M. Nature 2008, 452, 301-310.

(35) Schwarzenbach, R. P.; Escher, B. I.; Fenner, K.; Hofstetter, T. B.; Johnson, C. A.; von Gunten, U.; Wehrli, B. Science (Washington, DC, U.S.); Science (Washington, DC, United States) 2006, 313, 1072-1077.

(36) Oki, T.; Kanae, S. Science (Washington, DC, U.S.); Science (Washington, DC, United States) 2006, 313, 1068-1072.

(37) Lee, S. B.; Mitchell, D. T.; Trofin, L.; Nevanen, T. K.; Soederlund, H.; Martin, C. R. Science (Washington, DC, U.S.); Science (Washington, DC, United States) 2002, 296, 2198-2200.

(38) Wirtz, M.; Martin, C. R. Adv.Mater.(Weinheim, Ger.); Advanced Materials (Weinheim, Germany) 2003, 15, 455-458.

(39) Yang, S. Y.; Park, J.; Yoon, J.; Ree, M.; Jang, S. K.; Kim, J. K. Adv.Funct.Mater. 2008, 18, 1371-1377.

(40) Yang, S. Y.; Ryu, I.; Kim, H. Y.; Kim, J. K.; Jang, S. K.; Russell, T. P. Adv.Mater.(Weinheim, Ger.) 2006, 18, 709-712.

(41) Peinemann, K.; Abetz, V.; Simon, P. F. W. Nat Mater 2007, 6, 992-996.

(42) Olayo-Valles, R.; Guo, S.; Lund, M. S.; Leighton, C.; Hillmyer, M. A. Macromolecules 2005, 38, 10101-10108.

(43) Zalusky, A. S.; Olayo-Valles, R.; Wolf, J. H.; Hillmyer, M. A. J. Am. Chem. Soc. 2002, 124, 12761-12773.

(44) Zalusky, A. S.; Olayo-Valles, R.; Taylor, C. J.; Hillmyer, M. A. J. Am. Chem. Soc. 2001, 123, 1519-1520.

(45) Chen, L.; Phillip, W. A.; Cussler, E. L.; Hillmyer, M. A. J. Am. Chem. Soc. 2007, 129, 13786-13787.

(46) Angelescu, D. E.; Waller, J. H.; Adamson, D. H.; Deshpande, P.; Chou, S. Y.; Register, R. A.; Chaikin, P. M. Adv.Mater.(Weinheim, Ger.); Advanced Materials (Weinheim, Germany) 2004, 16, 1736-1740.

(47) Cavicchi, K. A.; Berthiaume, K. J.; Russell, T. P. Polymer 2005, 46, 11635-11639.

(48) DeRouchey, J.; Thurn-Albrecht, T.; Russell, T. P.; Kolb, R. Macromolecules 2004, 37, 2538-2543.

(49) Fasolka, M. J.; Harris, D. J.; Mayes, A. M.; Yoon, M.; Mochrie, S. G. J. Phys. Rev. Lett. 1997, 79, 3018-3021.

(50) Gunkel, I.; Stepanow, S.; Thurn-Albrecht, T.; Trimper, S. Macromolecules (Washington, DC, U.S.); Macromolecules (Washington, DC, United States) 2007, 40, 2186-2191.

(51) Hamley, I. W. Curr.Opin.Colloid Interface Sci.; Current Opinion in Colloid & Interface Science 2000, 5, 342-350.

(52) Horvat, A.; Lyakhova, K. S.; Sevink, G. J. A.; Zvelindovsky, A. V.; Magerle, R. J. Chem. Phys. 2004, 120, 1117-1126.

(53) Hwang, J.; Huh, J.; Jung, B.; Hong, J.; Park, M.; Park, C. Polymer 2005, 46, 9133-9143.

(54) Jeong, U.; Ryu, D. Y.; Kho, D. H.; Kim, J. K.; Goldbach, J. T.; Kim, D. H.; Russell, T. P. Adv.Mater.(Weinheim, Ger.); Advanced Materials (Weinheim, Germany) 2004, 16, 533-536.

(55) Karim, A.; Singh, N.; Sikka, M.; Bates, F. S.; Dozier, W. D.; Felcher, G. P. J. Chem. Phys. 1994, 100, 1620-1629.

(56) Knoll, A.; Horvat, A.; Lyakhova, K. S.; Krausch, G.; Sevink, G. J. A.; Zvelindovsky, A. V.; Magerle, R. Phys. Rev. Lett. 2002, 89, 035501.

(57) Knoll, A.; Magerle, R.; Krausch, G. J. Chem. Phys. 2004, 120, 1105-1116.

(58) Morkved, T. L.; Lu, M.; Urbas, A. M.; Ehrichs, E. E.; Jaeger, H. M.; Mansky, P.; Russell, T. P. Science (Washington, D.C.); Science (Washington, D.C.) 1996, 273, 931-933.

(59) Park, C.; Simmons, S.; Fetters, L. J.; Hsiao, B.; Yeh, F.; Thomas, E. L. Polymer 2000, 41, 2971-2977.

(60) Peng, J.; Xuan, Y.; Wang, H.; Yang, Y.; Li, B.; Han, Y. J. Chem. Phys. 2004, 120, 11163-11170.

(61) Sakurai, S. Polymer 2008, 49, 2781-2796.

(62) Sakurai, S.; Okamoto, S.; Sakurai, K. Dev.Block Copolym.Sci.Technol.; Developments in Block Copolymer Science and Technology 2004, 127-158.

(63) Thurn-Albrecht, T.; DeRouchey, J.; Russell, T. P.; Jaeger, H. M. Macromolecules 2000, 33, 3250-3253.

(64) Thurn-Albrecht, T.; Schotter, J.; Kastle, G. A.; Emley, N.; Shibauchi, T.; Krusin-Elbaum, L.; Guarini, K.; Black, C. T.; Tuominen, M. T.; Russell, T. P. Science (Washington, D.C.); Science (Washington, D.C.) 2000, 290, 2126-2129.

(65) Vigild, M. E.; Chu, C.; Sugiyama, M.; Chaffin, K. A.; Bates, F. S. Macromolecules 2001, 34, 951-964.

(66) Wu, L.; Lodge, T. P.; Bates, F. S. J.Rheol.(N.Y., NY, U.S.); Journal of Rheology (New York, NY, United States) 2005, 49, 1231-1252.

(67) Chen, Z.; Kornfield, J. A. Polymer 1998, 39, 4679-4699.

(68) Olayo-Valles, R.; Guo, S.; Lund, M. S.; Leighton, C.; Hillmyer, M. A. Macromolecules 2005, 38, 10101-10108.

(69) Kim, S. H.; Misner, M. J.; Xu, T.; Kimura, M.; Russell, T. P. Adv.Mater.(Weinheim, Ger.); Advanced Materials (Weinheim, Germany) 2004, 16, 226-231.

Chapter 2: Experimental Methods

The previous chapter helped to establish permeability and selectivity as key properties in evaluating the potential of a membrane separation. This chapter will detail how these properties were experimentally probed for the copolymer membranes fabricated in this work. Three experimental techniques – gas permeation, liquid convection and ultrafiltration – will be described in general terms without focusing on a specific copolymer system. Detailed descriptions of the membrane preparation and explanations of slight, but crucial, changes made to the methods discussed in this chapter will be saved for later chapters. Along with detailing the experimental set ups and procedures, this chapter will dedicate some time to discussing the data these techniques produce. Certain features of these data will be discussed; incorrect interpretations of these features lead to inaccurate reporting of results, while correct interpretations allow a deeper understanding to be gained.

2.1 Gas Diffusion Experiments

Gas permeabilties were measured using diffusion cells[1, 2] shown in Figure 2.1. Each cell consists of two compartments separated by the membrane. Two diffusion cells were used in our experiments, one constructed of brass and the other of stainless steel. Because ammonia is known to complex with copper, the majority component of brass, the stainless steel cell was required for the ammonia selective membrane experiments. The "donating" or "upstream" compartment and "receiving" or "downstream"

compartment in the steel cell each have a volume of 15.0 cm^3. The brass gas cell donating compartment has a volume of 22.1 cm^3 and the receiving compartment has a volume of 21.9 cm^3. Both compartments can be connected to 18 liter tanks to allow for longer experiments.

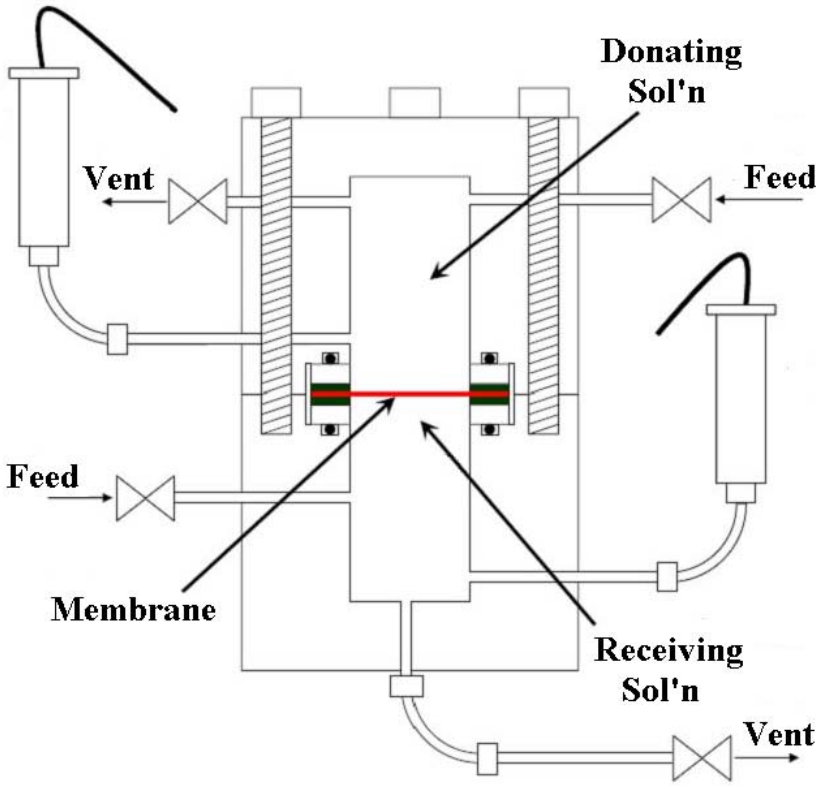

Figure 2.1: Gas Diffusion Cell. The membrane is clamped between two volumes at different pressures, and the pressure difference is measured vs. time.

Once the membrane is clamped in the cell, both compartments are thoroughly flushed with the gas being studied. After an hour, the donating vent valve is closed and the feed to the receiving compartment is cut off. This allows the receiving compartment pressure to drop to atmospheric pressure. At this point, the donating feed valve and receiving vent valve are closed and the data acquisition program is started. Upstream and

downstream compartment pressures are measured by electronic transducers (Cole Parmer Model 97356-61, Vernon Hills, IL) and the temperature is monitored with a thermocouple (National Semiconductor, Santa Clara, CA). Both the pressures and the temperature were recorded in Microsoft Excel using a Super Logics 8017 (Waltham, MA) interface. Experiments generally take between one and ten hours, depending on the permeability of the membrane being studied. Duplicate runs are performed after an additional twenty minutes of flushing.

To calculate a permeability from the pressure versus time data we write mass balances on the receiving and donating compartments.

$$V_{donating}\frac{dc_{1,donating}}{dt} = -Aj_1 \tag{2.1}$$

$$V_{receiving}\frac{dc_{1,receiving}}{dt} = +Aj_1 \tag{2.2}$$

Dividing each equation by the respective volume and subtracting the equations yields.

$$\frac{d\left(c_{1,donating} - c_{1,receiving}\right)}{dt} = -A\left(\frac{1}{V_{receiving}} + \frac{1}{V_{donating}}\right)j_1 \tag{2.3}$$

If we assume the flux across the membrane reaches steady-state quickly in comparison to changes in donating and receiving compartments, the flux is given by the result for a thin film:

$$j_1 = \frac{P_1}{\ell}\left(c_{1,donating} - c_{1,receiving}\right) \tag{2.4}$$

Inserting Equation (2.4) into Equation (2.3) yields a differential equation which can be integrated to give.

$$\frac{\Delta c_1}{\Delta c_{1o}} = \exp\left[-\frac{P_1 A t}{\ell}\left(\frac{1}{V'}+\frac{1}{V''}\right)\right] \tag{2.5}$$

In Equation (2.5), P_1 is the permeability, ℓ is the membrane thickness, A is the membrane area, t is the time, V' and V'' are the receiving and donating compartment volumes. By assuming the diffusing species is an ideal gas, we are able to account for temperature fluctuations and write the concentration difference in terms of a pressure difference: $\frac{\Delta p}{\Delta p_o} = \frac{\Delta c_1}{\Delta c_{1o}}$ where Δp_o and Δp are the pressure differences between the donating and receiving compartments initially and at time t. The cell geometric constants are grouped together in the variable β defined in Equation (2.6).

$$\beta = A\left(\frac{1}{V'}+\frac{1}{V''}\right) \tag{2.6}$$

The data are plotted as $\frac{1}{\beta}\ln\left(\frac{\Delta p_o}{\Delta p}\right)$ vs. $\frac{t}{\ell}$, and P_1 is determined from the slope.

$$\frac{1}{\beta}\ln\left(\frac{\Delta p_o}{\Delta p}\right) = P_1\frac{t}{\ell} \tag{2.7}$$

This is the key to an analysis.

Two examples of a typical gas permeation experiment are given in Figures 2.2 and 2.3, where the data are for ammonia permeating a porous polydicyclopentadiene[3] (PDCPD) and a dense polycyclooctene-b-polystyrene sulfonate[4] (PCOE-PSS) membrane, respectively. The shapes of these two plots are not similar. Diffusion across the PDCPD sample produces data that when plotted according to Equation (2.7) is linear, as expected.

The data for the PCOE-PSS is different. When plotted according to Equation (2.7) the initial data are curved for a period of time before becoming linear.

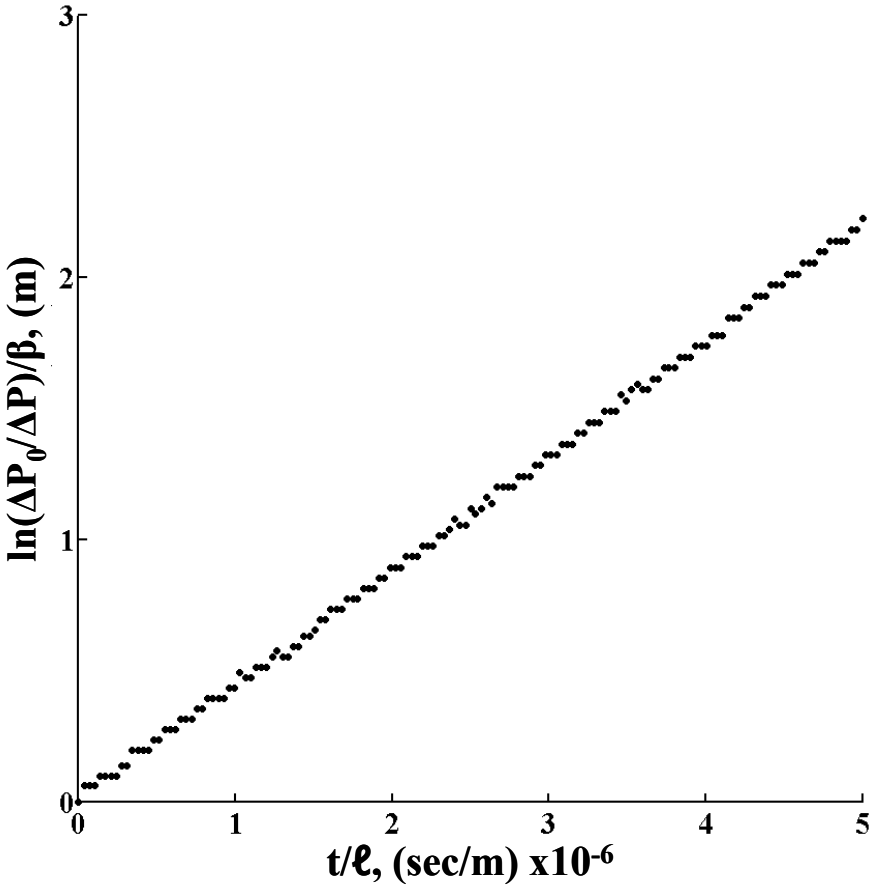

Figure 2.2: An Example of Experimental Data Which Does Not Show a Lag Time. Ammonia permeating a PDCPD membrane reaches steady-state quickly therefore a lag time is not observed.

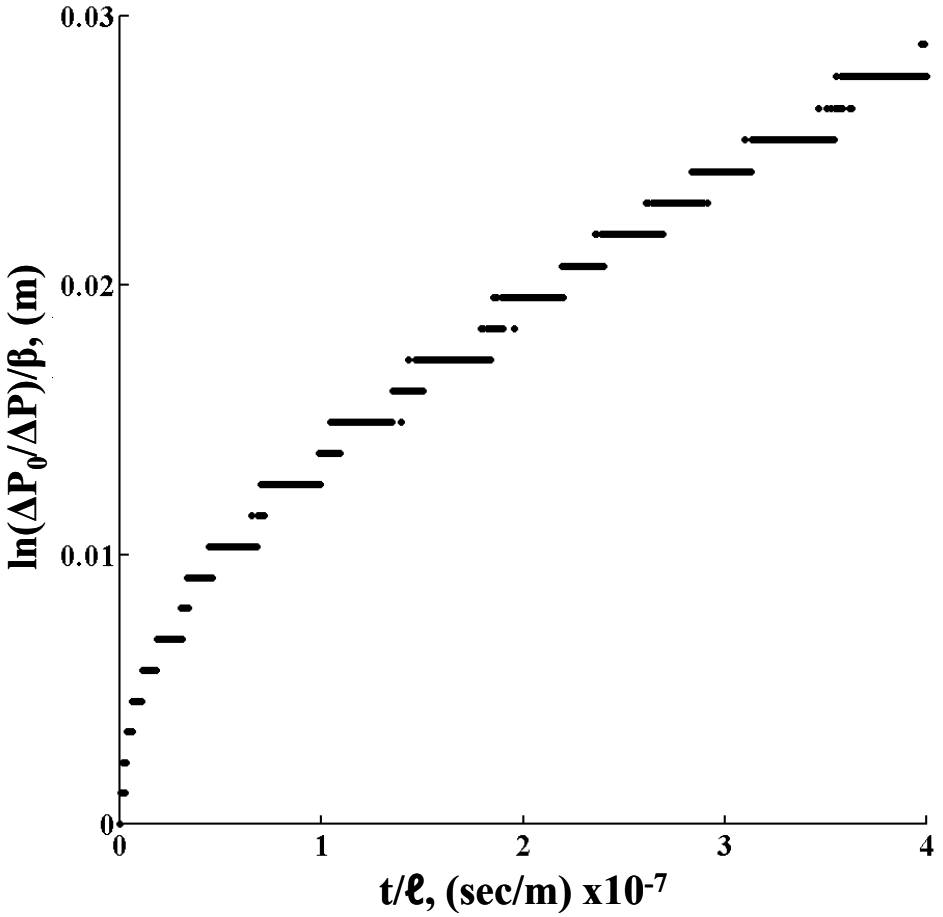

Figure 2.3: Experimental Data Which Shows a Lag Time. The later linear region of this plot is used to calculate the ammonia permeability of a PCOE-PSS sample.

Despite the difference in the shape of these two curves both were used to evaluate the ammonia permeability of the membranes. Implicit in the use of Equation (2.4) to describe the flux of species *i* across the membrane is the assumption that the system quickly reaches steady-state.[5] For thicker samples or those with low permeabilities this assumption may not be valid at small times. Instead a length of time, called the lag time,[1, 6-8] must pass before steady-state is reached. Once steady-state has been reached the data will follow the linear trend suggested by Equation (2.7). Knowing this, the permeability

of ammonia for the PCOE-PSS membrane is found from data in the later portion of the experiment.

In some of our experiments, we recognize the presence of a lag time and take steps to factor it out of our analysis. Moreover, there are cases when the lag time can be used as a useful experimental tool. The most common situation this occurs in are experiments when the upstream solute concentration is nearly constant with time and much higher than the downstream solute concentration, which is very dilute.[1, 6-12] In this case the downstream solute concentration at moderate times is predicted by Equation (2.8)

$$\frac{c_1}{c_{1o}} = \left[\frac{A}{V\ell}\right] D_1 H_1 \left(t - \frac{\ell^2}{6D_1}\right) \tag{2.8}$$

where c_1 is the concentration in the downstream; c_{1o} the concentration in the upstream; V the volume of the downstream compartment; and the permeability is written out as the product of the diffusion and partitions coefficients. The derivation of this equation, a discussion of the underlying assumptions as well as descriptions of experimental techniques consistent with the assumptions can be found in several references.[1, 6-12]

Equation (2.8) suggests plotting data from one of these experiments as c_1 vs. t. This results in a so called "breakthrough curve", a typical breakthrough curve is shown in Figure 2.4, which allows the solute permeability to be calculated from the slope and the lag time from the intercept.[7] Because the intercept only depends on the partition coefficient, the diffusion coefficient and partition coefficient can be separated. This tool has been widely used for many experimental investigations of membrane separations.

The lag time is also useful for studying a class of membranes known as barrier membranes. These membranes, designed to prevent the permeation of species, are often enhanced through the addition of impermeable inorganic flakes and/or reactive particles. The lag time can be used to investigate how the geometry and chemistry of these additives affect membrane performance.[6, 9, 10]

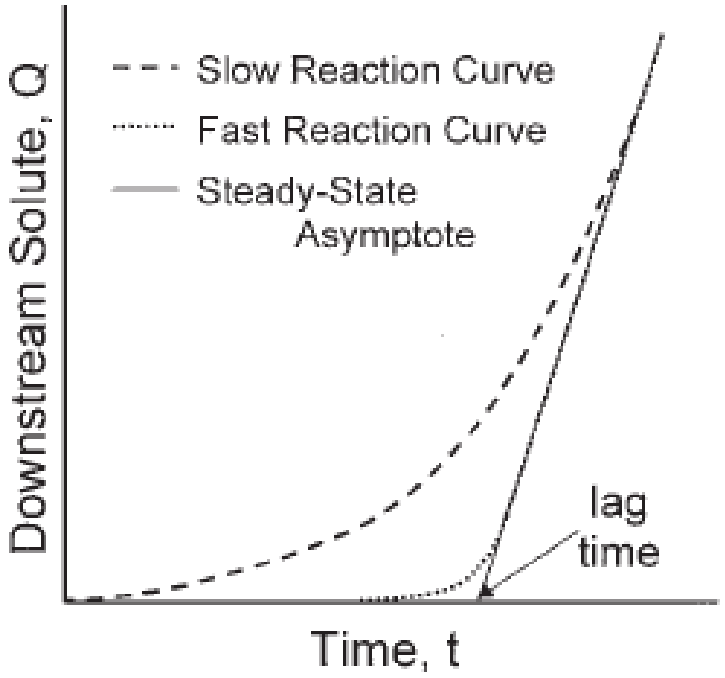

Figure 2.4: A Typical Breakthrough Curve for an Experiment Designed to Measure the Lag Time. The lag time and permeability are evaluated using Equation (2.8) to define the intercept and slope of the plot. Image reprinted from Ref. 7.

One question which may arise after the preceding discussion is "How can Equation (2.4), a steady-state result, be used to describe the behavior of an unsteady experiment?" There are two common responses to this question. One superficial answer given is that the approximation is valid because it works: diffusion coefficients measured

using a diffusion cell agree with those measured using alternative methods. The other answer tries to be a little more quantitative by comparing the relaxation time for the membrane with the relaxation time for a compartment.[13] The ratio of these values is shown in Equation (2.9) where we have assumed the two compartments have the same volume *V*.

$$\frac{\ell^2 / P_1}{2\ell / P_1 A V} = \frac{2A\ell}{V} \ll 1 \tag{2.9}$$

Equation (2.9) shows that the ratio of the relaxation times is equal to the ratio of the membrane to cell volumes. If the membrane volume is much smaller than the compartment volumes, which is often the case with our experiments, concentration changes occur much more rapidly in the membrane than in the compartment. Therefore transients which exist in the membrane can be ignored and the "pseudosteady-state approximation" used to analyze the collected data.[5, 14]

2.2 Liquid Convection Experiments

Liquid permeation experiments were performed on one of two experimental setups. Samples prepared as a thin film were run using the stirred filtration cell shown in Figure 2.5 (Amicon 8010, Millipore Co., Billerica, MA) that has an active area of 4.1 cm^2. Circular discs 2.5 cm in diameter were cut from larger cast sheets to fit into the stirred cell and sealed with a silicone O-ring. The pressure difference that drives convection was applied using N_2 gas (UHP N_2, Airgas, Radnor Township, PA). Prior to beginning flux measurements, the membrane was pre-wet using isopropyl alcohol for 30

min and flushed with pure water for 45 min to remove the alcohol. Besides wetting the membrane no other preconditioning was required; the observed flux of pure water through the membrane was not a function of time, indicating that little to no compaction occurred. This is to be expected given the rigidity of our membrane and the relatively low pressure drop. Once the membrane had been wet and flushed, the stir bar was turned off, and the pressure set to the desired value. The permeating water was collected in a glass vial, and its mass measured (Metler-Toledo, Inc., Columbus, OH) every five minutes for one hour. Flow rate measurements were performed three times at each pressure drop to check reproducibility.

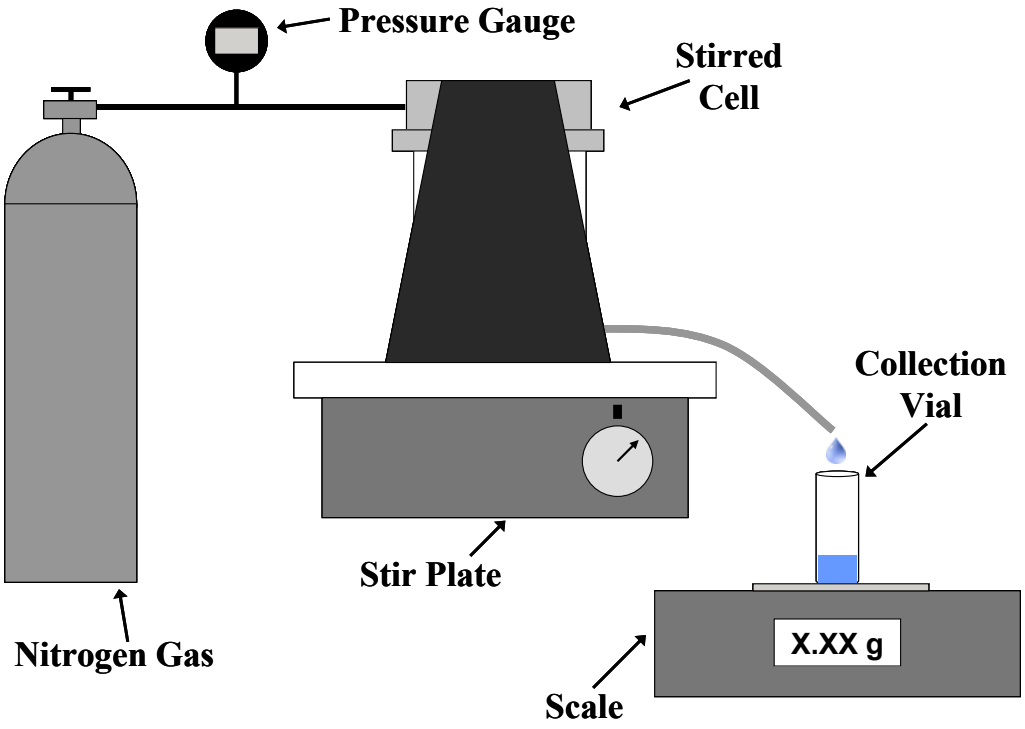

Figure 2.5: Stirred Cell Used for Liquid Phase Experiments with Thin Film Samples. The membrane pure water permeabilities and ability to reject dissolved solutes were both measured using this setup.

The liquid flux of monolith samples was measured using the diaphragm cell shown in Figure 2.6. The cell consists of two compartments separated by the monolith. The donating compartment is attached to a large reservoir and the receiving compartment to a precision bore capillary (Friedrich 8 Dimmock Inc., Millville, NJ). The height difference between the donating and receiving volumes is recorded by hand as a function of time using a cathetometer (Gaertner Scientific Corporation, Chicago, IL).

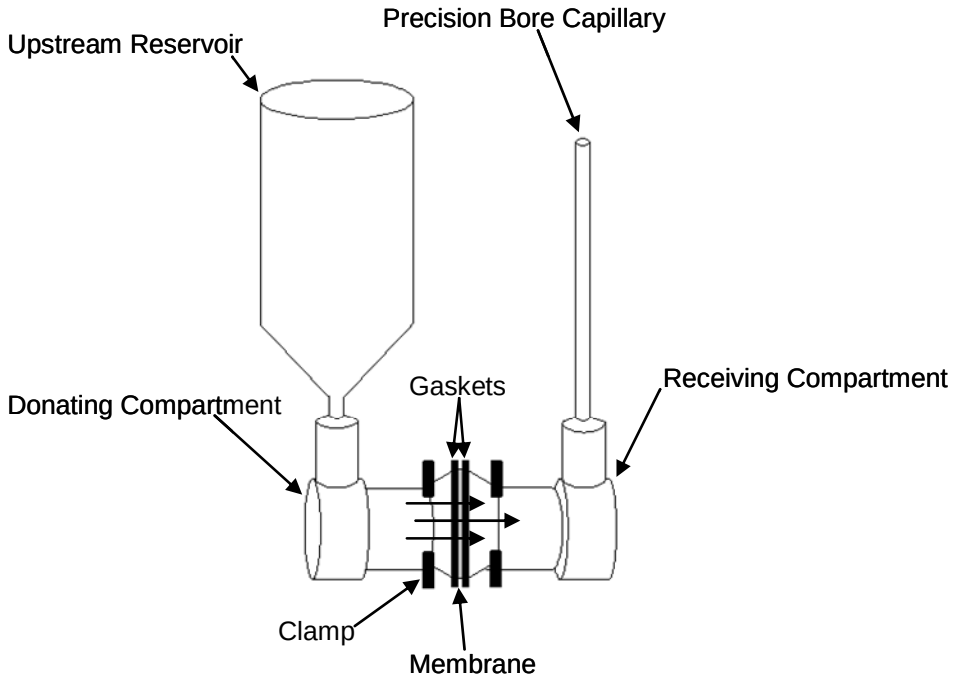

Figure 2.6: Diaphragm Cell. The diameter of the monolith's pores is found by measuring the height of water in the capillary vs. time.

Once the membrane is clamped in the cell, the two compartments are filled with distilled water so they partially fill both the large reservoir and the capillary. The meniscus height in the reservoir is greater than the meniscus in the capillary, so a

hydrostatic pressure difference drives the flow through the membrane. The pore diameter can be calculated from two mass balances for the donating and receiving compartments

$$A_{donating}\frac{dh_{donating}}{dt} = -Q \tag{2.10}$$

$$A_{receiving}\frac{dh_{receiving}}{dt} = +Q \tag{2.11}$$

Dividing each equation by the respective areas and then subtracting them yields

$$\frac{d\left(h_{donating} - h_{receiving}\right)}{dt} = -\left(\frac{1}{A_{receiving}} + \frac{1}{A_{donating}}\right)Q \tag{2.12}$$

The Hagen-Poiseuille relationship[14] for the flow through one pore gives a total volumetric flow rate, Q:

$$Q = n_p A_m \frac{\pi d^4 \Delta p}{128\mu\ell} \tag{2.13}$$

The experimental set up was selected such that the pressure difference was brought about by the height difference of the two compartments, $\Delta p = \rho g(h_{donating} - h_{receiving})$. Thus

$$\frac{\Delta h}{\Delta h_o} = \exp\left[-n_p A_m \frac{d^4 \rho g}{128\mu\ell}\left(\frac{1}{R'^2} + \frac{1}{R''^2}\right)t\right] \tag{2.14}$$

where d is the pore diameter, ℓ is the membrane thickness, A_m is the membrane area, ε is the membrane void fraction, ρ and μ are the density and viscosity of water, g is the acceleration due to gravity, t is the time, R' and R'' are the reservoir and capillary radii, respectively and Δh_o and Δh are the height differences between the donating and

receiving compartments initially and at time *t*. Normally the data are plotted as $\ln \frac{\Delta h_o}{\Delta h}$ vs. *t*, and *d* is determined from the slope.

2.3 Ultrafiltration Experiments

Two types of feed solutions were used to challenge the nanoporous membranes. The first type was a solution of a single polyethylene oxide (PEO) sample (Polymer Source Inc., Montreal, Quebec) with a narrow molecular weight distribution, dissolved at a concentration of 1.5 g L^{-1}. Single solute experiments were performed using eight different PEO molecular weights (0.8, 3.0, 9.0, 14.0 23.0, 34.5, 59.0 and 100.0 kg mol^{-1}), selected because the molecules have hydrodynamic radii in the size range of the pores (Table 2.1). The hydrodynamic radii were calculated using published data which show how the tracer diffusion coefficients[15] and intrinsic viscosities[16] vary with polymer molecular weight. The Stokes-Einstein equation (Equation (2.15)) is used to calculate the PEO hydrodynamic radius from experimental tracer diffusion data.[15]

$$D_t = \frac{k_B T}{6\pi\mu R_H} \tag{2.15}$$

where D_t is the diffusion coefficient of an individual polymer chain, k_B is Boltzmann's constant, T is temperature, μ is the liquid viscosity and R_H is the hydrodynamic radius. The hydrodynamic radius of the PEO molecules can also be estimated using intrinsic viscosity data[16] for the aqueous polymer solutions:

$$[\eta] = \frac{10\pi N_A R_H^3}{3M_n} \tag{2.16}$$

where [η] is the intrinsic viscosity of the polymer solution, N_A is Avogadro's number and M_n is the number average molecular weight of the polymer sample.

Table 2.1. Molecular Weight and Characteristic Size of PEO Solutes.

PEO sample M_n (kg mol^{-1})	D_t R_H[15] (nm)	[η] R_H[16] (nm)
0.75	0.6	0.8
3.40	1.5	1.8
8.90	2.6	3.2
14.0	3.4	4.0
23.5	4.5	5.4
35.0	5.7	6.8
59.0	7.8	9.0
100.0	10.6	12.1

The concentrations of PEO in the feed and permeate solutions were determined as total organic carbon (Sievers 900 portable TOC Analyzer, GE Analytical Instruments, Boulder, CO). Because the detection range of the TOC was 0–20 ppm, the collected feed and permeate samples were diluted 100 fold with water. Calibration solutions for each PEO molecular weight were made at 1, 5, 10, 15, and 20 ppm because there was concern about the higher MW samples not being fully oxidized.

The second type of feed solution used was a mixed solute solution consisting of polydisperse dextran fractions in 18 MΩ water. The concentration of the individual dextran fractions were selected to match the guidelines set out by the ASTM 1343: "Standard Test Method for Molecular Weight Cut-Off Evaluation of Flat Sheet Ultrafiltration Membranes".[17] These concentrations were analyzed using size exclusion chromatography (SEC) in a manner consistent with ASTM 1343. For both types of feed

solutions, sieving curves were calculated from the ratio of the concentrations in the filtrate to that of the feed solution.

Ultrafiltration experiments were performed with the same membrane preparation, wetting procedure and Amicon 8010 stirred cell as was used for the liquid convection experiments. Once the membrane was in place, wetted, and flushed, the pure water flux was checked for one hour at a pressure drop 13 psig to verify the sample performed in a manner consistent with the membranes used for liquid convection experiments. At this point, the stirred cell was filled with feed solution and the pressure drop returned to 13 psig. The system was run for one hour to flush the tubing running from the cell to the collection vial, thus avoiding artificial dilution of the collected permeate sample. After flushing, a clean glass vial was used to collect 1 mL of permeate which was analyzed using either TOC or SEC, depending on the solute. The system was then rinsed with water and flushed for an hour with 18 mΩ water. During this time, the flux was re-measured at a pressure drop of 13 psig to make sure no changes had occurred in the membrane. If the water flow rate was similar to that observed before challenging the membrane, the next solution was put into the cell and the process repeated. In this way we were able to move sequentially through the eight PEO solutions or repeat dextran experiments to check reproducibility.

2.4 References

(1) Yang, C.; Cussler, E. L. *AICHE J.* **2001***, 47*, 2725-2732.

(2) Phillip, W. A.; Rzayev, J.; Hillmyer, M. A.; Cussler, E. L. *J. Membr. Sci.* **2006***, 286*, 144-152.

(3) Phillip, W. A.; Amendt, M.; O'Neill, B.; Chen, L.; Hillmyer, M. A.; Cussler, E. L. *ACS Applied Materials & Interfaces* **2009***, 1*, 472-480.

(4) Phillip, W. A.; Martono, E.; Chen, L.; Hillmyer, M. A.; Cussler, E. L. *J. Membr. Sci.* **2009***, 337*, 39-46.

(5) Cussler, E. L. In *Diffusion, mass transfer in fluid systems;* Cambridge University Press: New York, 2009; , pp 654.

(6) Yang, C.; Nuxoll, E. E.; Cussler, E. L. *AICHE J.* **2001***, 47*, 295-302.

(7) Nuxoll, E. E.; Cussler, E. L. *AICHE J.* **2005***, 51*, 456-463.

(8) Lape, N. K.; Yang, C.; Cussler, E. L. *J. Membr. Sci.* **2002***, 209*, 271-282.

(9) DeRocher, J. P.; Gettelfinger, B. T.; Wang, J.; Nuxoll, E. E.; Cussler, E. L. *J. Membr. Sci.* **2005***, 254*, 21-30.

(10) Lape, N. K.; Nuxoll, E. E.; Cussler, E. L. *J. Membr. Sci.* **2004***, 236*, 29-37.

(11) Shimotori, T.; Nuxoll, E. E.; Cussler, E. L.; Arnold, W. A. *Environ. Sci. Technol.* **2004***, 38*, 2264-2270.

(12) Warta, A. M.; Arnold, W. A.; Cussler, E. L. *Environ. Sci. Technol.* **2005***, 39*, 9738-9743.

(13) Mills, R.; Woolf, L. A.; Watts, R. O. *AICHE J.* **1968***, 14*, 671-673.

(14) Bird, R. B.; Stewart, W. E.; Lightfoot, E. N. In *Transport phenomena;* J. Wiley: New York, 2002; , pp 895.

(15) Faraone, A.; Magazu, S.; Maisano, G.; Migliardo, P.; Tettamanti, E.; Villari, V. *J. Chem. Phys.* **1999***, 110*, 1801-1806.

(16) Meireles, M.; Bessieres, A.; Rogissart, I.; Aimar, P.; Sanchez, V. *J. Membr. Sci.* **1995***, 103*, 105-115.

(17) ASTM - ASTM International In Standard Test Method for Molecular Weight Cutoff Evaluation of Flat Sheet Ultrafiltration Membranes; 2001; Vol. ASTM E 1343 - 90 (reapproved 2001).

Chapter 3: Ammonia Selective Membranes

A number of research groups have investigated the use of a membrane separation to improve the Haber process.[1-8] The efforts of these groups have found that membranes made from polymers containing thiocyanate and sulfonic acid groups have significantly higher ammonia permeabilities than hydrogen and nitrogen permeabilities. While most of this work has focused on pure gas experiments, the reactor effluent from the Haber process contains a mixture of hydrogen, nitrogen and ammonia. Fully testing the potential of these membranes requires running experiments in mixed gas configurations. Unfortunately, in mixed gas experiments, the membrane loses its selectivity when the polymer swells in the highly soluble, a phenomenon known as membrane conditioning.[9-11]

This chapter will focus on our attempt to use block copolymers to make ammonia selective membranes which retain selectivity in mixed gas feeds. We use a copolymer which self-assembles into a bicontinuous microstructure with two interpenetrating nanoscopic domains.[12, 13] One domain is made from polystyrene sulfonate (PSS) known to have a high ideal selectivity, while the other domain will be made from crosslinked polycyclooctene (PCOE) or polydicyclopentadiene (PDCPD). Our hope is that the rigid structure of the PCOE/PDCPD phase will prevent the PSS phase from swelling, allowing the membrane to remain selective for mixed gas feeds.

3.1 Membrane Fabrication and Preparation

The membrane developed here uses the chemistry developed by Chen *et al.*[14] to produce a mechanically robust copolymer film with interpenetrating domains of crosslinked polycyclooctene or polydicyclopentadiene and polystyrene sulfonate . The three membranes cast using this type of copolymer had different molecular weights of the constituent blocks and different reactive monomers. This caused different PSS phase sizes and different degrees of crosslinking in the PCOE/PDCPD phase.

Table 3.1 summarizes the formulations of the three block copolymer membranes. The first column gives the membrane, and the second gives the molecular weight of the constituent blocks in the templating copolymer. The third through sixth columns give the weight percent of each component in the membrane casting solution where P(N-s-S)-b-PSSP is the templating block copolymer, COE is the reactive monomer cyclooctene, THF is the casting solvent tetrahydrofuran and the catalyst is the 2nd generation Grubbs metathesis catalyst. The structure generated is bicontinuous, with percolating sulfonated polystyrene and rigid matrix domains. The TEM image in Figure 3.1 shows these two regions for sample LC03. The bright areas are the PCOE matrix and the dark areas are the PSS stained by Pb^{+2}.

Table 3.1: Membrane Solutions for Each Sample.

Sample Name	poly(norboreneylethylstyrene)-b-poly(propyl styrene-sulfonate)		cyclooctene (wt %)	THF (wt %)	Grubbs Catalyst (wt %)
	Block M_n (kg mol^{-1})	(wt %)			
LC01	10-24	11.9	8.0	80.0	0.1
LC03	2.0-4.5	11.9	8.0	80.0	0.1
LC05	6.2-10	12.5	7.5 [a]	80.0	0.1

[a] For LC05, dicyclopentadiene and cyclooctene at a mass ratio of 1:1 was used.

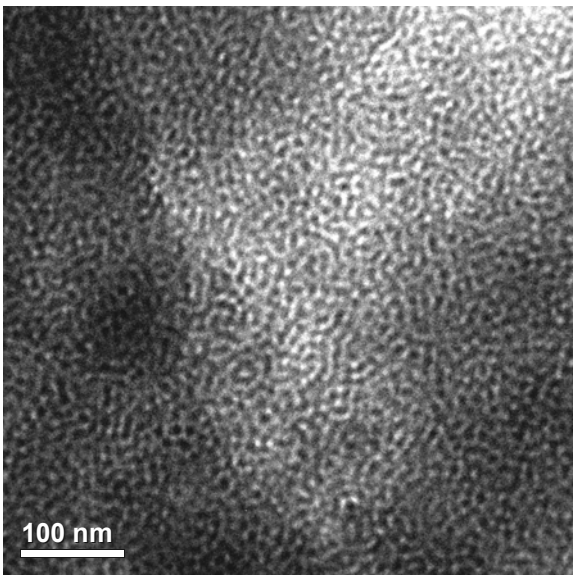

Figure 3.1: A TEM Image of the Copolymer Membrane. This image of the sample LC03 shows the microstructure of the copolymer membrane. The light areas of the image represent the PCOE phase and the dark areas show the PSS phase.

Our results with these block copolymer films are compared below with two other membranes. One is polypersulfonic acid (Nafion® 117, Sigma-Aldrich, St. Louis, MO), which was already shown to be highly permeable for ammonia and so provides a benchmark for these studies. The second membrane, an alumina disc, was used to verify our experimental set up was working properly. This membrane was made with 1.5 g aluminum oxide powder (Baikalox High Purity Alumina, Baikowski International,

Charlotte, NC), inserted into a stainless steel washer and clamped between two stainless steel rods at four tons pressure in a hydraulic press. After two minutes, the press was released and the washer inverted and recompressed to ensure good packing. The resulting disc is cured at 900 °C for 48 hrs.

The preparation of the membranes for gas diffusion experiments was straightforward. The copolymer and Nafion films were cut into 1 cm x 1 cm squares from the larger cast sheets. The alumina disc was used as is. All three types of membranes were glued using epoxy resin (DP-460 Off White, 3M, St. Paul, MN) to a stainless steel disc. The steel disc had a 1 mm diameter hole punched in the middle giving a membrane area of 7.9×10^{-3} cm^2 available for mass transfer. The assembly was cured in an oven at 40 °C for 4 hours, and placed between the two compartments of the stainless steel diffusion cell previously described.

The permeability of these membranes was determined under several conditions. For single pure gas experiments, both compartments were flushed for 1 hr with the gas to be studied. After flushing, the downstream compartment was emptied to 100 kPa (absolute), a 200 kPa (absolute) charge of gas is put into the upstream compartment, the cell was sealed and the data acquisition program was started. Mixed gas experiments differed. After the background gas was used to flush the cell for 1 hr, 200 kPa (absolute) of this gas was put in both the upstream and downstream compartments. The diffusing gas was then used to bring the upstream compartment to 300 kPa (absolute), the cell was sealed, and data acquisition was started.

The permeability of the block copolymer films was measured at different average pressures, defined as the arithmetic average of the upstream and downstream compartments. While the average pressure varied, the initial pressure drop was constant at 100 kPa. For example, for a mean pressure of 350 kPa (gauge), the upstream would initially be at 400 kPa (gauge) and the downstream at 300 kPa (gauge). In addition, initial experiments with ammonia were erratic, producing scattered data which suggested that the cell was leaking. This difficulty was due to incompatibility between NH_3 and the silicone O-rings and the valve lubricant. Buna N O-rings (Buna N, RT/Dygert International, Edina, MN) and Swagelok SS-41GS2 valves (SS-41GS2, Swagelok, Chaska, MN) do not interact with ammonia and were used in all experiments.

3.2 Results

3.2.1 Ammonia Selective Membrane Characteristics

The five membranes studied here all have a bicontinuous structure. Each also contains one phase that is much more permeable to ammonia than the other. The alumina membranes have solid alumina particles around gas filled vacancies. Nafion has a structure idealized as a perfluoronated hydrophobic phase surrounding a sulfonated hydrophilic phase, sometimes described as inverted micelles which are in contact.[15] The three copolymer templated films have a polycyclooctene or polydicyclopentadiene hydrophobic phase surrounding a hydrophilic polystyrene sulfonate phase. Because ammonia is hydrophilic, each of the membranes can be thought of as having “pores” (i.e. a phase which is significantly more permeable to ammonia).

The physical properties of these membranes are given in Table 3.2. The first column gives the membrane, and the second gives the anticipated mechanism for diffusion. Because the alumina has pores smaller than the mean free path of the gas molecules, the expected mechanism is Knudsen diffusion.[16] For Nafion and our block copolymer films, ammonia is expected to dissolve largely in the hydrophilic domain and diffuse through it.[16, 17] Nitrogen and hydrogen also proceed by this diffusion-solubility mechanism; because they are less polar than ammonia, they may dissolve slightly but significantly in both the hydrophilic and hydrophobic parts of the membrane.

Table 3.2: Summary of Membrane Characteristics.

Membrane	**Expected Mechanism**	**Thickness (μm)**	**Void or Sulfonated Fraction**	**"Pore" Diameter (nm)**	**Tortuosity**
Alumina	Knudsen Diffusion	1930	0.30	64	1.9
Nafion 117	Diffusion-Solubility	178	0.15	(3)	(3.0)
PCOE-PSS LC01	Diffusion-Solubility	124	0.42	(23)	(1.8)
PCOE-PSS LC03	Diffusion-Solubility	90	0.42	(7)	(1.8)
PDCPD-PSS LC05	Diffusion-Solubility	140	0.39	(11)	(1.8)

The third and fourth columns in Table 3.2 give the membranes' thickness and void/sulfonated fraction. The void fraction of the alumina membrane is calculated from its density; the sulfonated fraction of Nafion is taken from the literature;[15] and that for the copolymer membrane is assumed equal to the volume fraction of the hydrophilic phase. The last two columns in Table 3.2, the "pore" diameter (i.e., the actual pores in the alumina disc and the sulfonated domain size for the Nafion and block polymer

membranes) and the tortuosity, are estimated from diffusion and small angle X-ray scattering, as detailed later in the chapter. Recent work with similar nanoporous PDCPD membranes has shown that these methods give estimates of pore size for block copolymer membranes which are consistent with diffusion and flow measurements.[18]

3.2.2 Single Gas Experiments

The diffusion data for single gas experiments across alumina, Nafion, and a block copolymer membrane are summarized in Figures 3.2-3.4. The sample LC01 is chosen as a representative for the block copolymer templated membranes. The data, which for all membranes vary as predicted by Equation (2.7), are used to calculate the permeability of each gas, giving the results in Table 3.3. In this table, the first four columns give the membrane, the gas, the permeance $\frac{DH}{\ell}$ and the permeability DH.

Table 3.3: Permeance and Permeability for Five Membranes.[a]

Membrane	Gas	DH/ℓ (m/s)	DH[b] (m^2/s)	$D_{pore}(D_{Kn})$ ($x\ 10^5\ m^2/s$)
Alumina	H_2	6.53×10^{-3}	1.26×10^{-5}	7.98 (7.58)
	He	4.38×10^{-3}	8.46×10^{-6}	5.36 (5.36)
	N_2	1.92×10^{-3}	3.70×10^{-6}	2.34 (2.03)
	NH_3	2.36×10^{-3}	4.55×10^{-6}	2.88 (2.60)
poly(perfluorosulfonate) (Nafion 117)	H_2	2.53×10^{-6}	5.90×10^{-10}	
	N_2	2.11×10^{-6}	3.80×10^{-10}	
	NH_3	1.50×10^{-3}	2.67×10^{-7}	
PCOE-PSS (LC01)	H_2	8.15×10^{-8}	1.01×10^{-11}	
	N_2	7.42×10^{-8}	0.92×10^{-11}	
	NH_3	4.08×10^{-6}	5.06×10^{-10}	

[a] The values shown are for pure gases at 100 kPa and 25 ˚C.
[b] To convert these permeabilities to units of barrers multiply by 1.205×10^{12}.

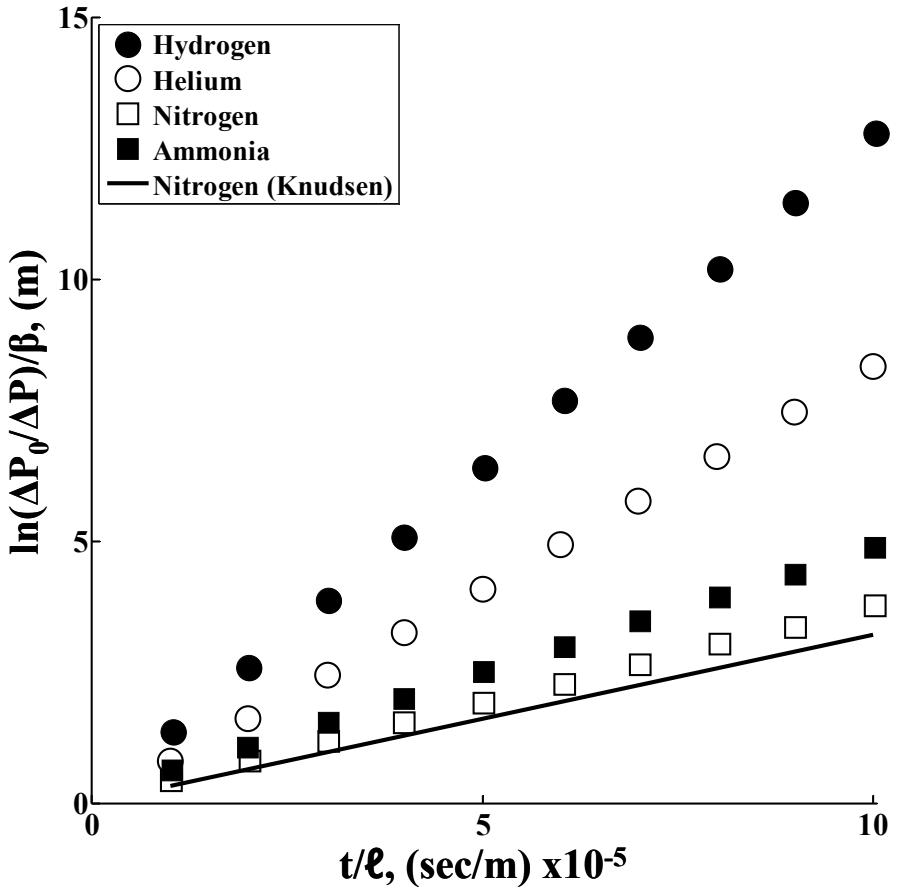

Figure 3.2: Gases Diffuse Across the Alumina Membrane by a Knudsen Mechanism. The measured gas permeabilities show an inverse square root dependence on the gas molecular weight as predicted by the Knudsen theory.

For the alumina membrane, we can easily find the diffusion coefficient itself D_{pore} using the membrane value of H which for this geometry equals ε/τ:

$$DH = \frac{\varepsilon}{\tau} D_{pore} \tag{3.1}$$

where ε is the void fraction and τ is the tortuosity. We can compare this D_{pore}, shown in the fifth column of Table 3.3, with that estimated for Knudsen diffusion[19, 20]

$$D_{Kn} = \frac{2d}{3}\sqrt{\frac{8k_B T}{\pi \tilde{m}}} \tag{3.2}$$

where d is the pore diameter, found from SEM to be 64 nm; k_B is Boltzmann's constant; $\tilde{m}$ is the molecular mass of the gas particle; and T is the temperature. We use the data for helium to calculate a tortusosity of 1.9. As Table 3.3 shows, the values of the other gases estimated on this basis agree with the experiments, with only modest differences between the fluxes of the different species. Any selective separations in the alumina membranes, which are based on Knudsen diffusion, are modest with little practical value.

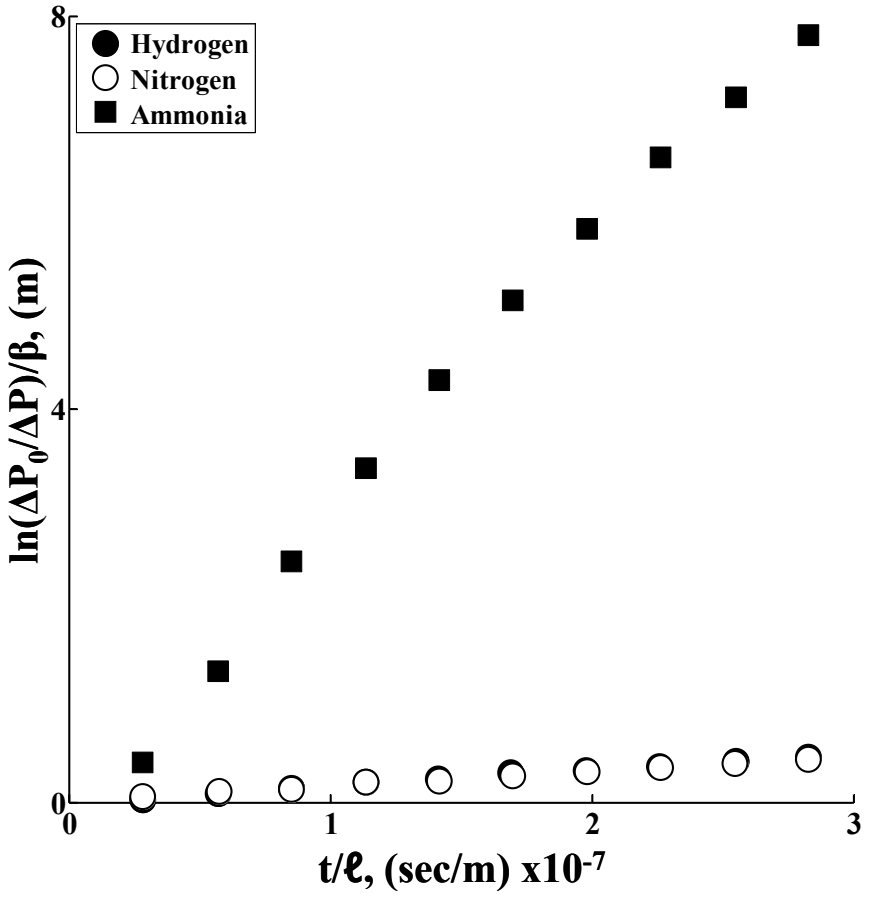

Figure 3.3: Ammonia Permeates Nafion More Rapidly Than Nitrogen and Hydrogen in Single Gas Experiments. These single gas permeabilities imply an ammonia to nitrogen selectivity greater than 400.

The data for Nafion, shown in Figure 3.3 and the middle of Table 3.3, are a dramatic contrast. The nitrogen and hydrogen permeabilities are over 10,000 times lower than those in the alumina membrane, which is due to diffusion in polymer rather than in dilute gas. The surprise is that the ammonia flux is over 400 times greater than the fluxes of nitrogen and hydrogen. In more common units, the fluxes of nitrogen and hydrogen are around 700 barrers, but that of ammonia is over 300,000 barrers. This implies the Nafion has an ideal selectivity (based on pure gases) of over 400:1 for ammonia vs. hydrogen and nitrogen.

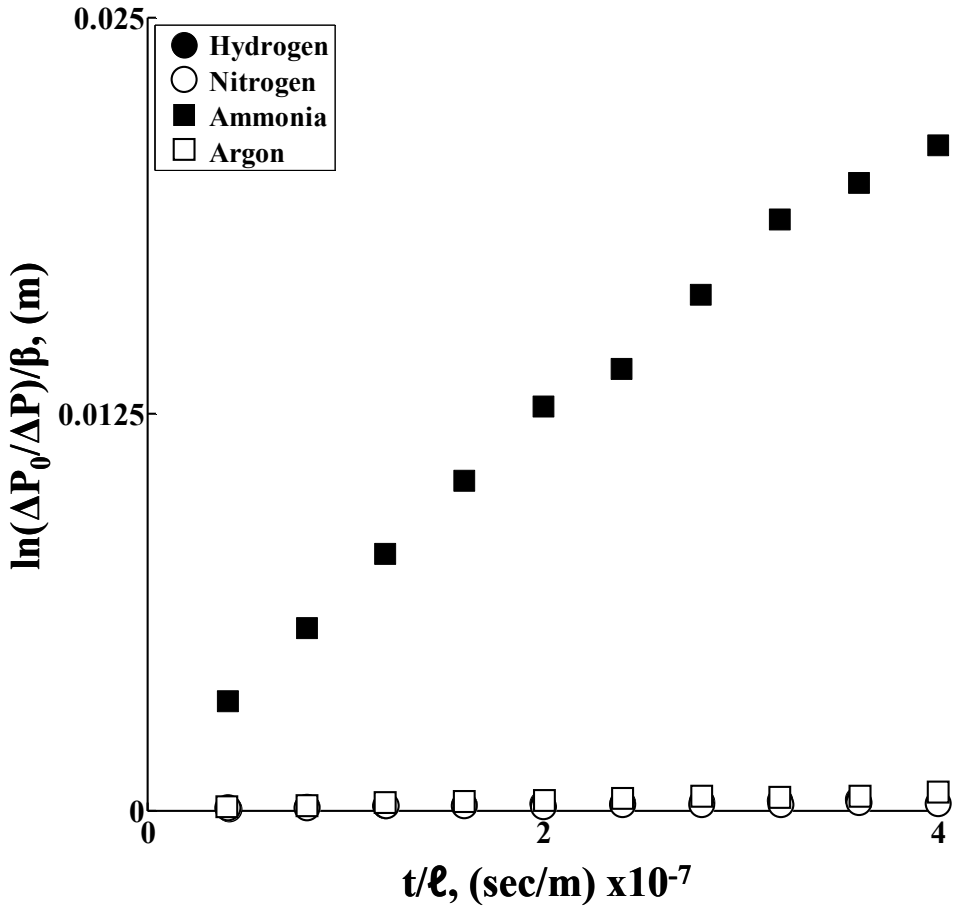

Figure 3.4: The LC01 Copolymer Membrane is Highly Selective in Single Gas Experiments. The selectivities implied by these experiments are over 50:1 for ammonia over nitrogen.

The fluxes across the block copolymer membrane LC01 are slower but show similarly high selectivity. As before, the data are consistent with Equation (2.7), as shown in Figure 3.4. The permeabilities found from these data are smaller, over 500 times less than those in Nafion, as shown in the bottom section of Table 3.3. Still, the ammonia flux is about 600 barrers, large enough to be practically interesting. As before, the membrane is selective: the flux of ammonia is over fifty times greater than those of nitrogen and hydrogen.

The high ideal selectivities for ammonia shown by Nafion and by our block copolymer are likely the result of a high solubility of ammonia in the sulfonated polymer. Ammonia is known to be extremely soluble in a wide variety of salts and ionic polymers.[1-8, 21] Nitrogen and hydrogen, which are less polar, are much less soluble. This difference in solubility and in the large selectivity it effects suggests that these membranes can be the basis for practical separation processes. However, the selectivities shown are inferred from measurements on pure gases. They are "ideal selectivites", not the actual ones based on gas mixtures.

3.2.3 Mixed Gases Results

The results for mixed gas experiments with Nafion and block copolymer membranes are shown in Figures 3.5 and 3.6, respectively. In both figures, the pressures reported are the changes in total pressure caused by a concentration difference in just one gas. For example, the open circles in these figures, labeled N_2, are the pressure changes caused by an initial pressure difference in nitrogen with a constant partial pressure of ammonia in the upstream and downstream. The pressure changes are assumed to be due to nitrogen permeation alone. This assumption implies that diffusion across these membranes has no multicomponent effects, that the diffusion flux of each gas is independent of the concentration gradient of all other gases. In more fundamental terms, this assumption is that the cross-term diffusion coefficients are near zero and the main term diffusion coefficients dominate transport.[16, 22] This is true in dilute solutions such as solutions of gases in polymer membranes. Note that this does not mean that the flux of,

for example, nitrogen is independent of the total ammonia pressure, but just independent of the pressure gradient of ammonia. We will return to this point below.

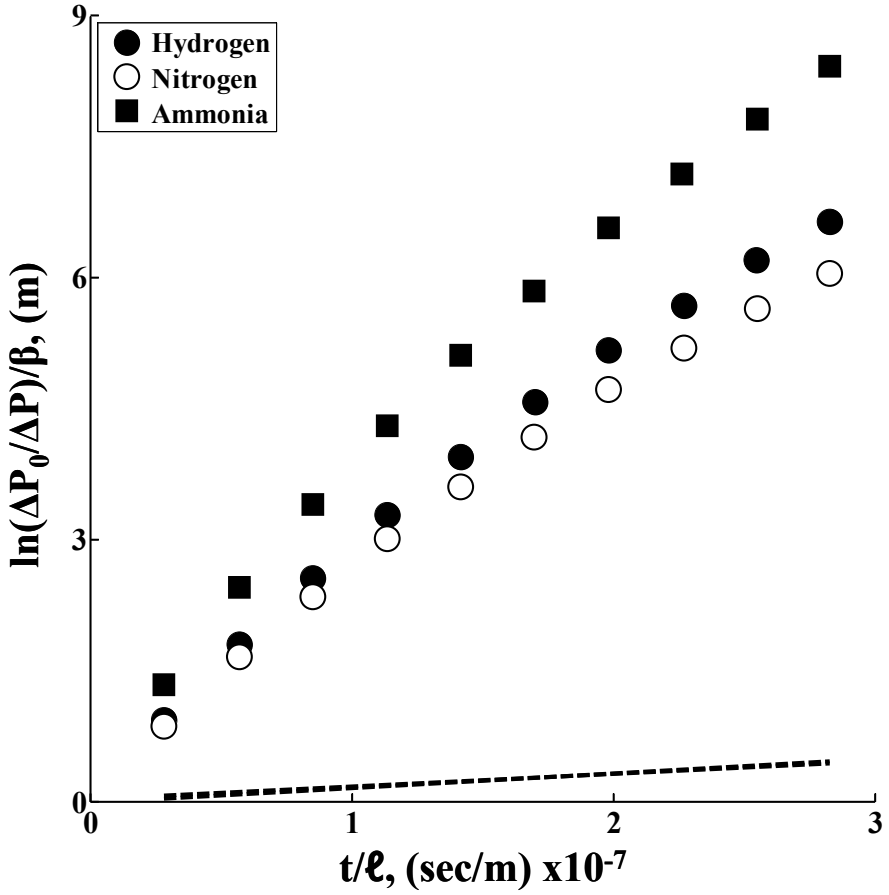

Figure 3.5: Nafion Loses Selectivity in Mixed Gas Experiments. Ammonia swells the Nafion membrane, plasticizing the polymer. The increased solubility and chain mobility after plasticization allows nitrogen and hydrogen to permeate more rapidly, resulting in a loss of selectivity. The loss of selectivity can be seen graphically by comparing the nitrogen and hydrogen single gas data (dashed lines) and mixed gas data (discrete points).

The mixed gas results for Nafion, shown in Figure 3.5, are disappointing. The high selectivity inferred by the pure gas experiments is almost completely lost. In this figure, the data points show the results for the mixed gas experiments and the dashed

lines show the changes for experiments with just one gas. The difference in permeabilities is detailed in Table 3.4. For pure gases diffusing across Nafion, the permeability of ammonia is over four hundred times that of nitrogen. For mixed gases diffusing across Nafion, the permeability of ammonia is only 20 percent higher than that of nitrogen and hydrogen. Selective separations across Nafion are not commercially interesting.

Table 3.4: Summary of Mixed Gas Diffusion.

Membrane	**DH (x10^8 m^2/s)**			**Selectivity**	
	H_2	**N_2**	**NH_3**	**NH_3/H_2**	**NH_3/N_2**
Nafion 117	0.059	0.038	26.7	>400	>700
+ 1 atm NH_3	22.9	21.3	27.0[a]	1.2	1.3
LC01	0.00101	0.00092	0.0506	>50	>50
+ 1 atm NH_3	0.00112	0.00086	0.0934[a]	>90	>100

a) An ammonia mixed gas experiment is identical to running a single gas ammonia experiment at a higher average pressure.

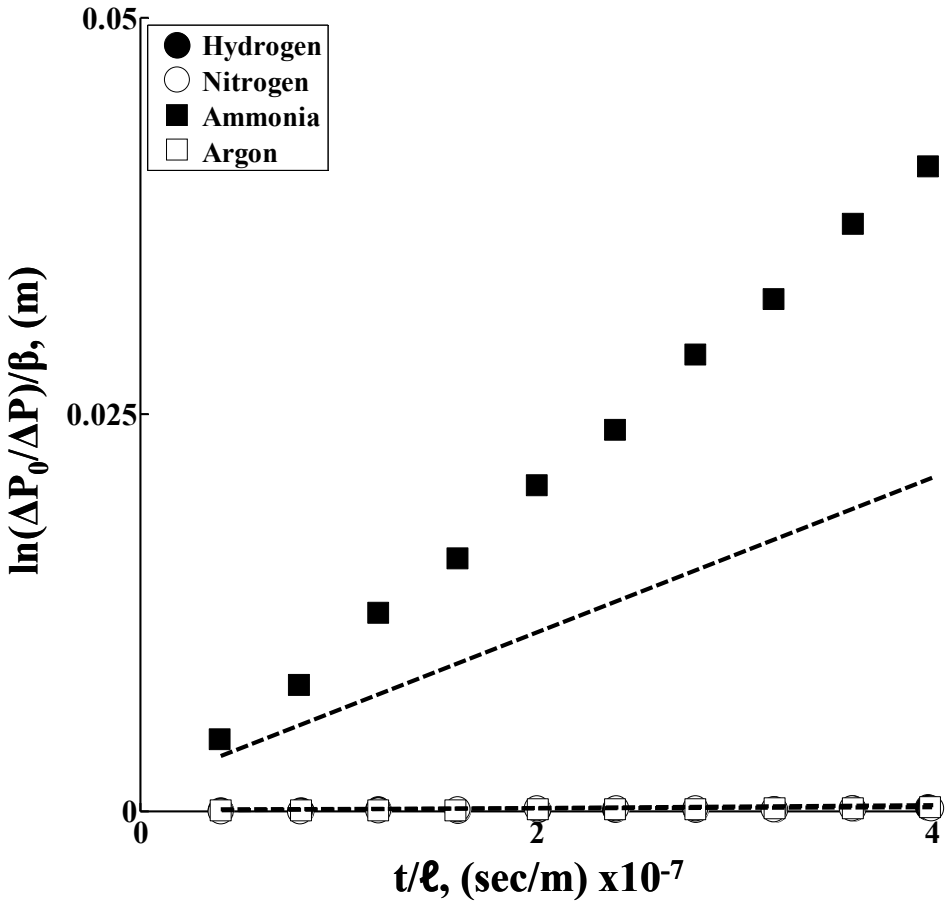

Figure 3.6: The Copolymer Membrane Remains Selective in Mixed Gas Experiments. The crosslinked PCOE/PDCPD phase prevents the PSS phase from swelling, so the membrane remains selective. Again, the dashed lines are the expectations drawn from the ideal permeabilities, i.e. from the pure gas experiments.

The block copolymer membrane results are much more promising. Figure 3.6 shows these results, which are a sharp contrast with Nafion. Though the values of the permeability are smaller than for Nafion, the ammonia permeability is larger when the membrane is run with a mixed gas feed. This result is addressed in more detail shortly. Importantly, the block copolymer membrane remains selective at high ammonia pressures. The permeability of ammonia remains over 90 times higher than hydrogen, and 100 times higher than nitrogen, as shown in Table 3.4.

3.2.4 Varying Membrane Sulfonated Domain Size and Degree of Crosslinkning

These results suggest exploring the limits of these membranes by varying the mean pressure in the diaphragm cell. The mixed gas permeabilities of nitrogen and ammonia are reported in Figures 3.7 and 3.8 for the three different block copolymer samples. As Table 3.2 showed, sample LC01 has 23 nm PSS domains in a PCOE matrix, sample LC03 has 7 nm PSS domains in a PCOE matrix, and sample LC05 has 11 nm PSS domains in a PDCPD/PCOE matrix. The properties of each membrane are discussed below.

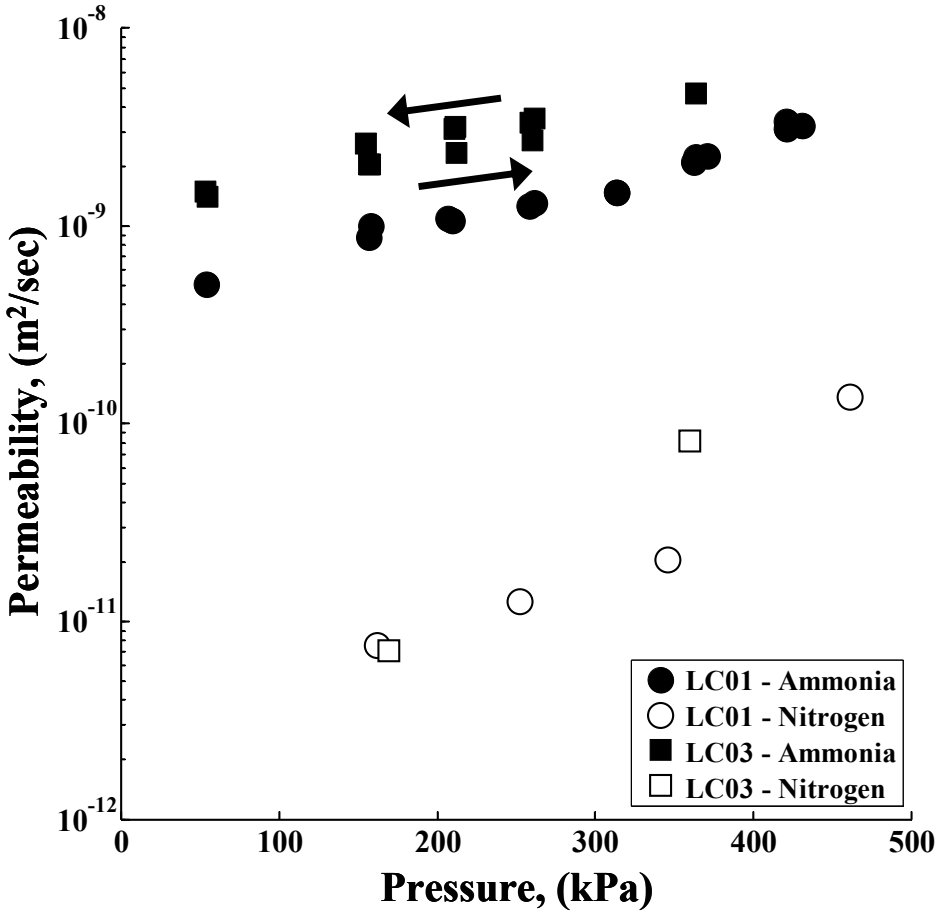

Figure 3.7: Ammonia and Nitrogen Permeability as a Function of Cell Pressure. The ammonia permeability increases with the average cell pressure due to increased ammonia solubility. The increased solubility results in the membrane plasticizing and losing selectivity. This loss of selectivity can be seen by the upturn in nitrogen permeability at a cell pressure of 350 kPa for sample LC03 and 450 kPa for sample LC01.

The plot of permeability vs. pressure for the LC01 and LC03 membranes (Figure 3.7) shows several characteristics are common to both samples. On a semilog scale, the ammonia permeabilities increase linearly over the pressure range explored: 50 kPa to 450 kPa. The LC03 membrane, which has smaller PSS domains than the LC01 membrane but the same PCOE matrix, has a higher ammonia permeability over this range. Also, the LC03 membrane demonstrates a hysteresis, indicated by the arrows, while the LC01

membrane does not. When the average pressure is increased from 50 kPa to 350 kPa, the measured ammonia permeabilties are those indicated by the lower path. The ammonia permeability measured with a decreasing average pressure are those following the higher path. If the cell is then flushed with nitrogen for one hour prior to repeating the experiments with an increasing average ammonia pressure, the data once again follow the lower path, indicating that the phenomenon is reversible.

The nitrogen permeability data for the two membranes also demonstrate similar trends. The nitrogen permeability of sample LC01 increases linearly from 150 kPa to 350 kPa. The mixed gas permeability for nitrogen in this range remains close to the pure gas measurement of 9.2×10^{-12} m^2/sec. Thus the membrane remains selective. However, at 450 kPa, the nitrogen mixed gas permeability increases nearly 100 times, resulting in a large decrease in selectivity. Sample LC03 loses selectivity at a lower pressure, at 350 kPa vs. 450 kPa (gauge). This suggests that in order to prevent membrane conditioning, larger pores are preferred.

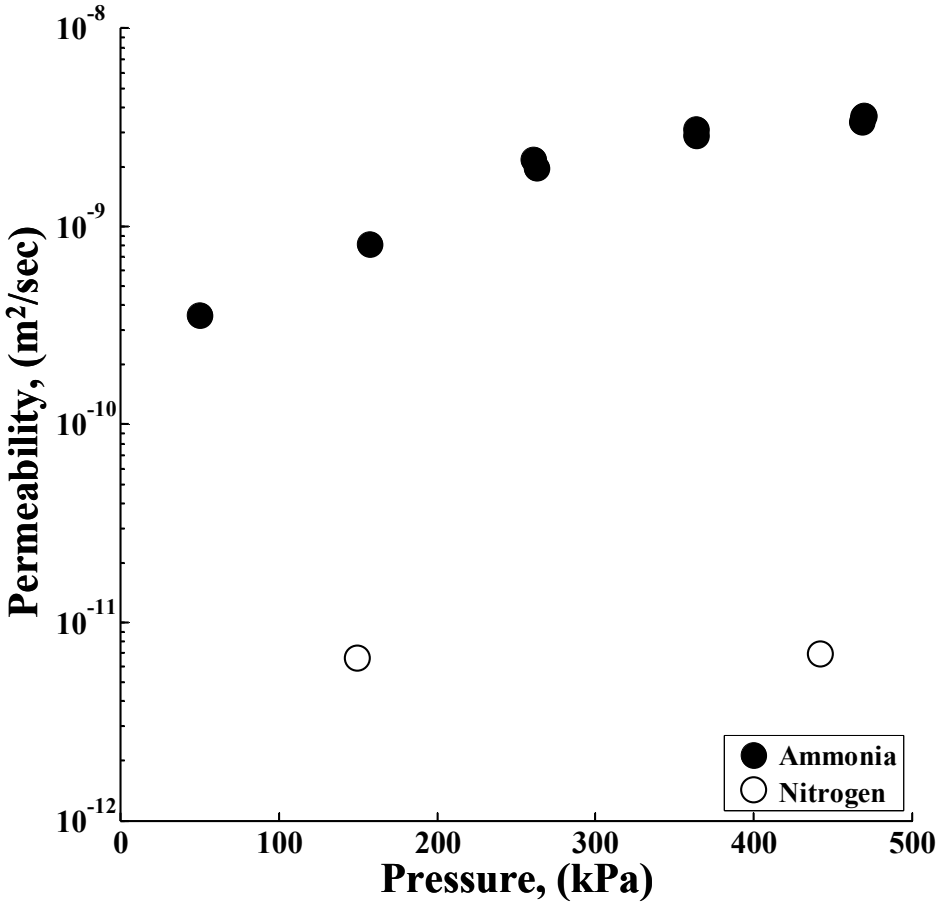

Figure 3.8: Increasing the degree of crosslinking results in the membrane retaining selectivity at higher pressures. Sample LC05 was made using dicyclopentadiene as the reactive monomer. Using a difunctional molecule results in a higher number of crosslinks in the hydrophobic phase.

The third block copolymer membrane LC05 has 11 nm PSS domains similar to sample LC03, but has a more rigid PDCPD/PCOE matrix instead of a pure PCOE matrix. As shown in Figure 3.8, the selectivity is retained over a wider range. From a mean pressure of 50 kPa to 450 kPa (gauge), the ammonia permeability increases, although not linearly as samples LC01 and LC03, while the mixed gas nitrogen permeability remains constant. Therefore the membrane remains over 100 times more selective for ammonia up to an NH_3 pressure of 450 kPa (gauge), the limit of our

experimental apparatus. We expect that with still higher average pressures, we will again see reduced selectivity. These characteristics and others are explored in more detail below.

3.3 Discussion of Ammonia Selective Membranes

3.3.1 Membranes for the Haber Process

The experiments investigating ammonia, hydrogen and nitrogen diffusion across membranes made of alumina, Nafion and PCOE-PSS block copolymer membranes raise two questions. First, do the block copolymer membranes studied have practical value in separating the Haber process reactor effluent? Second, why can some block copolymer membranes retain their selectivity at high ammonia feed pressures while the Nafion membranes cannot?

A membrane separation could enhance the current ammonia synthesis process in two configurations. One configuration would add the membrane directly onto the Haber process reactor. The membrane would continuously remove the ammonia driving the reaction to higher conversion. This would eliminate the steps required to process the effluent gas. However, for this configuration to be viable, the membrane must withstand the high temperature and pressure used in the Haber process. While several techniques exist to mechanically reinforce the block copolymer membrane so that it might stand the pressure,[23, 24] the operating high temperatures needed are likely a limiting factor for this system.[14, 25]

An alternative configuration for the Haber process would cool the effluent gases

and then feed them to a membrane module. This module separates the cooled gases for recycle. Because these gases are still at high pressure and because the ammonia selectively permeates the membrane, the nitrogen and hydrogen in the retentate would not need to be re-compressed before being recycled. Operating at these high pressures also requires supporting the selective layer mechanically on some sort of microporous membrane.[23, 24] This seems feasible with our current membranes.

To develop this configuration further, we must choose a microporous membrane support. Selecting the proper support requires balancing several parameters. The material selected needs to be mechanically robust, which is easiest if the material has small pores.[23] The support should not significantly contribute to the overall mass transfer resistance, which suggests a high concentration of large pores. In balancing these considerations, we seek mechanically robust membranes with pores sizes around 40 nm. Ideally, the support layer should be manufactured as a hollow fiber membrane because of the large surface area per volume provided by the fibers.[23]

Typical dimensions of hollow fiber membranes taken from literature and combined with our gas diffusion data provide an estimate of how thin we should aim to make our selective copolymer layer.[26, 27] We anticipate designing the resistance to mass transfer of our selective layer to be ten times more than that of the support layer, so we will not need to be concerned with the mass transfer through the support layer. When typical values for void fraction, tortuosity, pore diffusion coefficient and membrane thickness given in Table 3.5 are combined with the ammonia permeability of the LC01 copolymer membrane, we conclude that coating a selective layer thinner than 500 nm

will not greatly improve the composite membrane's performance. Such a coating is within existing technology.

Table 3.5. Summary of Support Membrane Properties.

Support Membrane Property	**Representative Value[26, 27]**
Ammonia Diffusion Coefficient (cm^2/sec)	0.04
Void Fraction	0.3
Membrane Thickness (μm)	200
Tortuosity	2

We can now estimate the membrane surface area required for a given production rate of ammonia. As a basis, we assume a plant which produces a modest one ton of ammonia per day. If the pressure drop across the membrane is 10 atm, the selective layer thickness of the membrane is 500 nm and the ammonia permeability is $5x10^{-6}$ cm^2/sec, the membrane area required is 0.17 m^2. This estimate is based on an idealized case; the operation of an industrial unit would require more area. Phenomena such as feed stream channeling and concentration polarization will increase the membrane area needed and must be accounted for in the design. Concentration polarization, a particular concern for membranes that are this permeable, would reduce the ammonia flux and selectivity.[23] Even knowing our estimate is optimistic, we conclude that these membranes have promise for the Haber process.

3.3.2 How Does Ammonia Pressure Affect Block Polymer Membrane Performance

The second question about these ammonia selective membranes is why the permeability and selectivity vary as a function of ammonia pressure. To begin, we recall

that the permeability of a solute is the product of its diffusion and solubility coefficients. Because the diffusion coefficient within the membrane is not a strong function of the pressure in the gas phase, the solubility probably causes the increase in permeability which we observed. The solubility coefficient between the gas phase ammonia and the dissolved ammonia phase reflects the equality of chemical potential in the gas phase just outside of the membrane surface and dissolved in the polymer just inside the membrane surface. Because at the low pressures used here the fugacity coefficient is one, the chemical potential in the gas phase $\mu_{1,\text{gas}}$ is

$$\mu_{1,\text{gas}} = \mu_1^+(T, p) + RT \ln\left(\frac{p_1}{p_1^{\text{vap}}}\right) \tag{3.3}$$

where $\mu_1^+(T, p)$ is the chemical potential at a reference temperature T and total pressure p, p_1^{vap} is the vapor pressure of ammonia at the experimental temperature, and p_1 is the average pressure of ammonia in the cell. The chemical potential of ammonia in the membrane $\mu_{1,\text{dis}}$ is given by

$$\mu_{1,\text{dis}} = \mu_1^\circ(T, p) + \Delta\mu_{1,\text{mix}} + \Delta\mu_{1,\text{inter}} + \Delta\mu_{1,\text{elas}} \tag{3.4}$$

$\mu_1^\circ(T, p)$ is the potential at a standard temperature and pressure, $\Delta\mu_{1,\text{mix}}$ is the change in potential due to mixing, $\Delta\mu_{1,\text{inter}}$ is the energy change due to ammonia shielding the unfavorable enthalpic interactions at the PSS-PCOE (or PDCPD/PCOE) interface, and $\Delta\mu_{1,\text{elas}}$ is the change arising from the increased pressure inside the membrane. The $\Delta\mu_{1,\text{mix}}$ term and the $\Delta\mu_{1,\text{inter}}$ terms, which favor the sorption of more ammonia into the

membrane, are resisted by the $\Delta\mu_{1,elas}$ term. Understanding how these terms depend upon the membrane properties of sulfonated domain size and degree of crosslinking suggests a way in which our experimental results can be understood.

The term $\Delta\mu_{1,inter}$, which accounts for the unfavorable enthalpic interactions between the PSS and PCOE blocks, can be used to rationalize the observed differences between samples LC01 and LC03. One way to mediate the unfavorable interactions between the two blocks is by absorbing ammonia at the PSS/PCOE interface to shield the polymer units from each other.[28] The amount of ammonia absorbed will depend upon the number of contacts between the PSS and PCOE. This number is proportional to the internal surface area of the membrane, which will scale as d^{-1} where the characteristic dimension d of the membrane microstructure is taken the diameter of the PSS domains. Because samples with smaller PSS domains at fixed PSS volume fraction will have larger internal surface areas, more ammonia will dissolve in membranes with these smaller pores. Thus, the LC03 membrane will absorb more ammonia at the same pressure than the LC01 membrane. This higher partition coefficient results in a higher permeability and explains why the LC03 membrane loses selectivity at lower pressures.

Others have discussed similar effects as "membrane conditioning" though not for the block polymer case explored here.[10, 11, 29, 30] For example, Visser and Wessling have shown that the non-Fickian diffusion,[11] which characteristically sets in when a membrane begins to lose selectivity, occurs at a single value of volume dilation. This value of volume dilation is proportional to the product of solvent concentration ϕ_1 and solvent

partial molar volume $\overline{V}_1$. Above this critical value of volume dilation, non-Fickian diffusion occurs and the membrane conditions. Because we are concerned here only with ammonia so $\overline{V}_1$ is constant across all membrane samples, ϕ_1 dictates when non-Fickian diffusion occurs. Because ϕ_1 is higher for small pores in sample LC03, the critical value of volume dilation is reached sooner and the membrane "conditions" at a lower pressure.

The $\Delta\mu_{1,\text{elas}}$ term explains why the higher degree of crosslinking in the LC05 sample results in selectivity being retained to higher pressures than both the LC01 and LC03 sample. The elastic stretching term arises because space must be made for the ammonia molecules which are being drawn into the membrane. To create this space, the polymer chains which make up the membrane are stretched, decreasing their entropy and exerting an additional pressure on the ammonia molecules inside the membrane.[31, 32]

Several theoretical models for the change in chemical potential resulting from the entropic stretching of a polymer chain exist.[32-34] Though these models range in complexity, all follow the general form

$$\Delta\mu_{1,\text{elas}} = G \times f\left(\phi_P\right) \tag{3.5}$$

where G is the shear modulus of the material and $f(\phi_P)$ is a function of the polymer volume fraction. While the magnitude of $f(\phi_P)$ will vary with the theoretical model used, it will always be positive. The shear modulus of an amorphous non-glassy polymer network can be expressed in terms of the number of elastically effective strands ν_e per volume V

$$G = k_B T \frac{\nu_e}{V} \tag{3.6}$$

where k_B is Boltzmann's constant and T is the temperature of the sample.[31] Thus by increasing the degree of crosslinking in a material, the number of effective strands is increased, resulting in a higher shear modulus. The increase in chemical potential for a given polymer volume fraction that results will be greater for a sample with a higher shear modulus. In our case, the more highly crosslinked sample LC05 will have a lower concentration of dissolved ammonia and hence be able to retain selectivity at higher pressures.

In conclusion, we have shown that both Nafion and block copolymer templated membranes are much more permeable to pure ammonia than to pure nitrogen and pure hydrogen. The Nafion membranes lose selectivity in mixed gas systems, but our block copolymer membranes retain selectivity. Further, we have showed that by tailoring the sulfonated block pore size and the degree of crosslinking, the membrane permeability and resistance to conditioning can be further improved. These block copolymer membranes are attractive in some applications for ammonia synthesis. The results in the chapter begin to address the more general issue of designing membranes which retain their selectivity with high pressure, mixed gas feeds.

3.4 References

(1) Bhown, A.; Cussler, E. L. *J. Am. Chem. Soc.* **1991,** *113*, 742-749.

(2) Pez, G. P.; Carlin, R. T.; Laciak, D. V.; Sorensen, J. C. United States Patent 4761164, 1988.

(3) Pez, G. P.; Laciak, D. V. Patent Application Country: Application: US; Patent Country: US Patent 4762535, 1988.

(4) He, Y.; Cussler, E. L. *J. Membr. Sci.* **1992**, *68*, 43-52.

(5) Sakai, T.; Takenaka, H.; Torikai, E. *J. Electrochem. Soc.* **1986**, *133*, 88-92.

(6) Sakai, T.; Takenaka, H.; Wakabayashi, N.; Kawami, Y.; Torikai, E. *J. Electrochem. Soc.* **1985**, *132*, 1328-1332.

(7) Timashev, S. F.; Vorobiev, A. V.; Kirichenko, V. I.; Popkov, Y. M.; Volkov, V. I.; Shifrina, R. R.; Lyapunov, A. Y.; Bondarenko, A. G.; Bobrova, L. P. *Journal of Membrane Science* **1991**, *59*, 117-131.

(8) Bikson, B.; Nelson, J. K.; Perrin, J. E. Patent Application Country: Application: US; Patent Country: US Patent 5009678, 1991.

(9) Baker, R. W.; Lokhandwala, K. *Ind Eng Chem Res* **2008**, *47*, 2109-2121.

(10) Visser, T.; Masetto, N.; Wessling, M. *J. Membr. Sci.* **2007**, *306*, 16-28.

(11) Visser, T.; Wessling, M. *Macromolecules* **2007**, *40*, 4992-5000.

(12) Bates, F. S. *Science (Washington, D.C., 1883-)* **1991**, *251*, 898-905.

(13) Bates, F. S.; Fredrickson, G. H. *Annu. Rev. Phys. Chem.* **1990**, *41*, 525-557.

(14) Chen, L.; Phillip, W. A.; Cussler, E. L.; Hillmyer, M. A. *J. Am. Chem. Soc.* **2007**, *129*, 13786-13787.

(15) Mauritz, K. A.; Moore, R. B. *Chem.Rev.(Washington, DC, U.S.)* **2004**, *104*, 4535-4585.

(16) Cussler, E. L. In *Diffusion, mass transfer in fluid systems;* Cambridge University Press: New York, 2009; , pp 654.

(17) Freeman, B. D. *Macromolecules* **1999**, *32*, 375-380.

(18) Phillip, W. A.; Amendt, M.; O'Neill, B.; Chen, L.; Hillmyer, M. A.; Cussler, E. L. *ACS Applied Materials & Interfaces* **2009**, *1*, 472-480.

(19) Huizenga, D. G.; Smith, D. M. *AICHE J.* **1986**, *32*, 1-6.

(20) Dullien, F. A. L. In *Porous media : fluid transport and pore structure;* Academic Press: San Diego, 1992; , pp 574.

(21) AnonymousPatent Country: GB; Priority Application Country: US Patent 1034197, 1966.

(22) Bird, R. B.; Stewart, W. E.; Lightfoot, E. N. In *Transport phenomena;* J. Wiley: New York, 2002; , pp 895.

(23) Baker, R. W. In *Membrane technology and applications;* J. Wiley: Chichester ; New York, 2004; , pp 538.

(24) Ho, W. S. W.; Sirkar, K. K. In *Membrane handbook;* Kluwer Academic Pub.: Boston, 2001; , pp 954.

(25) Park, K. R.; Kang, P. H.; Nho, Y. C. *React Funct Polym* **2005**, *65*, 47-56.

(26) Kim, J.; Hwang, J. R.; Kim, U. Y.; Kim, S. S. *J. Membr. Sci.* **1995**, *108*, 25-36.

(27) Koonaphapdeelert, S.; Li, K. *J. Membr. Sci.* **2007**, *291*, 70-76.

(28) Naughton, J. R.; Matsen, M. W. *Macromolecules* **2002**, *35*, 5688-5696.

(29) Lin, H.; Freeman, B. D. *Journal of Molecular Structure* **2005**, *739*, 57-74.

(30) Staudt-Bickel, C.; Koros, W. J. *J. Membr. Sci.* **1999**, *155*, 145-154.

(31) Hiemenz, P. C., Lodge, T. In *Polymer chemistry;* CRC Press: Boca Raton, FL, 2007; pp 608.

(32) Flory, P. J. In *Principles of polymer chemistry;* Cornell University Press: Ithaca, 1953; .

(33) Gusler, G. M.; Cohen, Y. *Ind Eng Chem Res* **1994**, *33*, 2345-2357.

(34) Freger, V. *Polymer* **2002**, *43*, 71-76.

Chapter 4: Ultrafiltration Membranes Templated By Self-Assembled Bicontinuous Block Polymers

Ultrafiltration is a water purification technique where a high pressure feed stream is forced across a porous membrane filter to give a purified permeate.[1-3] The key to ultrafiltration is the membrane, which should allow a high flux and show a sharp molecular weight cut-off. Current membranes, made by a phase inversion process, allow for high fluxes but are limited by a wide distribution of pore sizes.[4, 5] Ideally the membranes would have one well defined pore dimension.

Our research will produce such a membrane by taking advantage of block polymer self-assembly.[6, 7] We will use polymers which contain a polylactide block that can be selectively etched to create a porous structure.[8-10] The polymer chosen can assemble into either a cylindrical or bicontinuous network morphology since both have domain which span the membrane thickness. Our efforts to make these membranes will be the focus of the next three chapters. Because there are no alignment issues when working with a bicontinuous network, these experiments will be discussed first.

4.1 Transport in Small Pores

Prior to discussing the experimental techniques and results for our nanoporous membranes, we will review several theories for transport in small pores. These theories

help to guide our interpretation and understanding of the experimental results for the membranes discussed in this chapter as well as the membranes reported in Chapters 5 and 6.

4.1.1 Gas Diffusion in Small Pores

The mechanism of gas diffusion in small pores depends on the Knudsen number, i.e., the ratio of the mean-free path to the pore diameter.[11] When the mean-free path is much smaller than the pore size, the Knudsen number is small and diffusion is the result of random collisions between different molecules. In this case, the diffusion coefficient D_{CE} can be estimated from the Chapman-Enskog kinetic theory[11, 12]

$$D_{CE} = \left(\frac{4\sqrt{2}}{3\pi^{3/2}}\right)\frac{\left(k_B T\right)^{3/2}}{p\,\sigma^2\,\tilde{m}^{1/2}\,\Omega} \tag{4.1}$$

where k_B is Boltzman's constant, T is the temperature, p is the pressure, σ is the collision diameter, $\tilde{m}$ is the mass of one molecule, and Ω is a dimensionless function of temperature which is of order one. For small Knudsen number, kinetic theory predicts that the diffusion coefficient varies inversely with pressure but is independent of pore size.

The situation when the mean-free path is much larger than the pore diameter is different. Now, when the Knudsen number is large, diffusion is the result of collisions between the diffusing gas and the walls of the pores.[11] The diffusion coefficient D_{Kn} for this case of "Knudsen diffusion" is now given by

$$D_{Kn} = \frac{2d}{3}\left(\frac{2k_B T}{\pi \tilde{m}}\right)^{1/2} \tag{4.2}$$

where d is the pore diameter. While this prediction is more approximate than Equation (4.1), the important feature is that the diffusion coefficient now does not vary with the pressure but is proportional to the pore diameter.

Using our experiments we want to investigate the selectivity of the membranes for different gases. This selectivity should be proportional to the inverse square root of the molecular weight ratio. If modes of transport other than Knudsen diffusion are occurring, such as bulk diffusion, the selectivity would deviate from this predicted ratio. Though a $\sqrt{1/\tilde{m}}$ term does appear in Equation (4.1), the term that accounts for the Leonard-Jones 6-12 potential Ω, causes the ratio of bulk diffusion coefficients to deviate from an inverse square root dependence.

For a porous solid, the effective diffusion coefficient (i.e., the permeability) across the film in the Knudsen regime is predicted to follow a modified version[13, 14] of Equation (4.2)

$$D_{eff} = \frac{\varepsilon}{\tau}\frac{2d}{3}\left(\frac{2k_B T}{\pi \tilde{m}}\right)^{1/2} \tag{4.3}$$

where ε is the void fraction and τ is the tortuosity. The void fraction accounts for the experimental measurements being based on the total projected area of the membrane, not on the cross sectional area of the pores. The tortuosity accounts both for variations in the size and shape of the pore cross-section and for the additional distance required for a molecule to travel relative to the film thickness.

4.1.2 Liquid Flow in Small Pores

Like the experiments with gases, our measurements of liquid flow center on the calculation of a single transport property, the superficial velocity $\overline{v}$

$$\overline{v} = \frac{\varepsilon}{\tau}\langle v \rangle \tag{4.4}$$

where $\langle v \rangle$ is the Hagen-Poiseuille velocity[11, 12] of fluid in a single pore. The Hagen-Poiseuille relationship, based on the continuum approximation, gives a velocity of

$$\langle v \rangle = \frac{d^2 \Delta p}{32 \mu \ell} \tag{4.5}$$

where d is the characteristic pore dimension, Δp is the pressure drop, μ is the liquid viscosity and ℓ is the membrane thickness. Experiments with track-etched membranes validate the use of this equation to describe liquid flow in nanometer sized cylindrical pores. These experiments show that the viscosity of water confined to pores as small as 3 nm does not deviate significantly from its bulk value of at 25 ˚C.[15]

We want to use the results of our gas diffusion and liquid flow experiments to further investigate the microstructure of the thin films. As shown in Equations (4.3) and (4.5), the effective diffusion coefficient and superficial velocity are functions of ε, τ and d, three parameters related to the pore structure. The void fraction is readily calculated from the known volume fraction of the etchable component. However, the tortuosity and pore diameter are not well defined. The effective diffusion coefficient and superficial velocity depend on the pore diameter differently, namely d vs. d^2, respectively. Therefore we can combine our results in order to separate the variables and obtain estimates for d

and τ. These estimated values can then be compared to values obtained using independent material characterization techniques. In particular, the pore dimension can be inferred from scanning electron microscopy (SEM), from N_2 adsorption/desorption,[13] or from small angle x-ray scattering (SAXS) experiments.[16] In addition, several attempts have been made to calculate tortuosities for known geometries using simulations.[17] We will compare our values with these calculations.

4.1.3 Rejection of Dissolved Solutes

We also want to explore the use of these nanoporous membranes as ultrafilters which reject dissolved solutes. To analyze our rejection data, we will use the model which pictures the dissolved solutes as rigid spheres in a cylindrical pore[18-23] as shown in Figure 4.1. Several assumptions are made regarding the system shown.

1) The characteristic solute and pore sizes are significantly greater than the solvent size, which is treated as a continuum.
2) The solute concentration is dilute, allowing the solute-solute interactions to be neglected.
3) The pore length is much larger than its radius. This allows the velocity profile $V(r)$ to fully develop and the solute molecule velocity U to be considered constant (i.e., the system is at steady-state).

We will use this model to compare experiments and theory.

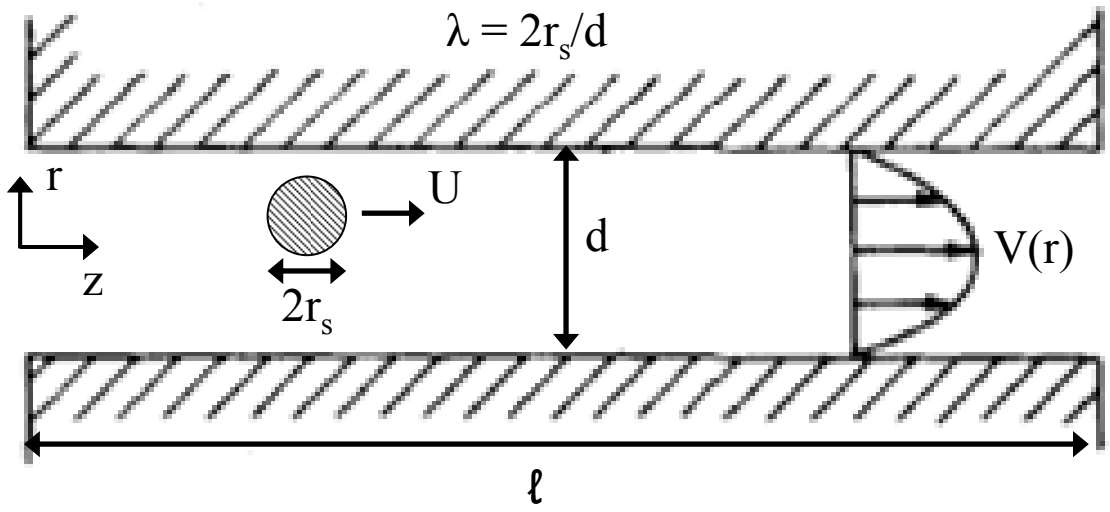

Figure 4.1: A Spherical Solute in a Cylindrical Pore. The solute and pore are nearly the same size resulting in a higher drag on the solute than if it were in an unbounded fluid. The magnitude of this additional drag is expressed as a function of the ratio of the solute size to pore size.

The driving force for diffusion, the chemical potential gradient, can be viewed as a body force acting upon the solute molecule. Because the system is at steady-state, this body force is exactly balanced by the hydrodynamic drag:

$$\underbrace{-k_B T \frac{\partial \ln(c_i)}{\partial z}}_{\substack{\text{Diffusional} \\ \text{Body Force}}} - \underbrace{6\pi\mu r_s K(U - GV)}_{\substack{\text{Hydrodynamic Drag} \\ \text{Force}}} = 0 \tag{4.6}$$

where K, the enhanced drag, and G, the lag coefficient, account for the effects of the finite pore size. In an unbounded fluid, K=G=1, and the drag term is equivalent to Stokes law.

Equation (4.6) can be rearranged by recognizing $Uc_i = N_i$, so

$$N_i = -K^{-1} D_i \frac{\partial c_i}{\partial z} + GVc_i \tag{4.7}$$

where N_i is the solute flux and D_i is the solute diffusion coefficient in an unbounded fluid. The quantities V, G, K and c_i all depend on the radial position within the pore, so it is more useful to express the flux averaged over the pore cross section.

$$\langle N_i \rangle = -K_d D_i \frac{\partial \langle c_i \rangle}{\partial z} + K_c \langle v \rangle \langle c_i \rangle \tag{4.8}$$

where K_d and K_c are the averaged hydrodynamic coefficients, both of which depend on the ratio of the solute radius to pore radius, $\lambda = {2r_s}/{d}$. Although the jump from Equation (4.7) to Equation (4.8) may seem trivial, several subtle assumptions are made to allow for this transition. We continue without detailing these assumptions but refer the reader to articles that cover the topic in more detail.[18-23]

Relating the steady-state flux to the concentrations in the adjacent solutions requires integrating Equation (4.8) subject to boundary conditions at $z = 0$ and $z = \ell$. Because we have assumed ${d}/{\ell} \ll 1$, the solute concentrations just inside the pore mouth and just outside the pore mouth can be considered in equilibrium.

$$\Phi = \frac{\langle c_i \rangle_o}{c_{io}} = \frac{\langle c_i \rangle_\ell}{c_{i\ell}} \tag{4.9}$$

where $c_{i\ell}$ and c_{io} are the solute concentrations at the downstream and upstream outer membrane surfaces and $\langle c_i \rangle_\ell$ and $\langle c_i \rangle_o$ are the concentrations inside the pores at the same locations. For a system where there are no long range interactions between the solute and pore wall, the partition coefficient Φ can be obtained using either geometric[24] or

statistical thermodynamic arguments[22]. We will use the geometric arguments because these are more intuitive. A solute molecule which is approaching a pore will only enter the pore if its projected area will fit within the pore cross sectional area. As Figure 4.2 helps to show, this restriction means the center of a solute molecule cannot sit a distance further than $R - r_s$ from the pore center. This leads to the following expression for the partition coefficient.

$$\Phi = (1 - \lambda)^2 \tag{4.10}$$

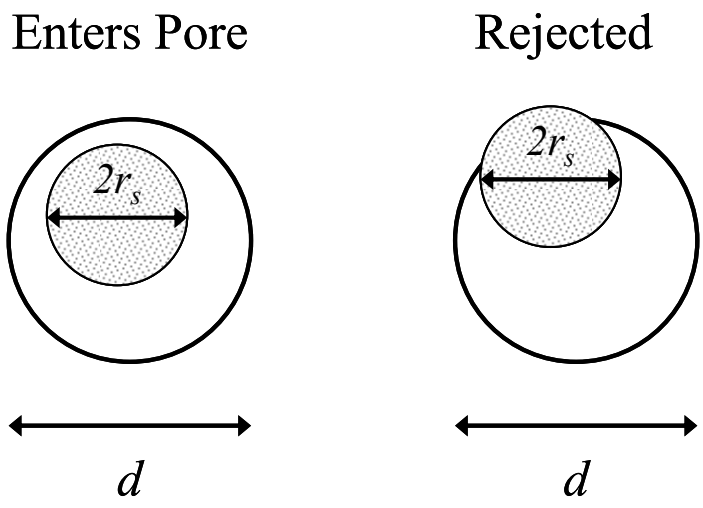

Figure 4.2: Solute Molecules Approaching a Pore Mouth. If a solute molecule hits the membrane surface it will bounce back into the bulk solution.

Integrating Equation (4.8) subject to the given boundary conditions gives an equation for the desired quantity, the macroscopic flux of species *i*:

$$\langle N_i \rangle = \left(\Phi K_c \langle v \rangle\right) \frac{c_{io} \exp\left(\dfrac{\langle v \rangle K_c \ell}{D_i K_d}\right) - c_{i\ell}}{\exp\left(\dfrac{\langle v \rangle K_c \ell}{D_i K_d}\right) - 1} \tag{4.11}$$

The dimensionless quantity in the square brackets is the Peclet number, a measure of the speed of convection relative to the speed of diffusion. Equation (4.11) has interesting forms for extremes of this number. When transport is dominated by diffusion, i.e., $Pe \ll 1$ the solute flux is given by

$$\langle N_i \rangle = \frac{\Phi K_d D_i}{\ell}\left(c_{io} - c_{i\ell}\right) \quad \left(Pe \ll 1\right) \tag{4.12}$$

When convection dominates transport i.e., $Pe \gg 1$, the solute flux is given by.

$$\langle N_i \rangle = \Phi K_c \langle v \rangle c_{io} \quad \left(Pe \gg 1\right) \tag{4.13}$$

Note K_d and K_c are not equal. The evaluation of these coefficients will be discussed shortly.

The common practice is to describe the ability of a membrane to reject a dissolved solute using a sieving coefficient. The sieving coefficient is the ratio of the solute concentration in the downstream to the concentration in the upstream. Defining the downstream solute concentration as $c_{i\ell} = \langle N_i \rangle \big/ \langle v \rangle$ allows the actual membrane sieving coefficient to be expressed as a function of λ and Pe:

$$S_a = \frac{c_{1\ell}}{c_{1o}} = \frac{K_c\left(1-\lambda\right)^2}{1-\left(1-K_c\left(1-\lambda\right)^2\right)e^{-[Pe]}} \tag{4.14}$$

Remember that Pe varies with K_d and K_c.

The use of Equation (4.14) relies on quantifying the additional drag functions K_c and K_d. As written, K_c and K_d are radially averages of the functions G and K, respectively. The math required to average these functions is quite rigorous so it is typically performed for asymptotic solute sizes i.e., $\lambda < 0.1$ or $\lambda > 0.9$.[18, 19, 23] Results for wide ranges of λ are available, but only for cases where the solute sits on the pore centerline, $r = 0$.[20] Evidence that this "centerline approximation" leads to reasonably accurate estimates for K_c and K_d supports its use.[21] Because we are interested in solutes that span the whole range of λ we use a theory developed by Bungay & Brenner for $0 \le \lambda < 1$.[20] The tabulated values for K_c and K_d found using this theory are given below in Equation (4.15) and Table 4.1:

$$K_c = \frac{\Phi(2-\Phi)K_s}{2K_t} \quad K_d = \frac{6\pi\Phi}{K_t}$$
$$\begin{pmatrix} K_t \\ K_s \end{pmatrix} = \frac{9}{4}\pi^2\sqrt{2}(1-\lambda)^{-5/2}\left[1+\sum_{n=1}^{2}\begin{pmatrix} a_n \\ b_n \end{pmatrix}(1-\lambda)^n\right]+\sum_{n=0}^{4}\begin{pmatrix} a_{n+3} \\ b_{n+3} \end{pmatrix}\lambda^n \tag{4.15}$$

Table 4.1. Hydrodynamic Coefficients for Spheres in Cylindrical Pores.[20]

n	a_n	b_n
1	$-\frac{73}{60}$	$\frac{7}{60}$
2	$\frac{77,293}{50,400}$	$-\frac{2,227}{50,400}$
3	-22.5083	4.0180
4	-5.6117	-3.9788
5	-0.3363	-1.9215
6	-1.216	4.392
7	1.647	5.006

4.1.4 Concentration Polarization

The material in the previous subsection lets us predict the actual sieving coefficient, S_a. However, this coefficient is distinct from the observed coefficient, S_o. The actual sieving coefficient is calculated using the solute concentration immediately adjacent to the membrane surface, while the observed sieving coefficient replaces this with the bulk upstream solute concentration.[3, 4] While the bulk concentration is more easily obtained in experiments, it can often be lower than the concentration at the membrane surface due to concentration polarization. During experiments, convective flow carries the feed mixture toward the membrane; at the membrane surface some of the species selectively permeate the membrane while others are rejected. The concentration of the rejected species increases at the membrane surface, resulting in a diffusive flux back into the bulk. If the diffusive back flux relative to the convective flux is large, the feed mixture will be well mixed, and the bulk and wall concentrations of rejected species will be nearly equal. If, however, the diffusive flux is small compared to the convective flux, the bulk and wall concentrations will be different and the concentration is said to be polarized. In order for S_o to accurately reflect S_a and not artifacts of the operating conditions, polarization needs to be minimized.

In ultrafiltration systems, concerns about polarization on the downstream side of the membrane are usually small because the rejected solutes are dilute.[1, 3] Quantifying concentration polarization on the upstream side of the membrane is a more important problem. Several methods have been used to estimate the degree of concentration polarization.[1, 3] We will make our estimates based on the thin film model pictured in

Figure 4.3. Species *i*, with a bulk concentration of c_{ib}, is carried toward the membrane surface at a velocity $\bar{v}$ where it is rejected, resulting in permeate concentration of $c_{i\ell}$ and the wall concentration to c_{io}.

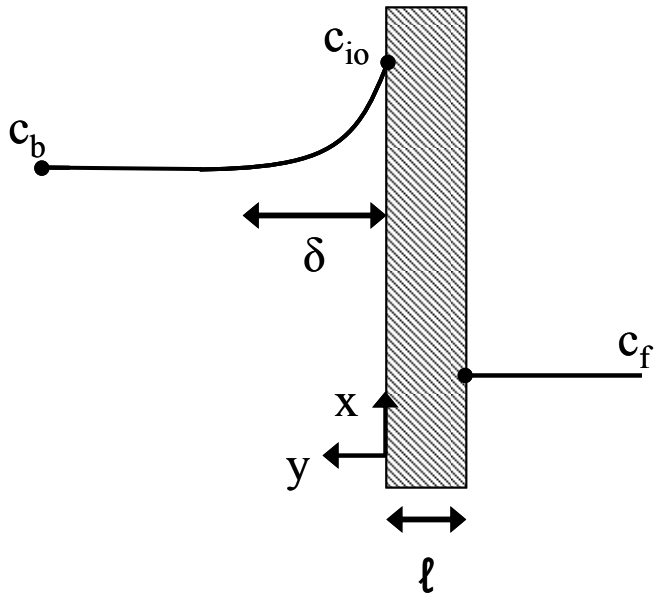

Figure 4.3: Concentration Polarization in a Membrane System. Convective flow carries the rejected solute towards the membrane surface while diffusion causes the solute to return to the bulk feed. When convection dominates diffusion the system cannot remain well mixed and the concentrations in the bulk and at the membrane surface differ.

For a system operating at steady-state a mass balance on species *i* shows that the flux of *i* does not change with position in the y-direction. The flux on the upstream side can be written as the sum of the convective and diffusive contributions while on the downstream side only the convective portion contributes. Furthermore, these two expressions can be equated because they are different ways of representing the same flux.

$$\underbrace{D_i \frac{dc_i}{dy} - \overline{v} c_i}_{\text{Upstream}} = \underbrace{N_i}_{\substack{\text{Flux of} \\ \text{Species } i}} = \underbrace{\overline{v} c_{i\ell}}_{\text{Downstream}} \tag{4.16}$$

Rearranging and then integrating this expression from the membrane wall to δ yields:

$$\overline{v} = \frac{D_i}{\delta} \ln\left(\frac{c_{io} - c_{i\ell}}{c_{ib} - c_{i\ell}} \right) \tag{4.17}$$

Because experimentally determining δ is complex, we avoid this difficulty by recognizing D_i/δ as the mass transfer coefficient k without polarization, and evaluating k using correlations developed for specific geometries. For the stirred cell used in our experiments, we use the correlation developed by Zeman and Zydney:[3]

$$\frac{kb}{D_i} = 0.23 \left(\frac{\omega b^2}{\nu} \right)^{0.567} \left(\frac{\nu}{D_i} \right)^{0.333} \tag{4.18}$$

where b is the radius of the stirred cell, ω is the angular velocity of the stir bar, and v is the kinematic viscosity of the feed solution. Equations (4.17), (4.18) and the definitions of S_o and S_a can be combined to give:

$$S_a = \frac{S_o}{(1 - S_o) \exp\left(\overline{v}/k \right) + S_o} \tag{4.19}$$

Note that as the quantity $\overline{v}/k$, which represents the ratio of convection to diffusion, becomes small, $S_a = S_o$. We aim to run experiments where $\overline{v}/k$ is small, but recognize that such experiments may not always be possible.

4.2 Membrane Fabrication and Preparation

Thin films of nanoporous polymer were produced by Mark Amendt using the method reported by Chen *et al.*[25] Three samples of polynorbornenylethylstyrene-b-polylactide (P(N-s-S)-b-PLA), the doubly reactive block polymer that templates the nanopores, are used in this work. All samples have a P(N-s-S) block with a number average molecular weight (M_n) of 27 kg mol^{-1}. In order to observe the effect on pore size, the molecular weight of the etchable PLA block is varied between the samples. The general membrane preparation procedure is as follows. A (P(N-s-S)-b-PLA) sample is combined with dicyclopentadiene (DCPD) and the second generation Grubbs metathesis catalyst[26] in the solvent tetrahydrofuran (THF), mixed for about 10 seconds, cast onto a glass plate, and allowed to react and dry at room temperature for 6 h. The specific recipes for each membrane sample are given in Table 4.2.

Table 4.2. Membrane solutions for each sample.[a]

Sample Name	PLA M_n (kg mol^{-1})	P(N-s-S)-b-PLA (mg)	DCPD (mg)	THF (mL)	Catalyst (mg)	f(PLA)
A	32	400	104	2.1	2.9	0.43
B	42	402	109	1.6	2.1	0.47
C	65	402	200	2.0	3.3	0.47

[a] The M_n of the P(N-s-S) block in each of the examples is 27 kg mol^{-1}.

After casting the optically transparent films (ca. 100 cm^2 and 100 μm thick) are then cured at 100 °C for 1 h. After curing, the films are removed from the glass plate and exposed to 0.5 M NaOH solution (in 60/40 (*v/v*) methanol/water) at 70 °C to etch the

PLA. After PLA removal, the films are generally treated by an oxygen-reactive ion etch to remove a submicron, nonporous PDCPD "skin" that formed at the surface of the films.

The resulting films, nanoporous composite polyDCPD membrane, can be used for gas diffusion, liquid convection and ultrafiltration experiments. Typical SEM images of the film's surface (left) and fractured cross section (right) showing the nanoporosity are given in Figure 4.4. The distribution in pore sizes visible in the image of the film's surface is due to the bicontinuous nature of the material. If we cut across a pore at an angle other than perpendicular then the pore will appear to be larger than it actually is. The SEM image of the fracture cross section demonstrates that the pore structure is homogeneous along the length of the membrane.

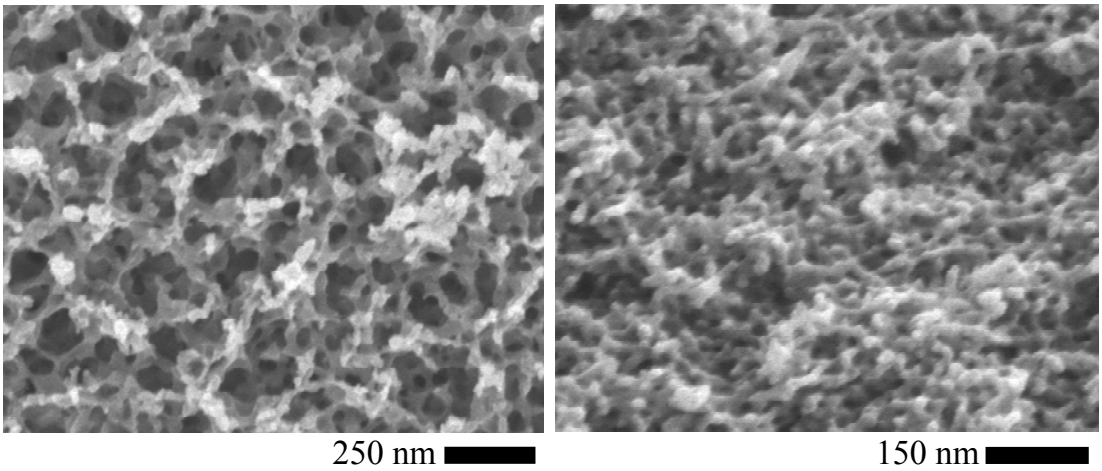

Figure 4.4: SEM Image of a Typical Nanoporous Membrane Used in This Study. The percolating pore structure was templated using a PLA-b-P(N-s-S) polymer. The P(N-s-S) crosslinked the DCPD matrix and the PLA was etched with a NaOH solution to create the pores.

Thin films approximately 7 mm x 7 mm were cut from the larger samples for mounting into the gas diffusion cell. The section was fixed over a 0.3 cm diameter hole in

a stainless steel disc, giving an active area of 0.071 cm^2. The section of thin film was held in place using epoxy (DP-460 Off White, 3M, St. Paul, MN) applied using a spatula and allowed to cure overnight at room temperature. The sample was then mounted in the diffusion cell. Circular samples 2.5 cm in diameter for liquid convection and ultrafiltration experiments were cut using shears from the larger cast sheet.

This research included three different groups of experiments: gas diffusion, liquid convection, and ultrafiltration. The gas diffusion and liquid convection experiments elucidate transport properties of the self-assembled, etched membrane pores, while the ultrafiltration studies begin to explore whether these structures have practical applications. Descriptions of the three different experimental procedures can be found in Chapter 2. The following paragraphs provide a discussion of the three groups of results.

4.3 Results

4.3.1 Gas Diffusion Results

These studies measure the pressure difference across the membrane as a function of time for thin films made from polymer sample B. The results, shown in Figure 4.5, vary as predicted by Equation (2.7). The slope of the curves is used to calculate the effective diffusion coefficient for each gas. These effective diffusion coefficients, which are reported in Table 4.3, are reproducible, varying less than ±3 percent for duplicate experiments with the same membrane or for repeated experiments with different membranes.

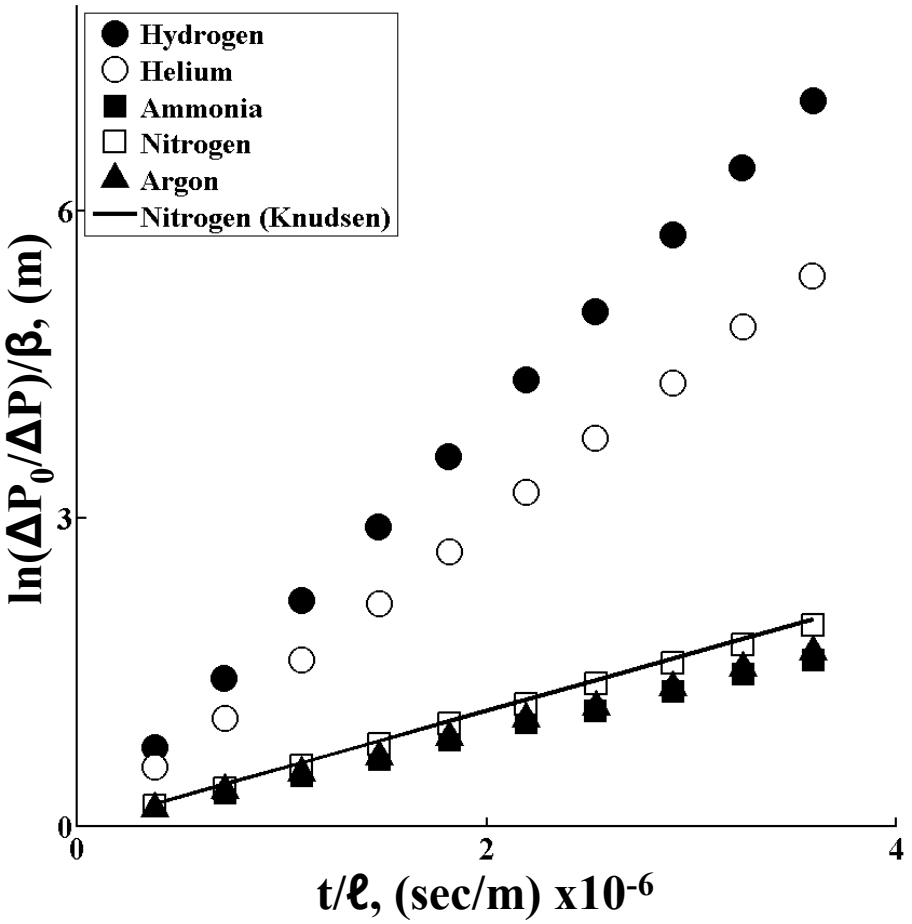

Figure 4.5: Gases Diffuse Across the Membrane by a Knudsen Mechanism. The slope of the experimental data is proportional to the gas permeability. Knudsen theory, shown for N_2 as a solid line, predicts a $\sqrt{1/\tilde{m}}$ dependence.

Table 4.3. Summary of gas diffusion data.[a]

Solute	D_{eff}	D_{eff}/ε[b]	D_{Kn}/τ[c]	$D_{C\text{-}E}$	α_{exp}[d]	α_{Kn}[d]	$\alpha_{C\text{-}E}$[d]
H_2	0.0184	0.0391	0.0464	0.9474	0.84	0.71	1.18
He	0.0154	0.0328	0.0328	1.1184	1.00	1.00	1.00
NH_3	0.0043	0.0091	0.0159	0.1299	3.58	2.06	8.61
N_2	0.0055	0.0117	0.0124	0.1350	2.80	2.66	8.28
Ar	0.0047	0.0100	0.0104	0.1219	3.27	3.15	9.17

[a] All diffusion coefficients are reported with units of cm^2/sec

[b] Assuming $\varepsilon = 0.47$

[c] Assuming d = 14.2 nm and $\tau = 1.81$

[d] All selectivities are defined as $\alpha_i \equiv D_{He}/D_i$

The experimental diffusion coefficients can be compared with coefficients calculated using the Knudsen and Chapman-Enskog theories. Except for ammonia, the experimentally measured coefficients are within 10 percent of those calculated using Equation (4.3). The use of Equation (4.3) relies on the assumption of a pore diameter and tortuosity. Here, we assumed d = 14.2 nm and $\tau = 1.81$. These choices are explained below. Table 4.3 also presents the selectivities for the gases relative to helium diffusion. Helium is chosen as the reference gas because it is not expected to interact with the solid membrane.[27] The experimental selectivities for all gases except ammonia are within an average of 10 percent of those predicted, demonstrating they have a molecular weight dependence consistent with Knudsen diffusion, i.e. $\sqrt{1/\tilde{m}}$. These results show conclusively that transport through the pores occurs by a Knudsen mechanism, which is expected because the mean-free paths of these gases are about ten times larger than the pore diameter.[11] The results also indicate that the membranes have nanoscopic pores

which span the entire membrane thickness, as transport through macroscopic defects would occurs by mechanisms other than Knudsen diffusion.

The somewhat lower values observed for Knudsen diffusion of ammonia are probably a result of an interaction of ammonia with groups on the pore walls left after etching. These interactions are not strong enough to cause ammonia to adsorb onto the pore wall and in turn to reduce the effective pore diameter. Experimental evidence for this can be found in the helium diffusion coefficient measured in the presence of an ammonia atmosphere. In the Knudsen regime, diffusing molecules do not collide with each other, so there is no interaction between the ammonia and helium molecules that would affect the measured helium coefficient. However, if ammonia did adsorb onto the pore wall, the effective pore diameter would be decreased, causing a decrease in the measured helium coefficient. Measurements of helium transport in the presence of ammonia do not show such a decline in the helium diffusion coefficient (i.e., the mixed gas and single gas values are the same), implying that ammonia is not adsorbing onto the pore walls. The interactions between ammonia and groups on the pore wall calls into question a key assumption of our simple Knudsen model of diffusion, that the collisions between the diffusing solute and pore wall are elastic; more accurate theories of Knudsen diffusion include such features as a sticking coefficient to correct for nonelastic collisions.

4.3.2 Liquid Flow Results

Next, we turn from the diffusive flux of dilute gases to the convective flux of liquids. The convective flux of water in m^3 per m^2 sec, is plotted in Figure 4.6 *vs* the pressure drop, in kPa. The linear relation expected from Equation (4.5) is observed. The fluxes are small, around 1×10^{-6} m^3/m^2 sec (4 gal/ft^2 day) at a pressure drop of 30 kPa. However, if the membrane thicknesses were decreased from 100 μm to 0.5 μm and the pressure drop was increased to 200 kPa, the flux is predicted to be 2.8×10^{-3} m^3/m^2 sec (5,600 gal/ft^2 day). If this larger flux could be achieved it would be competitive with typical fluxes observed through membranes made by phase inversion. These fluxes are found to range from 3.0×10^{-5} to 4.0×10^{-4} m^3/m^2 sec. These experiments do not show these high fluxes, though they do suggest the potential of these membranes.

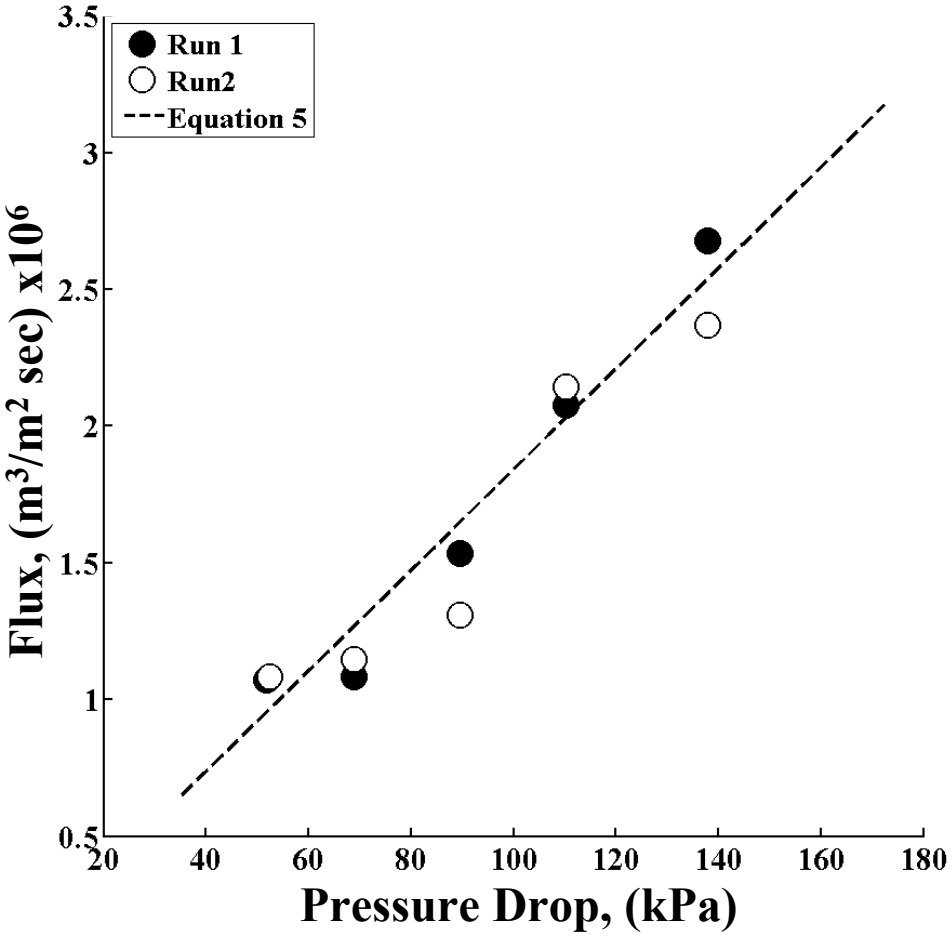

Figure 4.6: Water Flux is Proportional to Pressure Drop. Experimentally observed fluxes for polymer sample B are compared to Equation 5.

The convective flux observed is independent of ionic strength over a range of 10^{-3} to 10^{-1} mol/L of NaCl at a pH of 5.5. However, the convective flux is a function of pH as shown by the data in Figure 4.7. Because the membranes are stored in water exposed to room air, their initial pH is 5.5; it is raised or lowered by adding sodium hydroxide or hydrochloric acid. The 60 percent decrease in flux as the pH changes from 2 to 12 suggests an effective 3 nm decrease in pore size. This can be rationalized as a chemical

reaction producing hydrophilic groups within the pore, which then extend further into the center of the pore, reducing its effective diameter. We have no independent experimental support for this hypothesis, which does not explain the near-linear variation with pH observed.

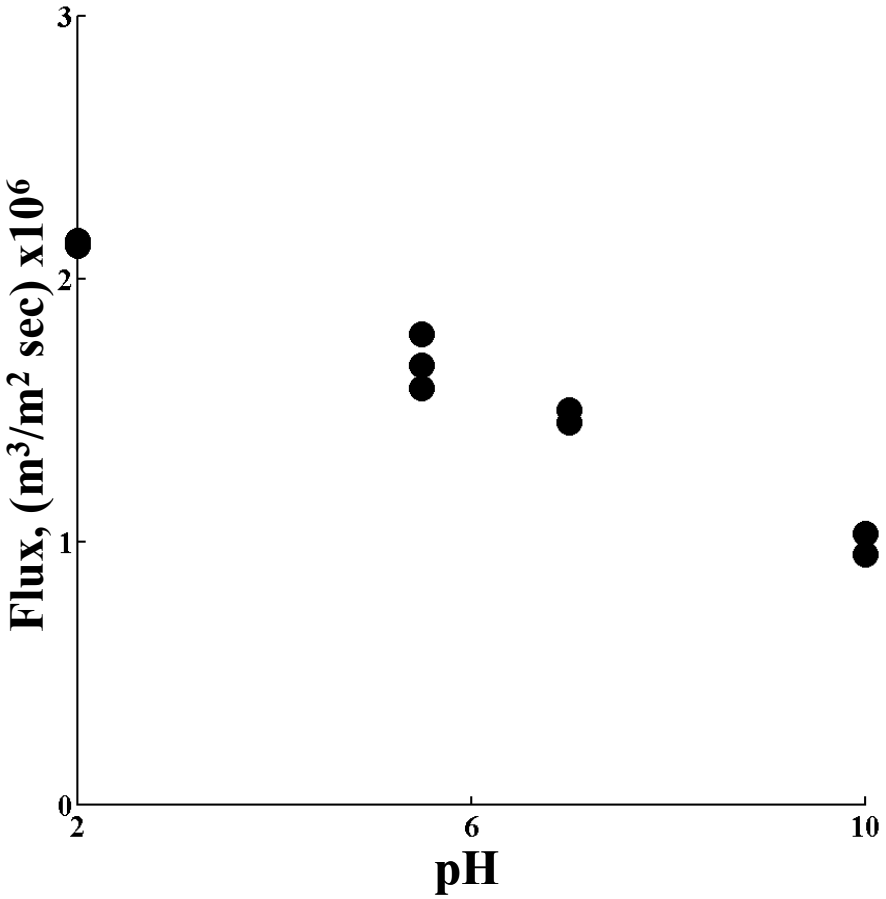

Figure 4.7: Water Flux as a Function of pH. The flux is shown to be a function of pH at $I = 10^{-3}$ M. The reason for the decrease in flux with increasing pH is not known but may be due to acid groups left in the pore after etching.

A hysteresis is observed when the pH of the permeating solution is changed. Each datum in Figure 4.7 represents the steady-state flow rates at a particular pH. After changing the pH of the permeating solution, there is a period of time over which the steady state value is slowly approached. The observed effect occurrs for both increases and decreases in pH, with the sign of variation depending on the direction of the pH change. For example, after an experiment at pH = 2, flow rates measured at pH = 5.5 would be higher for about 2 hours. Over that time, the flow rate slowly decays to a steady value. After an experiment at pH = 10, the flow rates measured at pH = 5.5 would be lower. This effect is completely reversible: given enough time, flow rates return to their original steady state value.

The predictions of Knudsen diffusion and liquid convection do rest on the assumption of a pore diameter and membrane tortuosity. The pore diameter and tortuosity were inferred from experiments by using the measured diffusion coefficient for helium, the hydraulic permeability of water at pH = 5.5, and Equations (4.3)─(4.5). This method gave d = 14.2 nm and τ = 1.81. These values are compared with other measurements of the pore diameter and tortuosity in Table 4.4. In Reference 25 we estimated a tortuosity of 2.29 for a similar membrane using only gas diffusion experiments. Here we have assumed the tortuosity for gas diffusion and liquid flows is the same and by doing so are able to use the complementary techniques to estimate a tortuosity of 1.81. We are more confident in this value given its agreement with supportive computational work.[17]

Table 4.4. Comparison of pore diameter and membrane tortuosity.

Characterization Technique	d (nm)	τ
Gas Diffusion/Liquid Flow	14.2	1.81
BET[a]	15.1	--
SAXS C[b] SAXS L	22.3 11.6	-- --
BJH[c]	16.0-23.0	--
SEM	20.0	--
Theory[d]	--	1.56

[a] The method used to calculate pore diameter is described in Reference 13.
[b] The domain spacing was calculated according to Reference 16. SAXS C and SAXS L refer to assuming a cylindrical or lamellar morphology, respectively.
[c] The Barret-Hallendar-Joyner method is described in Reference 29.
[d]The tortuosity was taken from simulations in Reference 17.

The size from diffusion and flow is consistent with values from BET and SAXS, with a level of agreement comparable to that observed earlier for cylindrical pores.[28] The values inferred from diffusion and flow are expected to be somewhat less than those measured by other methods because diffusion and flow implicitly reflect the resistances of pore diameters in series, and thus imply a harmonic average of pore diameters. The average size should be smaller than those from methods which average pore sizes differently, as the BJH (Barrett-Joyner-Halenda) analysis does.[29] However, the detailed relation between these values is not known because the exact pore geometry is not known.

4.3.3 Ultrafiltration Results

Finally, we consider the flow of solutions containing macromolecular species across these membranes. Because the dissolved solutes' sizes are on the same order of

magnitude as the membrane pore size, the solutes should be at least partially retained. The membrane's ability to perform such a separation is described by the sieving coefficient S_a, defined as the concentration in the permeate $c_{1\ell}$ divided by that at the upstream membrane surface c_{10} (Equation (4.14)). In practical studies, the concentration at the membrane surface is replaced by the bulk upstream concentration, c_F. The bulk value is often lower than c_{10} due to concentration polarization, where the ultrafiltration itself causes higher solute concentrations at the upstream membrane surface than in the bulk solution. This higher surface concentration in turn reduces the flux.[1, 3]

This effect is illustrated by the ultrafiltration of a 2 percent solution of a 35 kDa PEO, shown as circles in Figure 4.8. The flux drops off as the pressure drop increases. This drop is absent in the ultrafiltration of pure water, shown as triangles; it is also absent when the upstream solution is rapidly stirred, shown by squares. By always making ultrafiltration experiments with rapid stirring, we avoid this complexity and measure the sieving coefficients of the membrane directly.

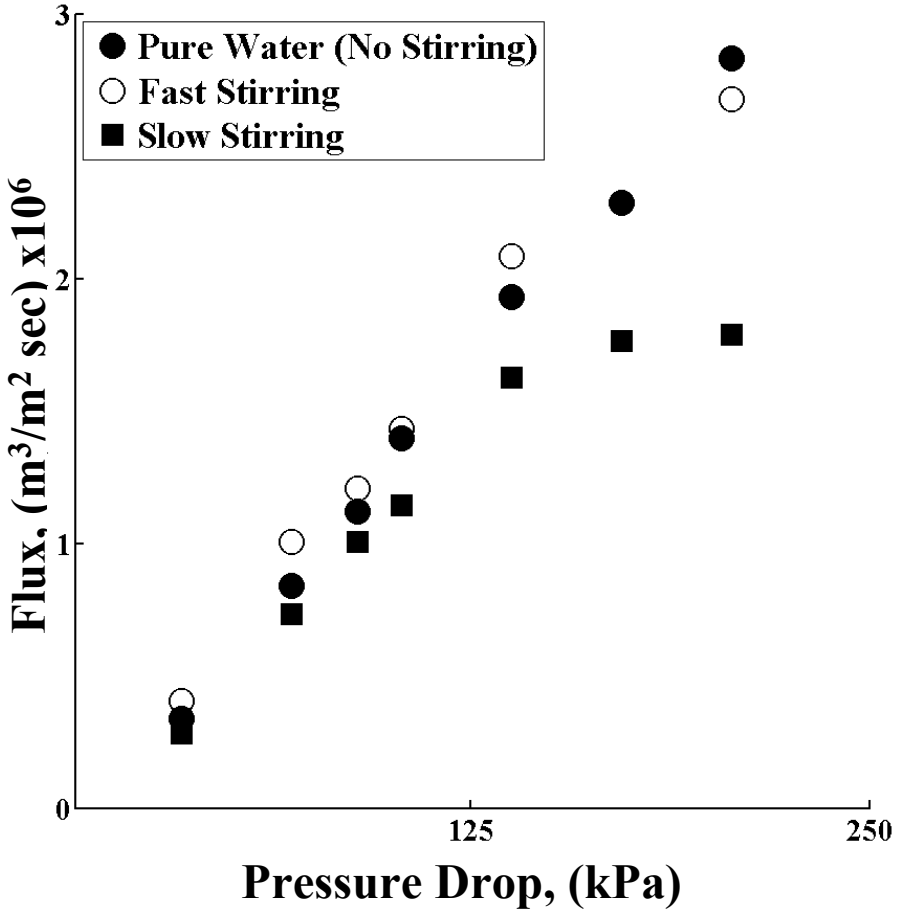

Figure 4.8: The Flux of a 2 wt% PEO Solution is a Function of the Stirring Rate. Rejected solutes accumulate at the pore wall causing a decrease in the observed flux. Rapid stirring allows for rapid mass transport of these solutes back to the bulk solution and prevents a decrease in flux.

That concentration polarization is negligible is supported by comparing the mass transfer coefficient of solute in the bulk solution, k, to the flux of the permeate, $\overline{v}$, across the membrane. The ratio of these values determines how closely the experimentally observed sieving coefficient reflects the membrane's actual sieving coefficient. Using the correlation given by Zeman and Zydney[3] for a stirred cell geometry at a stirring speed of

400 rpm, we calculate a mass transfer coefficient of 1.1 x 10^{-5} m/sec. This mass transfer coefficient and the filtrate flux at 80 kPa give a value for $\overline{v}/k$ of 0.09. At this flux and stirring speed, the system is not highly polarized and our experiments reflect the actual sieving coefficient.

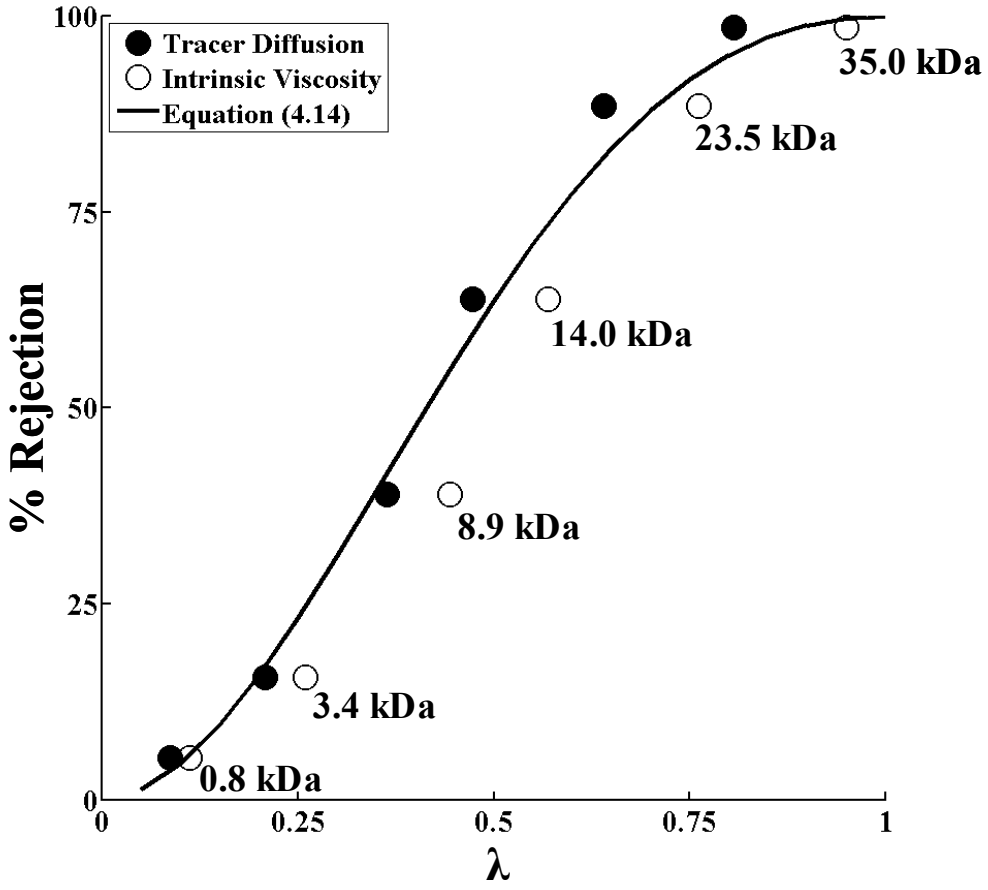

Figure 4.9: PDCPD Membrane Rejects PEO Solutes as Expected. Single solute PEO solutions were used to challenge a PDCPD membrane made using polymer sample B. The resulting rejection curve is compared with the predicted curve using the hindrance coefficients of Brenner[20] for a 14.2 nm pore. The filled circles and open circles are for PEO hydrodynamic radii calculated from tracer diffusion coefficient[30] and intrinsic viscosity data[31], respectively.

These ultrafiltration experiments are summarized for a series of PEO solutes in Figure 4.9. The molecular weight of each solute is given next to each data point. The figure plots the percent rejected (1-S_a)x100 *vs* the solute diameter (i.e., two times the hydrodynamic radius) divided by the pore diameter, λ. The solute diameters are estimated as a function of molecular weight from tracer diffusion and intrinsic viscosity measurements given in the literature.[30, 31] The pore diameter is taken as a constant 14.2 nm, determined as described above by gas diffusion and liquid flow. This diameter is consistent with the flows in Figure 4.6 and with the diffusion data in Table 4.3. As expected, the rejection of the 1 kDa sample is small, around 4 percent; it increases with solute molecular weight until the rejection of the 35 kDa sample is near complete, over 98 percent.

The curve shown in Figure 4.9 is not a best fit of the data, but a prediction without adjustable parameters based on Equation (4.14). This prediction depends on the membrane thickness and void fraction, on the fluid velocity, on the solute diffusion coefficient, and on the ratio of solute diameter to pore diameter λ, that is, on the values on the abscissa of Figure 4.9. From values of λ, we find the parameters K_c and $K_{d.}$ using the equations developed by Bungay and Brenner[20] and then can calculate the curve in Figure 4.9. The agreement of this curve with the experimental results implies that the membrane pores are nearly monodisperse and reproducible across membranes made from the same polymer sample.

Finally, we made a series of experiments with a mixed feed of dextrans. These experiments imitate membrane quality control studies carried out industrially. In

experiments like these, all solutes are fed simultaneously, and the flux of each out of the membrane is determined using SEC equipped with a differential refractometer detector. A sample of the output from the differential refractometer is presented in Figure 4.10. The ratio of the appropriate peak areas is used to calculate the rejection curves shown in Figure 4.11.

Using this method, two types of membranes were tested, our nanoporous PDCPD membranes and a commercial membrane made by phase inversion. Two PDCPD membranes were used, one with a 32 kDa etchable PLA block and the other with a 65 kDa block. This change was made to observe the influence of the PLA molecular weight on the pore dimension. The commercial membrane made by phase inversion is still under development, so details regarding its specific characteristics are not available. The scientist who assisted with these experiments selected this membrane because it has a MWCO similar to that of our PDCPD materials. While this membrane could have a particularly poor rejection curve, it is frequently selected by its manufacturer to test the accuracy of detection equipment. Experiments with both our nanoporous PDCPD membranes and commercial membranes made by phase inversion were run at a constant pressure drop of 13 psig.

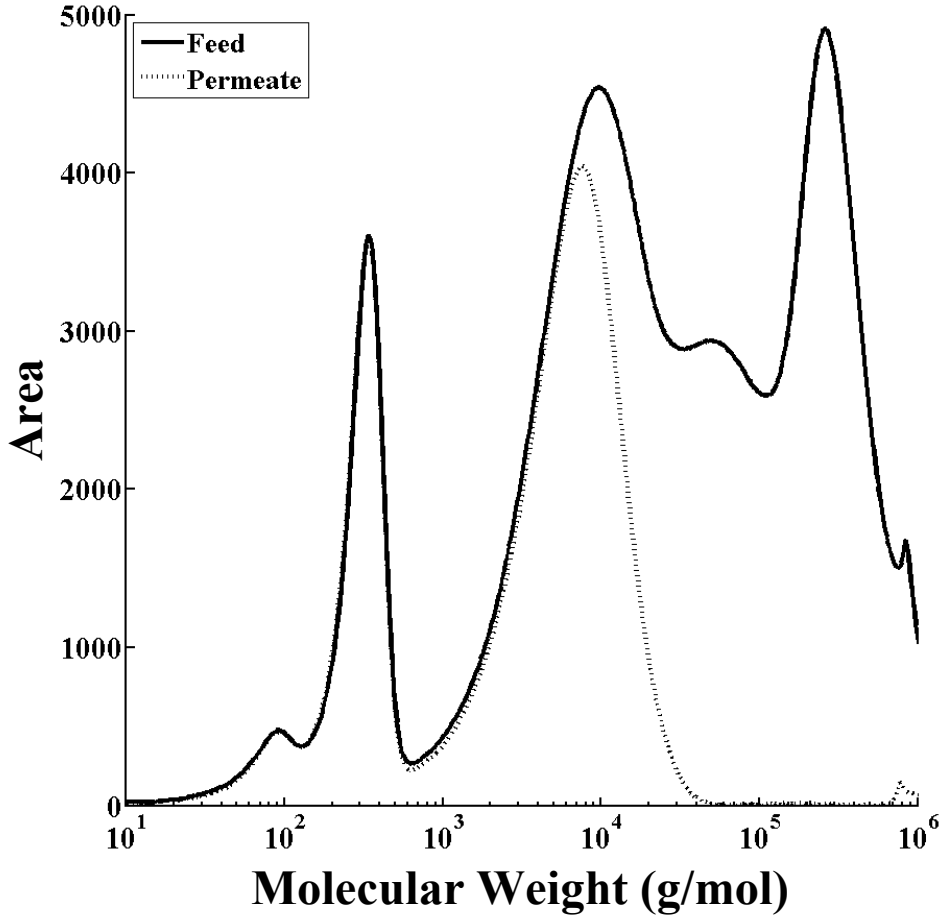

Figure 4.10: Typical SEC Data Used to Calculate Rejection Curve for Dextran Solutions. The mass concentration of dextran in solution is proportional to peak area. Percent rejection is calculated from (1 – *Permeate Area/Feed Area*) x 100.

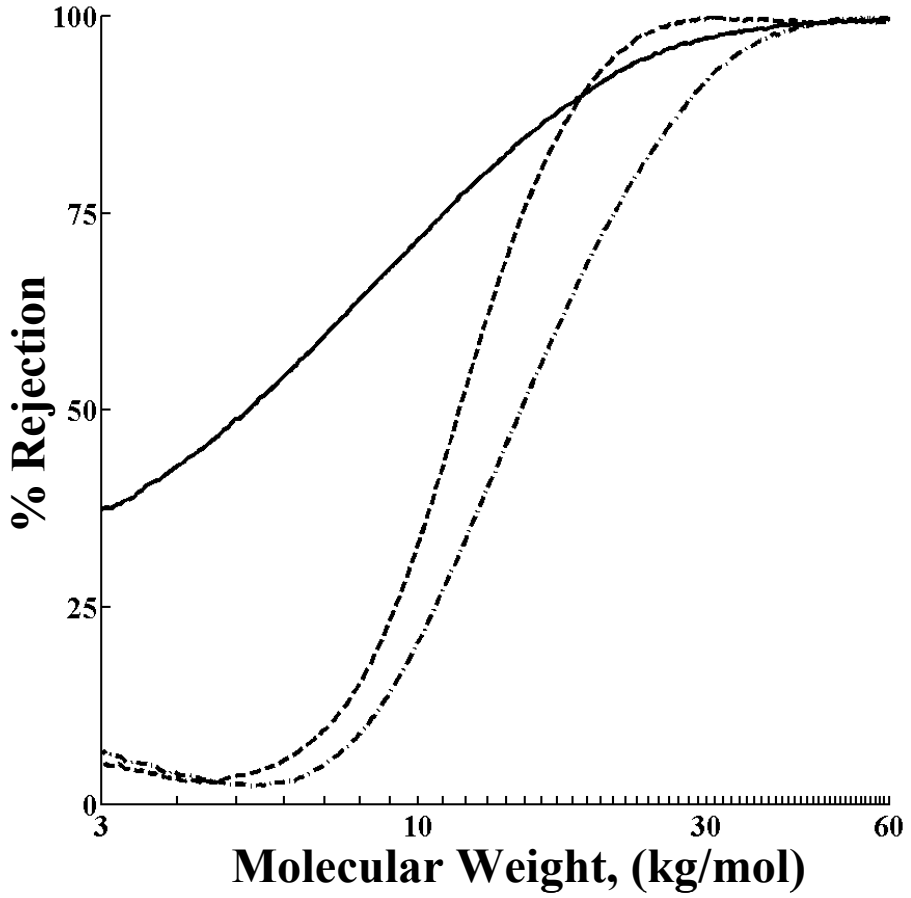

Figure 4.11: PDCPD Membranes Show a Sharper MWCO Than a Membrane Made by Phase Inversion. The solid line is the membrane made by phase inversion. The dashed and dash-dot lines are rejection curves for the membranes developed in this work from polymer samples A and C, respectively. By tailoring the molecular weight of the etchable block, the pore size can be modified.

Ideally, we would like these curves to be step functions with no rejection until a critical molecular weight and then complete rejection above this critical weight. However, this is inconsistent with the underlying theory for Figure 4.9, where the rejection is gentler because of altered free volume and drag of the solute within the pores. Even though step functions are not possible, the results in Figure 4.11 are encouraging.

The data for our two membranes based on etched, self-assembled, block polymer-based membranes show a sharper rejection than those of a commercial ultrafiltration membrane. Moreover, the data for a membrane with a 32 kDa PLA block reassuringly show a cut-off at lower molecular weight for a 65 kDa PLA block. This suggests that block polymer membrane properties can be further tuned to perform a specific desired separation.

4.4 Discussion

The results of our experiments are encouraging. Block copolymer derived nanoporous materials demonstrate some of their potential as an alternative route to ultrafiltration membranes. The MWCO experiments with a mixed dextran feed show that our films provide a more precise cut-off than ultrafiltration membranes made by phase inversion. These experiments also show that control over the etchable blocks molecular weight provides finer control over the cut-off. The gas diffusion, liquid flow, and MWCO experiments all agree with existing theories. The pore diameter inferred from these theories, 14.2 nm, is corroborated by BET and SAXS measurements. These results suggest that ultrafiltration membranes made from block copolymers have considerable potential.

To evaluate this potential, we remember that ultrafiltration membranes are judged by three criteria: selectivity, flux, and resistance to fouling. The results in Figures 4.9 and 4.11 show superior selectivity which can be predicted on the basis of existing theories for cylindrical pores. The fluxes reported in Figure 4.6–4.7 will be over ten times higher than those currently used if the membrane thickness can be reduced.

However, these positive results should be tempered by concerns with membrane thickness and pore diameter. At present, these membranes, cast without a support, have a thickness of 100 μm. Such thick membranes result in low fluxes because the flux is inversely proportional to the membrane thickness. Casting 0.5 μm membranes on a non-woven support is a high priority. Casting membranes which are dramatically thinner than 0.5 μm is less important, because the resistance to flow of the support becomes dominant.[1] While the membranes studied here have not yet been cast on either flat sheet or hollow fiber supports, techniques exist for such casting.[1-3] We are confident these methods can be tailored to our system.

The membranes studied are based on self-assembled bicontinuous structures of a polylactide phase and a polydicyclopentadiene-based phase. When these structures are etched with dilute base, a porous membrane consisting of predominantly polydicyclopentadiene remains. Because this porous structure is isotropic, it requires no alignment to be permeable. Because the pores fill about 40 percent of the membrane volume, the flux is potentially high. However, because the porous structure is periodic, the pore diameter changes from a small value to a larger one, and then back to a smaller one.

Such a structure means that the pore diameter varies along the pore length. Diameters estimated from micrographs represent only the surface, and diameters found from SAXS are arithmetic averages of size. Diameters from surface area (i.e., from BET measurements) should be best for convective measurements because fluid drag is also proportional to surface area. These expectations seem supported by experiment.

The superior selectivity and higher fluxes promised for these easily fabricated membranes may be lost if the membranes foul easily. There is some reason to expect that they will: their internal structure probably does contain some double conical structures which should plug quite easily. At the same time, the overall surface of the membranes appears on a micrometer scale to be much smoother than existing ultrafiltration membranes.[32] Therefore it is critical to experimentally probe the fouling of these membranes.

4.5 References

(1) Baker, R. W. In *Membrane technology and applications;* J. Wiley: Chichester ; New York, 2004; , pp 538.

(2) Ho, W. S. W.; Sirkar, K. K. In *Membrane handbook;* Kluwer Academic Pub.: Boston, 2001; , pp 954.

(3) Zeman, L. J.; Zydney, A. L. In *Microfiltration and ultrafiltration : principles and applications;* M. Dekker: New York, 1996; , pp 618.

(4) Mehta, A.; Zydney, A. L. *J. Membr. Sci.* **2005***, 249*, 245-249.

(5) Mochizuki, S.; Zydney, A. L. *J. Membr. Sci.* **1993***, 82*, 211-227.

(6) Bates, F. S. *Science (Washington, D.C., 1883-)* **1991***, 251*, 898-905.

(7) Bates, F. S.; Fredrickson, G. H. *Annu. Rev. Phys. Chem.* **1990***, 41*, 525-557.

(8) Olayo-Valles, R.; Guo, S.; Lund, M. S.; Leighton, C.; Hillmyer, M. A. *Macromolecules* **2005***, 38*, 10101-10108.

(9) Zalusky, A. S.; Olayo-Valles, R.; Taylor, C. J.; Hillmyer, M. A. *J. Am. Chem. Soc.* **2001***, 123*, 1519-1520.

(10) Zalusky, A. S.; Olayo-Valles, R.; Wolf, J. H.; Hillmyer, M. A. *J. Am. Chem. Soc.* **2002***, 124*, 12761-12773.

(11) Cussler, E. L. In *Diffusion, mass transfer in fluid systems;* Cambridge University Press: New York, 2009; , pp 654.

(12) Bird, R. B.; Stewart, W. E.; Lightfoot, E. N. In *Transport phenomena;* J. Wiley: New York, 2002; , pp 895.

(13) Huizenga, D. G.; Smith, D. M. *AICHE J.* **1986***, 32*, 1-6.

(14) Dullien, F. A. L. In *Porous media : fluid transport and pore structure;* Academic Press: San Diego, 1992; , pp 574.

(15) Anderson, J. L.; Quinn, J. A. *J.Chem.Soc., Faraday Trans.1* **1972***, 68*, 744-748.

(16) Teubner, M.; Strey, R. *J. Chem. Phys.* **1987***, 87*, 3195-3200.

(17) Tassopoulos, M.; Rosner, D. E. *Chem. Eng. Sci.* **1992***, 47*, 421-443.

(18) Anderson, J. L.; Quinn, J. A. *Biophys. J.* **1974***, 14*, 130-150.

(19) Brenner, H.; Gaydos, L. J. *J. Colloid Interface Sci.* **1977***, 58*, 312-356.

(20) Bungay, P. M.; Brenner, H. *Int. J. Multiphase Flow* **1973***, 1*, 25.

(21) Deen, W. M. *AICHE J.* **1987***, 33*, 1409-1425.

(22) Giddings, J. C.; Kucera, E.; Russell, C. P.; Myers, M. N. *J. Phys. Chem.* **1968***, 72*, 4397-4408.

(23) Mavrovouniotis, G. M.; Brenner, H. *J. Colloid Interface Sci.* **1988***, 124*, 269-283.

(24) Renkin, E. M. *J. Gen. Physiol.* **1954***, 38*, 225-243.

(25) Chen, L.; Phillip, W. A.; Cussler, E. L.; Hillmyer, M. A. *J. Am. Chem. Soc.* **2007***, 129*, 13786-13787.

(26) Scholl, M.; Ding, S.; Lee, C. W.; Grubbs, R. H. *Org. Lett.* **1999***, 1*, 953-956.

(27) Yang, R. T. In *Gas separation by adsorption processes;* Series on chemical engineering; Imperial College Press ;$aSingapore; Distributed by World Scientific: London; River Edge, NJ, 1997; Vol. ol. 1, pp 352.

(28) Phillip, W. A.; Rzayev, J.; Hillmyer, M. A.; Cussler, E. L. *Journal of Membrane Science,* **2006***, 286*, 144-152.

(29) Barrett, E. P.; Joyner, L. G.; Halenda, P. P. *J. Am. Chem. Soc.* **1951***, 73*, 373-380.

(30) Faraone, A.; Magazu, S.; Maisano, G.; Migliardo, P.; Tettamanti, E.; Villari, V. *J. Chem. Phys.* **1999***, 110*, 1801-1806.

(31) Meireles, M.; Bessieres, A.; Rogissart, I.; Aimar, P.; Sanchez, V. *J. Membr. Sci.* **1995***, 103*, 105-115.

(32) Zhu, X.; Elimelech, M. *Environ. Sci. Technol.* **1997***, 31*, 3654-3662.

Chapter 5: Gas Diffusion and Liquid Flow Across Nanoporous Block Polymers with a Cylindrical Morphology

The previous chapter discussed our efforts to use a bicontinuous network block polymer morphology to template ultrafiltration membranes with a very narrow distribution of pore sizes. This chapter will focus on similar efforts with a cylindrical morphology.[1-5] Unlike the network structure, the cylinders are anisotropic, and must be oriented in the direction of mass transport. The method we discuss in this chapter uses shear forces to align the cylindrical domains,[6, 7] which are then removed via selective etching to create the pores.[2, 8] Here, we utilize a polystyrene-poly(dimethylacrylamide)-polylactide (PS-PDMA-PLA) triblock polymer precursor, where PS constitutes the continuous matrix, PLA is the etchable component, and PDMA remains as a coating on the nanochannel walls.[4, 5] The PDMA shell facilitates the PLA etching and results in hydrophilic channels. Using this polymer, 1-2 mm thick monoliths are made and used to study gas diffusion and liquid flow through cylindrical nanochannels.

5.1 Background

The membrane behavior reported below reflects Knudsen diffusion of gases and laminar flow of liquids. In the Knudsen regime, the mean free path of the gas molecules is larger than the diameter of the pores i.e., $Kn \gg 1$. This means that collisions of gas

molecules are with the pore walls, not with other gas molecules.[9] A simple model for Knudsen diffusion in a single pore predicts the diffusion coefficient D_{Kn} is

$$D_{Kn} = \frac{2d}{3}\left(\frac{2k_B T}{\pi \tilde{m}}\right)^{1/2} \tag{5.1}$$

where d is the pore diameter, k_B is Boltzmann's constant, T is the temperature, and $\tilde{m}$ is the mass of a diffusing gas molecule. Note that this theory predicts that the diffusion coefficient is independent of pressure, but proportional to pore size.

The situation when the mean-free path is much smaller than the pore diameter is different. Now, when the Knudsen number is small, diffusion is the result of collisions between the gas molecules.[9] In this case, the self diffusion coefficient D_{CE} can be estimated from the Chapman-Enskog kinetic theory

$$D_{CE} = \left(\frac{4\sqrt{2}}{3\pi^{3/2}}\right)\frac{\left(k_B T\right)^{3/2}}{p\,\sigma^2\,\tilde{m}^{1/2}\,\Omega} \tag{5.2}$$

where T is the temperature, p is the pressure, σ is the collision diameter, $\tilde{m}$ is the mass of one molecule, and Ω is a dimensionless function of temperature which is of order one. Note that the kinetic theory predicts that the diffusion coefficient varies inversely with pressure but is independent of pore size.

The result for liquid flowing through the pores in these membranes is different again. The Knudsen number is small and molecular collisions are frequent. The fluid density is so high that the liquid behaves as a continuum. Because the pores are so small, the fluid velocity for a single pore v is laminar and described by the Hagen-Poiseuille law[9, 10]

$$v = \frac{\Delta p d^2}{32 \mu \ell} \tag{5.3}$$

where Δp is pressure drop across a membrane of thickness ℓ, and μ is the liquid viscosity. Of course, we can rewrite this expression as an apparent diffusion coefficient, but this obscures the physical mechanism.

Because our experiments are based on the total membrane area, and not the cross sectional area of the pores, Equations (5.1) and (5.3) are multiplied by ε. Because the pores are formed from a cylindrical morphology we assume the tortuosity $\tau = 1$. We use these equations as a comparison for our results for diffusion and flow through the new membranes developed in the following sections. First, how the membranes are made and prepared in order to measure diffusion coefficients and liquid flow will be described. Then we compare these measured values with those predicted by the above theories.

5.2 Polymer Synthesis and Alignment

The PS-PDMA-PLA triblock copolymer is prepared by Dr. Javid Rzayev using a combination of controlled ring-opening and free-radical polymerization protocols. First, the polylactide segment is synthesized by an aluminum-catalyzed ring-opening polymerization of D,L-lactide. The reaction is conducted in toluene at 90 ˚C to produce PLA with M_n = 11 x 10^3 (NMR) and M_w/M_n = 1.05 (GPC). The native hydroxyl end-group of PLA is then linked to *S*-1-dodecyl-*S*'-(α,α'-dimethyl-α''-acetic acid)trithiocarbonate[11] via an acid chloride intermediate to provide a macrochain-transfer agent (PLA-TC) in quantitative yield (NMR). Subsequently, PLA-TC is employed under

the reversible addition-fragmentation chain-transfer (RAFT) polymerization conditions to grow PDMA and PS blocks sequentially. The analysis by NMR and GPC after each step corroborates the efficient re-initiation, and the final PS-PDMA-PLA triblock copolymer was obtained with block molecular weights of 25 x 10^3 – 2.2 x 10^3 – 11 x 10^3, respectively, and M_w/M_n = 1.14.

The powdery samples of PS-PDMA-PLA were pressed in a rectangular mold, and then forced through a channel die (L x W = 50 mm x 2 mm) at 160 ˚C to provide 1 - 2 mm thick monoliths.[6, 7] Following annealing in a vacuum oven at 190 ˚C for 16 hours, the monoliths are analyzed by small-angle X-ray scattering (SAXS), which confirms the formation of the aligned cylindrical morphology with hexagonal symmetry in the direction of flow. The degree of alignment, quantified using the second-order orientation factor F_2,[2, 12, 13] is as high as 0.94 – 0.96. Figure 5.1 shows an end-on view of a fractured monolith surface demonstrating the hexagonally packed pore structure.

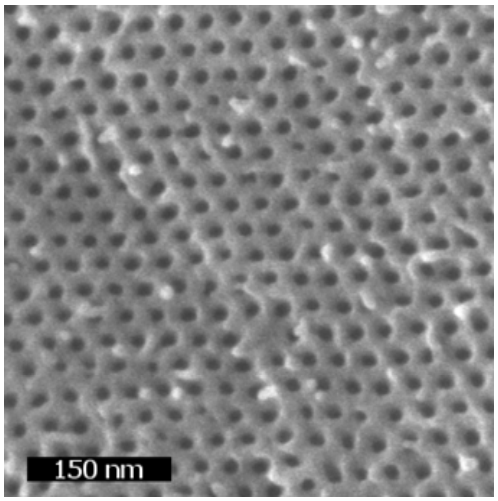

Figure 5.1: SEM Image of Etched Nanoporous PS-PDMA-PLA Block Polymer. Image shows 16.8 nm aligned pores in hexagonally packed structure.

5.3 Membrane Preparation

We use two different membranes in our experiments. The first uses commercially available track-etched polycarbonate membranes as a standard. The second is based on the block copolymer monoliths whose synthesis is described above. The preparation of these two membranes differs, as described below.

The preparation of the track-etched membranes was straightforward. A typical membrane (Steriltech, Kent, WA) is mounted between two sheets of aluminum foil using epoxy in order to avoid contamination of the membrane by silicon grease used on the sealing gaskets. A sheet of aluminum foil is folded in half and a 1.1 cm diameter hole is punched through both layers. The PCTE membrane, which has a diameter of 1.3 cm, is glued between the layers using epoxy (Loctite Corporation, Rocky Hill, CT). Once the epoxy cures the membrane is now ready for mounting as shown in Figures 5.2 and 5.3. The track-etched film, clad with aluminum foil, is put between a sieve plate and a metal ring with gaskets and clamped in place.

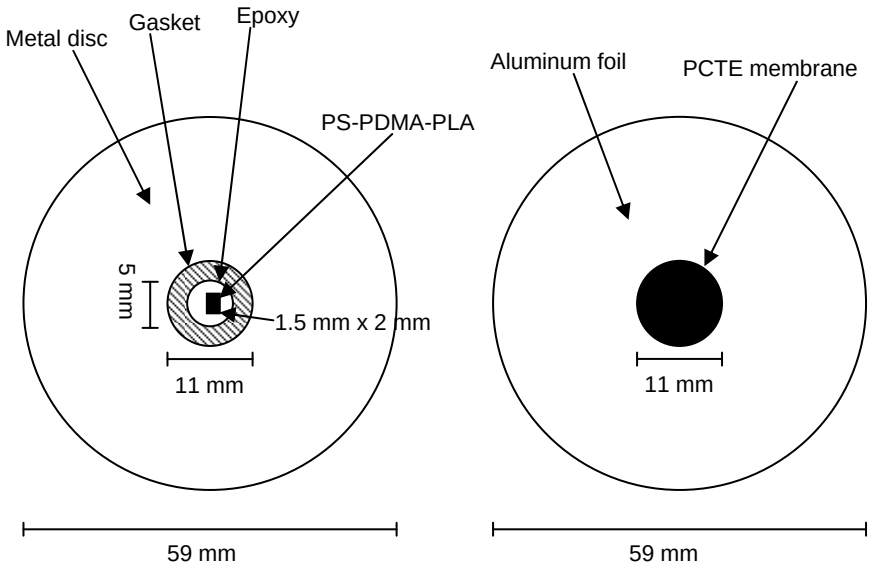

Figure 5.2: Mounted Monolith and Poretics Standard. Mounting membranes in this manner ensures all relevant flux occurs through the porous materials.

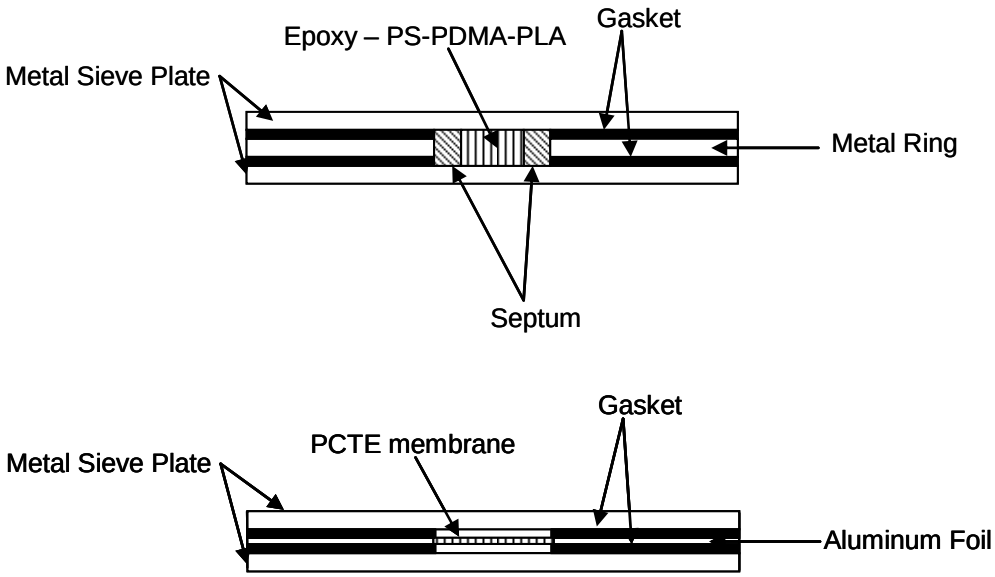

Figure 5.3: Clamping Setup for Each Membrane. Due to the differing thicknesses of the two types of membranes, a different clamping procedure is necessary for the PS-PDMA-PLA and PCTE membranes.

The procedure to prepare the block copolymer membranes is described in more detail than normal, because many who have attempted this preparation have not been

successful. Prior to being potted the extruded, aligned monoliths of PS-PDMA-PLA are cut into 2 mm lengths. A 3 mm length of 5 mm I.D. Teflon tubing is filled with epoxy (DP-460 Off White, 3M, St. Paul, MN) and the copolymer chunk is submerged in the epoxy with the extruded direction (i.e., the pores) parallel to the axis of the tubing. The tubing containing the epoxy and monolith chunk is placed in an oven at 75 ˚C for one hour to cure the epoxy. Upon removal from the oven, the cured epoxy with the PS-PDMA-PLA chunk inside slides out of the PFTE tubing. The PS-PDMA-PLA is exposed by whittling away the epoxy at each end using a razor blade. The final sample is approximately 2 mm thick and 5 mm in diameter, with an exposed area of copolymer around 1.5 mm x 2 mm. The cylindrical epoxy-monolith sample is inserted into a gasket made by punching a hole in a GC septum. This assembly is then inserted into a metal disk, as shown in Figure 5.2. The disk is clamped between two metal sieve plates, causing the gasket to compress in the vertical direction and expand in the horizontal direction. This deformation creates a good seal between the sample and the metal disk. At this point, the polymer had *not* been etched.

The process with the PS-PDMA-PLA monoliths begins with an unetched sample because each film is tested before degradation of the PLA block to ensure that a good seal is formed. This shows that almost all the flux through the membrane will be due to the pores and not to leaks at the epoxy-copolymer or gasket-metal disk interface. Earlier attempts to pot the entire 1-2 cm extruded PS-PDMA-PLA sample and then cut off 2 mm lengths resulted in leaks, probably because the cohesion between the epoxy and the

PS-PDMA-PLA is not sufficient to counteract the stress caused by the razor blade. To eliminate this problem, we found it necessary to cut the PS-PDMA-PLA before potting it.

If the unetched copolymer membrane is found to be impermeable, it is removed and immersed in a stirred 0.5 M NaOH, 60:40 (v:v) methanol/water solution at room temperature. Earlier experiments at 70 ˚C were not successful because the methanol swelled the epoxy, destroying the cohesion between the epoxy and PS-PDMA-PLA. The use of lower temperatures results in a longer time required for the complete etching of the PLA block. At room temperature, degradation takes about eight days for the 2 mm thick monolith. The sample is removed from the solution and rinsed thoroughly with 60:40 (v:v) methanol/water. The sample is then dried under vacuum for approximately eight hours. The resulting membrane does have the highly aligned nanoporous structure with hexagonal symmetry, as verified by SAXS and Scanning Electron Microscopy (Hitachi S-900 FE-SEM). In the dry state, the pore diameter calculated from the volume fractions of the PS-PDMA-PLA precursor and the SAXS data is 16.8 nm. This membrane can now be clamped in the diffusion cell for experiments with a variety of gases.

The preparation of the monoliths for liquid flux measurements and preparation for diffusion measurements varied in only for one detail. The PFTE tubing used to shape the membrane for the diffusion measurements was replaced with a cylindrical die bored out of a Teflon block. Using the Teflon block we made a sample approximately 2 mm thick and 31 mm in diameter with an exposed area of copolymer around 1.5 mm x 2 mm. These dimensions were chosen because they allowed the sample to be directly inserted

into the liquid diaphragm cell. The preparation of the track-etched membranes for the liquid flux experiments remained unchanged.

5.4 Results

We first show typical data for our diffusion experiments and then compare the results of these experiments with the predictions summarized above. We conclude with our measurements of liquid flows. Typical data for nitrogen diffusion across the PS-PDMA-PLA triblock copolymer membranes are shown in Figure 5.4. The data, plotted as suggested by Equation (2.7), show that the logarithm of the ratio of pressure differences is linear in time. The slope of this plot is equal to the permeability: a larger slope means a larger permeability. The slope for the unetched membrane is near zero because it has no pores, and diffusion through the polymer itself is small. The slope of two different etched membranes is much larger and equal within 5 percent. We believe that this is typical of the reproducibility of our experiments.

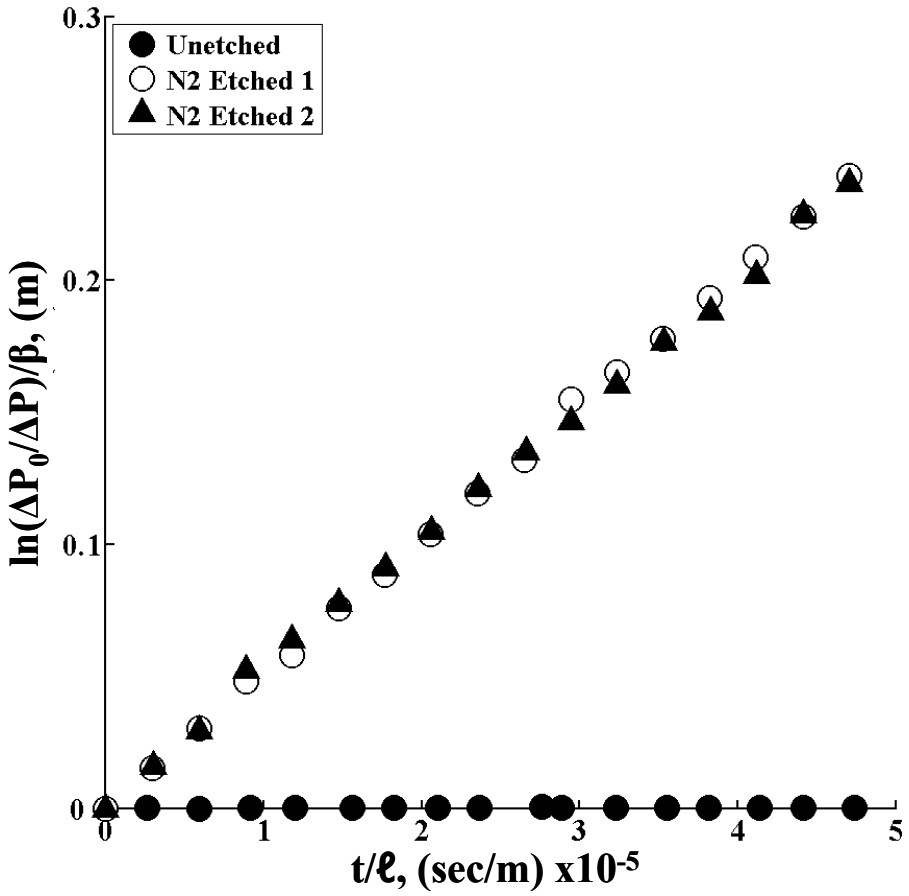

Figure 5.4: Diffusion Data vs. Etching. The pressure with time is reproducible for etched films, but very small for nonetched films.

As expected, different gases have different permeabilities, as shown in Figure 5.5. The permeability of helium is greater than oxygen, which is in turn greater than argon. This inverse dependence on molecular weight is that expected for either conventional or Knudsen diffusion, described by Equations (5.2) and (5.1), respectively. This dependence reflects the larger velocity of the smaller species, which is the basis of both models of diffusion.

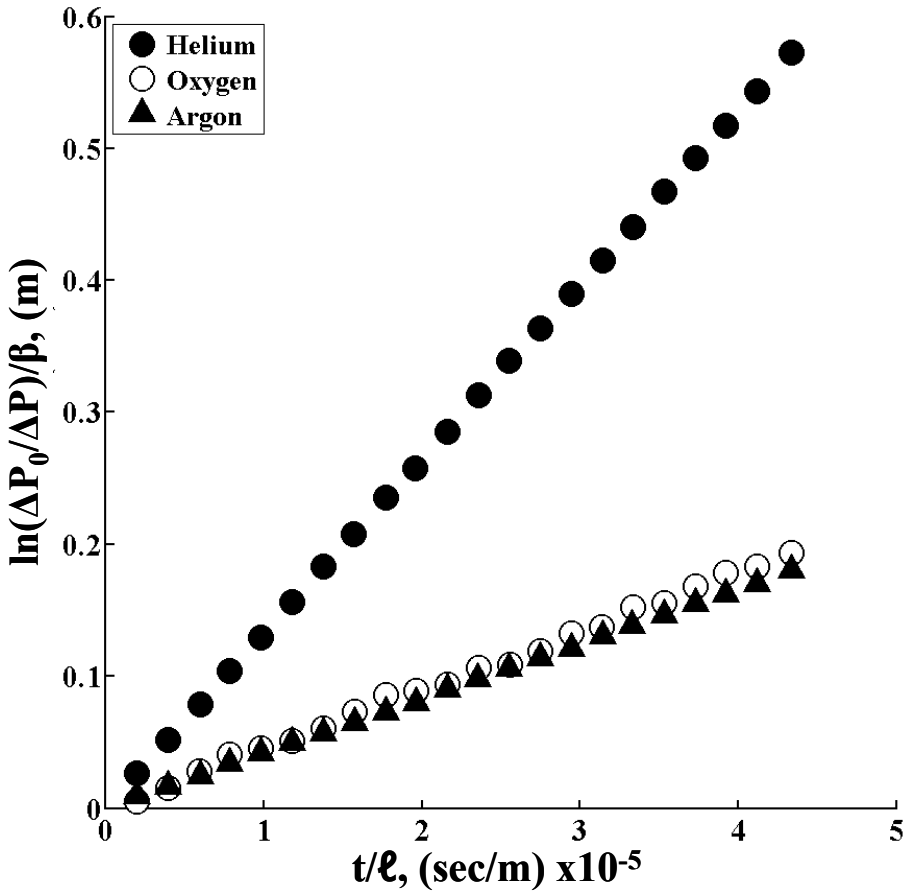

Figure 5.5: Diffusion Data for Different Gases. As expected, permeabilities are higher for gases with smaller molecular weights.

The transport mechanism in these membranes is Knudsen diffusion, as shown by the summary of results in Table 5.1. The upper part of this table gives the results for the PS-PDMA-PLA etched block copolymer membranes, and the lower part is for the track-etched membranes studied as a benchmark. The organization of the results within these two parts is the same. The first column gives diffusing gas, the second column gives the membrane permeability and the third column gives the experimentally determined diffusion coefficient. These values depend on the void fraction occupied by the pores,

which is 0.26 for the block copolymer membrane (based on the PLA volume fraction) and 0.0060 for the track-etched membrane. The next two columns give the diffusion coefficients calculated from Equations (5.1) and (5.2), respectively. The last three columns give the membrane selectivities relative to helium found from experiment and calculated for Knudsen and kinetic diffusion theories.

Table 5.1. Results of Gas Diffusion.[a]

A. Data for PS-PDMA-PLA monoliths.

Solute	D_{eff}	D_{eff}/ε[b]	D_{Kn}[c]	$D_{C\text{-}E}$	α_{exp}[d]	α_{Kn}[d]	$\alpha_{C\text{-}E}$[d]
He	0.0133	0.051	0.051	1.12	1.00	1.00	1.00
N_2	0.0049	0.019	0.019	0.135	2.59	2.65	8.28
O_2	0.0044	0.017	0.018	0.137	2.90	2.83	8.16
Ar	0.0044	0.017	0.016	0.122	3.08	3.16	9.17

[a] All diffusion coefficients are reported with units of cm^2/sec

[b] Assuming $\varepsilon = 0.26$

[c] Assuming d = 12.2 nm

[d] All selectivities are defined as $\alpha_i \equiv D_{He}/D_i$

B. Data for Commercial Track-Etched Membranes.

Solute	D_{eff}	D_{eff}/ε[a]	D_{Kn}[b]	$D_{C\text{-}E}$	α_{exp}[c]	α_{Kn}[c]	$\alpha_{C\text{-}E}$[c]
He	0.000077	0.128	0.123	1.12	1.00	1.00	1.00
Ar	0.00024	0.040	0.390	0.122	3.21	3.16	9.17

[a] Assuming $\varepsilon = 0.006$

[b] Assuming d = 29.5 nm

[c] All selectivities are defined as $\alpha_i \equiv D_{He}/D_i$

The results in Table 5.1 show conclusively that transport through the pores etched in the block copolymer occurs by Knudsen diffusion. The measured coefficients are within 5 percent of those calculated from the Knudsen mechanism. They are about six times smaller than the values expected from kinetic theory. This is expected because estimates of the mean-free path of these gases average about ten times larger than the

pores themselves. In addition, the selectivities measured relative to helium are close to those calculated from Equation (5.1). They are a function only of the inverse square root of the molecular weight and are not dependent on factors like the collision diameter and the Leonard-Jones potential, which alter kinetic theory estimations. Finally, the experiments with the track-etched membranes used as a benchmark give very similar results, justifying our procedure.

The results in Table 5.1 begin to realize the promise of etched block copolymer membranes for fast ultrafiltration with a sharp molecular weight cut-off. However, the predicted values of Knudsen diffusion coefficients are based on a pore diameter of 12.2 nm, less than the value of 16.8 nm found from both electron microscopy and SAXS. We believe that this difference reflects both limitations in the theory summarized by Equation (5.1) and consequences of the detailed chemistry, especially of the PDMA left at the pore walls. We will discuss this in detail later in the chapter.

We did explore this discrepancy by measuring flow of water liquid through the etched pores. The results are shown in Figure 5.5, where the data plotted as the logarithm of the ratio of height difference are linear in time, as predicted by Equation (2.14). The average pore diameter as calculated from the slope in Figure 5.5 is 13.0 nm, in close agreement with the diffusion results. We have not measured changes in flux as a function of pH or solute concentration. We understand that these changes may be major, as we showed for the membranes developed in Chapter 4.[14, 15]

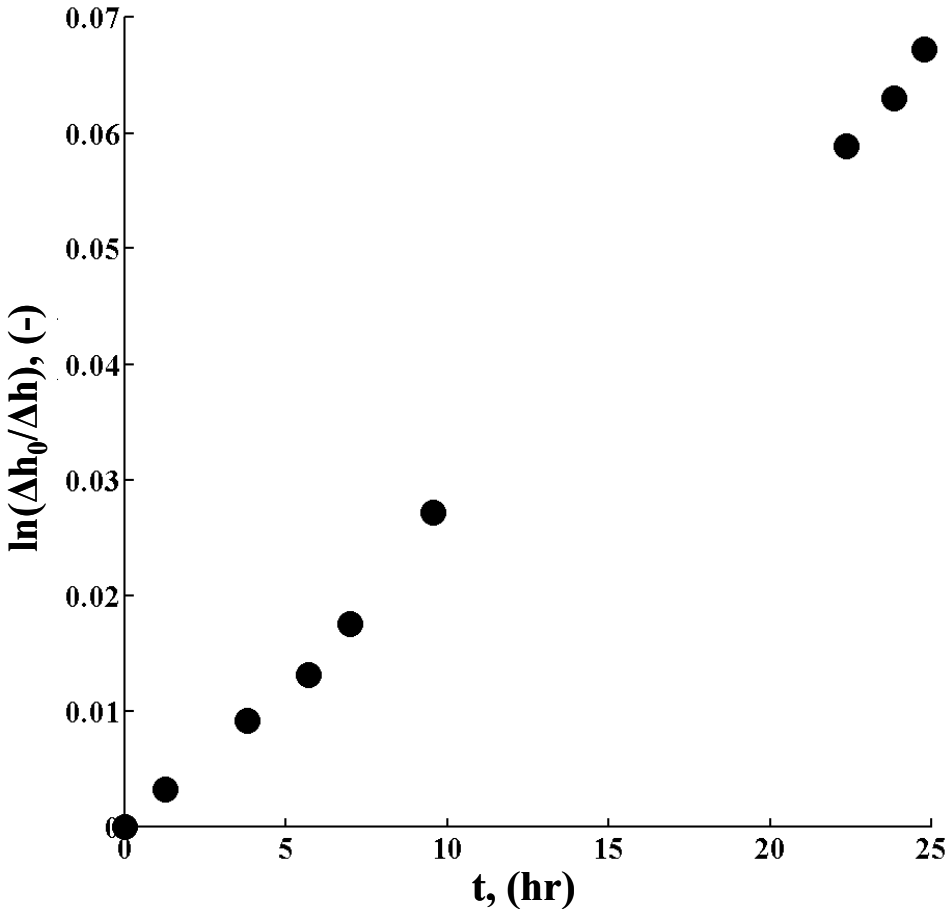

Figure 5.6: Liquid Water Flow Through Nanoetched Pores. The slope of these data implies an average pore diameter of 13.0 nm.

5.5 Discussion

5.5.1 What the Diffusion Results Mean

The results given above further establish the promise of ultrafiltration membranes based on etched block copolymers. The diffusion coefficients that are observed are consistent with those expected for Knudsen diffusion. The nearly monodisperse pores within these films should give sharp molecular weight cut-offs like those observed using track-etched membranes. We can make this comparison with track-etched films more

explicit by comparing the permeances across a 0.5 μm film, as shown in Table 5.2. The permeance of the block copolymer films is over 100 times higher than that of a track-etched film, even though the block copolymer film is thicker and has significantly smaller pores. If the pores were the same size, the permeance of the block copolymer films would be 4000 times larger.

Table 5.2. Predicted permeances.[a]

A. PS-PDMA-PLA membrane.[b]

Solute	D_{eff}/ℓ	$D_{Kn}\varepsilon/\ell$[c,d]
He	265	265
N_2	98.8	98.8
O_2	89.4	93.6
Ar	86.3	83.2

[a] All permeances are reported in cm/sec
[b] Assuming ℓ = 500 nm.
[c] Assuming ε = 0.26.
[d] Assuming d = 12.2.

B. Track-etched membrane.[a]

Solute	D_{eff}/ℓ	$D_{Kn}\varepsilon/\ell$[b,c]
He	1.54	1.49
Ar	0.48	0.47

[a] Assuming ℓ = 5 μm.
[b] Assuming ε = 0.006.
[c] Assuming d = 29.5 nm.

The close agreement between theory and experiment implies that the pore geometry we have obtained is close to that of right circular cylinders with an aspect ratio of over 10^6:1. Any branching or constrictions in the pores would mean that the agreement between theory and experiment would be weaker. At the same time, the diffusion data are consistent with a large body of earlier literature that explores whether these simple theories of membrane transport are valid for very small pores.[16-18] Our data,

which seem reliable, do support these simple theories, both for gases and liquids.[9, 18] Our data are also consistent with earlier efforts using etched block copolymers, though these make no comparisons with predictions.[8] However, our results and most earlier data are inconsistent with results for water liquid transport in aligned carbon nanotubes, where a new, different transport mechanism suggested by quantum mechanics may be operating. We found no evidence whatsoever of any new transport mechanism in our work.[19-22]

At the same time, we recognize that the pore diameter of 12.2 nm, which is consistent with our diffusion and flow results, is less than 16.8 nm which is observed in our SEM and SAXS measurements. We are not sure what causes this discrepancy. The obvious explanation is that our experimental procedure is somehow flawed. However, our experiments with track-etched films, which use the same procedure, give pore diameters from diffusion measurements that do agree with those from our SEM measurements. Thus our procedure seems correct.

Another possible reason for this discrepancy is that the pore geometry implied by the picture at the right of Figure 5.1 is misleading. That picture implies straight monodisperse cylindrical pores. Perhaps the pores have big mouths and narrow bodies within the film. Perhaps they are branched, or have many dead ends. Perhaps they are somehow polydisperse. In other words, perhaps their geometry may not be what it seems. However, SEM images from related monoliths are consistent with well-aligned straight pores with uninterrupted lengths over several microns. Moreover, if the pores had wide mouths and narrow bodies, the SEM results would suggest larger diameters than the SAXS results. They do not. If the pore geometry were complex and polydisperse, then

the gas diffusion and liquid flow results would be inconsistent. They are not. We conclude that the pore geometry is probably close to our simple picture.

The most likely cause of this discrepancy is due to the chemistry in the pores. Once the poly(lactide) blocks are removed by etching with base, we expect that the pores will be coated with poly(dimethylacrylamide). This will create a polymer brush on the inside of the pores that will extend into the fluid the pores. If a PDMA coating of 0.8 nm swells to 1.4 nm, in both gas and liquid, it would reduce the 16.8 nm measured from SAXS to the 14.0 nm closer to that measured by diffusion. Other changes in pore chemistry may include adsorption and desorption kinetics, which are often summarized as a "sticking coefficient." We could analyze our data in these terms, but we would then introduce a new parameter that we have no independent way to measure. However, any chemical interactions like those postulated in these analyses should be different for the different gases, and we find the same 12.2 nm diameter explains data for He, N_2, O_2, and Ar.

5.5.2 Potential of These Membranes

We recognize that many will be interested in the results of diffusion of gases, but that many more will be interested in the results of ultrafiltration of liquid solutions. After all, while the gas results are interesting scientifically the liquid results may have considerable practical value. We decided to begin our results with gases for two reasons. First, the diffusion of gases is chemically simple. It is unaffected by solvation, by solute charge, or by polymer polarity. It provides a chance to see if the geometry of etched

pores show in the right panel of Figure 5.1 is really as simple as it looks. The results are a definitive yes.

The second reason that we began by studying gases rather than liquid solutions is the difficulty of the experiments themselves. Once the basic synthesis and the etching of the block copolymers is established, it is relatively easy to get micrographs and X-ray scattering indicating that the aligned pore geometry exists. It is considerably more difficult to show that these materials can show the transport properties that are expected. In this case, we wanted to establish a preliminary baseline before moving onto experiments with liquid solutions. This chapter establishes that baseline.

We do want to speculate about what the performance of these membranes will be when they are used for ultrafiltration. To do so, we consider the case of bovine serum albumin, because the separation of this protein has been carefully studied.[23] One way to evaluate this case is to plot the separation factor vs. the hydraulic permeability. The separation factor, defined as the inverse of the membrane sieving coefficient, is a measure of the membrane selectivity; the hydraulic permeability is inversely proportional to the membrane resistance to flow.

We seek a high separation factor and a high hydraulic permeability. Not surprisingly, we get either a membrane with a high separation factor or a membrane with a high hydraulic permeability, as the data in Figure 5.7 show for commercially available membranes.[23] This figure also shows as the solid line the results expected for etched block copolymer membranes. These data were calculated by assuming a pore diameter,

and then calculating the hydraulic permeability from Equation 3 and the separation factor α from[24]

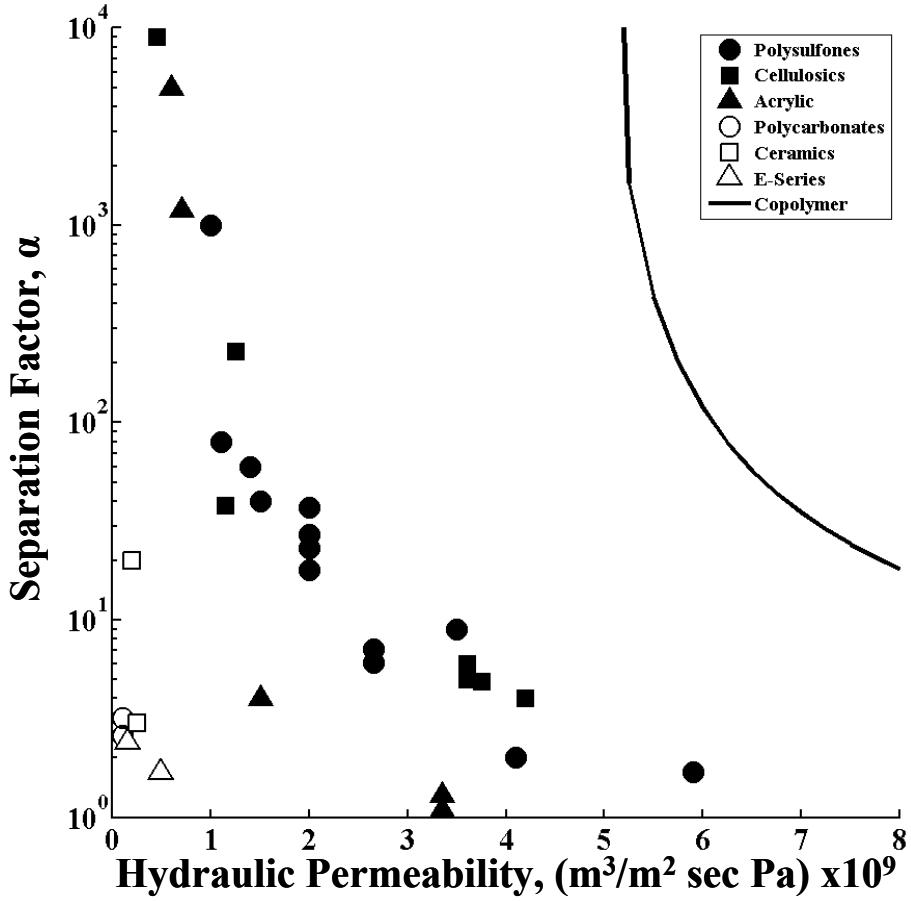

Figure 5.7: Separation Factor vs. Hydraulic Permeability. The data points, reviewed in Ref. 23, are for commercially available membranes. The solid curve is estimated for the membranes being developed here.

$$\frac{1}{\alpha} = S_a = \left(1-\lambda\right)^2\left[2-\left(1-\lambda\right)^2\right]e^{-0.71\lambda^2} \tag{5.4}$$

where λ is the ratio of the diameter of BSA (7.3 nm) to the diameter of the pores. The estimates for membranes like that used here - the solid line - have both a faster flow and a more abrupt increase in separation factor. We look forward to finding out if this expected improvement can be achieved.

5.6 References

(1) Zalusky, A. S.; Olayo-Valles, R.; Taylor, C. J.; Hillmyer, M. A. *J. Am. Chem. Soc.* **2001***, 123*, 1519-1520.

(2) Zalusky, A. S.; Olayo-Valles, R.; Wolf, J. H.; Hillmyer, M. A. *J. Am. Chem. Soc.* **2002***, 124*, 12761-12773.

(3) Olayo-Valles, R.; Guo, S.; Lund, M. S.; Leighton, C.; Hillmyer, M. A. *Macromolecules* **2005***, 38*, 10101-10108.

(4) Rzayev, J.; Hillmyer, M. A. *Macromolecules* **2005***, 38*, 3-5.

(5) Rzayev, J.; Hillmyer, M. A. *J. Am. Chem. Soc.* **2005***, 127*, 13373-13379.

(6) Chen, Z.; Kornfield, J. A. *Polymer* **1998***, 39*, 4679-4699.

(7) Chen, Z.; Kornfield, J. A.; Smith, S. D.; Grothaus, J. T.; Satkowski, M. M. *Science (Washington, D.C.); Science (Washington, D.C.)* **1997***, 277*, 1248-1253.

(8) Cooney, D. T.; Hillmyer, M. A.; Cussler, E. L.; Moggridge, G. D. *Crystallogr.Rev.; Crystallography Reviews* **2006***, 12*, 13-24.

(9) Cussler, E. L. In *Diffusion, mass transfer in fluid systems;* Cambridge University Press: New York, 2009; , pp 654.

(10) Bird, R. B.; Stewart, W. E.; Lightfoot, E. N. In *Transport phenomena;* J. Wiley: New York, 2002; , pp 895.

(11) Lai, J. T.; Filla, D.; Shea, R. *Macromolecules* **2002***, 35*, 6754-6756.

(12) Sakurai, S.; Aida, S.; Okamoto, S.; Ono, T.; Imaizumi, K.; Nomura, S. *Macromolecules* **2001***, 34*, 3672-3678.

(13) de Gennes, P. G.; Prost, J. In *The physics of liquid crystals;* The International series of monographs on physics; Clarendon Press; Oxford University Press: Oxford; New York, 1993; Vol. 83, pp 597.

(14) Liu, G.; Ding, J.; Hashimoto, T.; Kimishima, K.; Winnik, F. M.; Nigam, S. *Chem.Mater.; Chemistry of Materials* **1999***, 11*, 2233-2240.

(15) Phillip, W. A.; Amendt, M.; O'Neill, B.; Chen, L.; Hillmyer, M. A.; Cussler, E. L. *ACS Applied Materials & Interfaces* **2009***, 1*, 472-480.

(16) Anderson, J. L.; Quinn, J. A. *J.Chem.Soc., Faraday Trans.1* **1972***, 68*, 744-748.

(17) Liu, G.; Ding, J.; Stewart, S. *Angew.Chem., Int.Ed.; Angewandte Chemie, International Edition* **1999***, 38*, 835-838.

(18) Beck, R. E.; Schultz, J. S. *Biochim.Biophys.Acta, Biomembr.; Biochimica et Biophysica Acta, Biomembranes* **1972***, 255*, 273-303.

(19) Majumder, M.; Chopra, N.; Andrews, R.; Hinds, B. *Nature (London, U.K.); Nature (London, United Kingdom)* **2005***, 438*, 930.

(20) Skoulidas, A. I.; Ackerman, D. M.; Johnson, J. K.; Sholl, D. S. *Phys. Rev. Lett.* **2002***, 89*, 185901/1-185901/4.

(21) Sholl, D. S.; Johnson, J. K. *Science (Washington, DC, U.S.); Science (Washington, DC, United States)* **2006***, 312*, 1003-1004.

(22) Holt, J. K.; Park, H. G.; Wang, Y.; Stadermann, M.; Artyukhin, A. B.; Grigoropoulos, C. P.; Noy, A.; Bakajin, O. *Science (Washington, DC, U.S.); Science (Washington, DC, United States)* **2006***, 312*, 1034-1037.

(23) Mehta, A.; Zydney, A. L. *J. Membr. Sci.* **2005***, 249*, 245-249.

(24) Zeman, L.; Wales, M. *ACS Symp. Ser.* **1981***, 154*, 411-434.

Chapter 6: Preparation of Composite Ultrafiltration Membranes Templated by Block Polymer Self-Assembly

The previous two chapters discussed the fabrication and characterization of relatively thick nanoporous membranes. As discussed in those chapters, achieving commercially interesting hydraulic permeabilities requires membranes with a thin selective layer. Our effort to produce a membrane with a thin selective layer from a polystyrene-b-polylactide (PS-PLA) copolymer that forms a cylindrical morphology is the focus of this chapter. Using a cylinder forming copolymer adds the complication of orientation.[1-4] Rapid solvent evaporation is shown to produce the perpendicular orientation necessary for making filtration membranes. This chapter will discuss our understanding of how the cylinder orientation depends on the copolymer properties, solvent properties and the solvent evaporation rate.

Our knowledge of controlling cylinder orientation along with existing techniques for making composite membranes[5-7] will be used to produce block polymer templated ultrafiltration membranes. A thin copolymer layer is solution cast onto a microporous membrane. After etching the lactide domains with a dilute sodium hydroxide solution, the resulting composite membrane consists of a thin nanoporous PS layer which carries out the desired separation, mechanically reinforced by the underlying microporous support. Reports of liquid flow and ultrafiltration experiments explore the value of these new membranes.

6.1 Background

The membranes produced in this chapter have pores with a diameter on the order of tens of nanometers. Because the pores are small, the fluid velocity for a single pore $\langle v \rangle$ is laminar and described by the Hagen-Poiseuille law[8, 9]

$$\langle v \rangle = \frac{d^2 \Delta p}{32 \mu \ell} \tag{6.1}$$

where Δp is pressure drop across a membrane of thickness ℓ with pores of diameter d, and μ is the liquid viscosity. For a porous solid, the superficial velocity $\bar{v}$ is a more useful quantity:[10]

$$\bar{v} = \frac{\varepsilon}{\tau} \frac{d^2 \Delta p}{32 \mu \ell} \tag{6.2}$$

where ε is the void fraction and τ is the tortuosity. The void fraction accounts for the experimental measurements being based on the total projected area of the membrane, not on the cross sectional area of the pores. The tortuosity accounts for both variations in the size and shape of the pore cross-section as well as the additional distance required for a molecule to travel relative to the film thickness. We will compare predictions of this equation with our experimental results.

This chapter will also explore the ability of these ultrafiltration membranes to reject dissolved solutes. To analyze our rejection data, we will again use the model developed by Bungay and Brenner[11] as described in Chapter 4. This model pictures the dissolved solute as a sphere moving in a cylindrical pore described by λ, the ratio of

solute diameter to pore diameter. The rejection data are described in terms of a sieving coefficient

$$S_a = \frac{c_{1\ell}}{c_{10}} = \frac{K_c\left(1-\lambda\right)^2}{1-\left(1-K_c\left(1-\lambda\right)^2\right)e^{-\left[\frac{\langle v\rangle K_c \ell}{D_i K_d}\right]}} \tag{6.3}$$

where $c_{1\ell}$ and c_{10} are the solute concentrations at the downstream and upstream membrane surface, D_i is the solute's diffusion coefficient in bulk liquid, and K_c and K_d are tabulated dimensionless factors describing the hinderance in small pores.[11, 12] Note that the dimensionless quantity in square brackets is the Peclet number, a measure of the speed of convection relative to the speed of diffusion.

We note that the actual sieving coefficient, S_a, is distinct from the observed coefficient, S_o.[5, 13] The actual sieving coefficient is calculated using the solute concentration immediately adjacent to the membrane surface, while the observed sieving coefficient replaces this with the bulk upstream solute concentration. While the bulk concentration is more easily obtained in experiments, it can often be lower than the concentration at the membrane surface due to concentration polarization. We will report experiments here without such polarization, but recognize that such experiments may not always be possible. We now turn to describing how the membranes are made and prepared for liquid flow and solute rejection measurements. Then we compare the results of these measurements with those predicted by the above theories.

6.2 Polymer Synthesis and Characteristics

A series of asymmetric polystyrene-b-polylactide block copolymers are used as templates for the nanoporous membranes fabricated in this work. The PS-PLA copolymer samples were prepared by Marc Rodwogin using a combination of anionic and controlled ring-opening polymerization protocols.[14-16] First, the polystyrene segment is synthesized by the anionic polymerization of styrene using a sec-butyl-lithium initiator in cyclohexane at 40 °C. The reaction was terminated with excess ethylene oxide and the PS precipitated into a 50:50 (v:v) solution of methanol and isopropanol. Subsequently, the hydroxyl-terminated PS was placed in a high pressure vessel. This vessel was put into an inert atmosphere, where toluene and triethylaluminum were added and allowed to stir overnight. D,L-lactide was then added to the vessel before sealing it and placing it in a 90 °C oil bath. After 8 hours, the reaction was terminated with aqueous hydrochloric acid. The PS-PLA sample was precipitated in methanol and dried overnight under vacuum at 60 °C.

The overall polymer molecular weight and volume fraction were determined using ^{1}H NMR and the PDI was determined using size exclusion chromatography. Table 6.1 summarizes the properties of the different samples. The first column gives the sample name; the next two columns give the molecular weights of the styrene and lactide blocks, respectively; the fourth column gives the PDI; and the last column gives the volume fraction of lactide in the sample. Note the first four samples have a near constant M_n and increasing values of f_{PLA}, while the last three have an increasing M_n but a near constant

f_{PLA}. Small angle X-ray scattering was used to confirm that all of the samples formed a cylindrical morphology.

Table 6.1. Copolymer properties for each sample.

Sample Name	PS M_n (kg mol^{-1})	PLA M_n (kg mol^{-1})	PDI	f(PLA)
27k-26	26.6	11.0	1.05	0.26
27k-28	26.6	12.1	1.05	0.28
27k-30	26.6	13.3	1.05	0.30
27k-32	26.6	14.6	1.06	0.32
42k-25	41.6	15.4	1.05	0.27
52k-27	52.0	19.4	1.05	0.27
79k-25	70.5	24.3	1.09	0.26

6.3 Membrane Preparation

The procedure for preparing a membrane was the same for all the thin films, but the copolymer and solvent were varied. The casting procedure started by putting a clean dust-free glass plate on a level surface inside a fume hood. A 5 cm by 5 cm square of the microporous support membrane was cut from a larger sheet and floated on top of water in a Petri dish. The support sat on top of the water for 30 seconds allowing the water to wick into the pores. A noticeable change occurred once the membrane pores were wet – the initially opaque white membrane became a slightly translucent off-white. The support was then removed from the Petri dish, gently shaken to remove excess water and placed on top of the glass plate.

The membrane casting solution, prepared two hours prior to membrane fabrication, consisted of 8 wt% polymer dissolved in solvent. The time that it took for the solution to appear homogenous depended on the solvent quality and polymer molecular

weight, but never took longer than two hours. With the wetted support membrane in place, 1 mL of casting solution was dispensed onto the glass plate, and then drawn across the support membrane using a wire-wound rod. After the solvent was allowed to evaporate for 30 seconds, the glass plate was moved to a 60 ˚C oven where it was kept for 20 minutes. The oven was then turned down to 30 ˚C and the membrane left to dry overnight. The images on the left and right of Figure 6.1 show a scanning electron microscopy (SEM) image of the top surface of the support membrane and the composite membrane after the casting procedure, respectively.

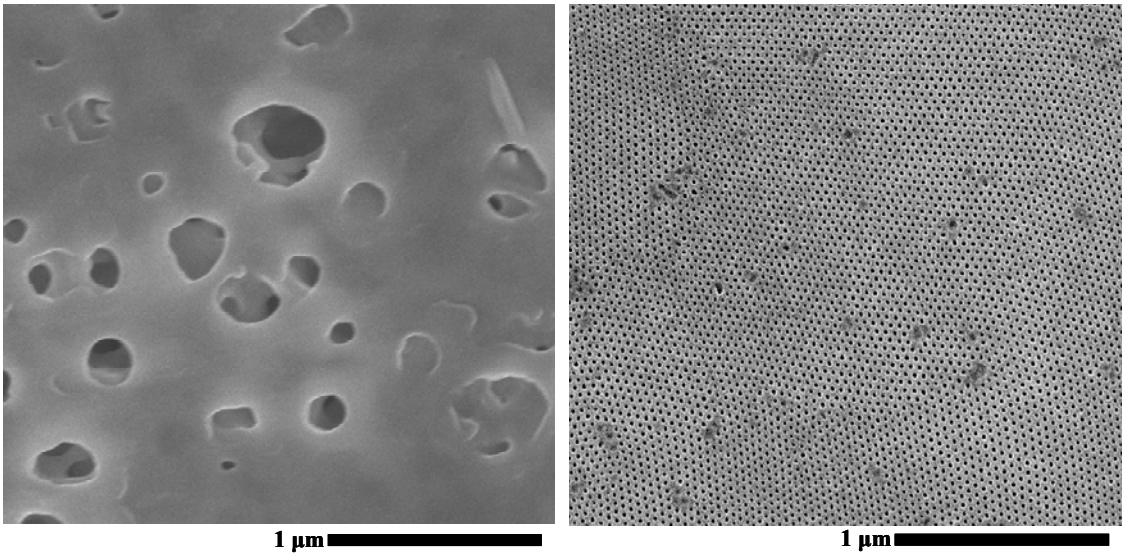

Figure 6.1: A Selective Copolymer Layer is Coated Onto a Microporous Support Membrane. The image on the left shows the structure of the polyether sulfone support membrane and the image on the right shows the monodisperse pores of the copolymer templated thin selective layer.

A few points should be made about this casting procedure. The solvents used for the casting solution were all water immiscible; therefore, the casting solution was excluded from the support's water filled pores. Once the solvent had evaporated, a thin

block polymer film was left sitting on top of the microporous support layer yielding the two layer composite structure we seek. Early attempts to make membranes were plagued by small cracks in the copolymer layer, which we attributed to residual stresses. By drying the film at 60 ˚C, the polymer remains above its glass transition temperature longer and the residual stresses are allowed to relax. Cooling the samples slowly by turning the oven to 30 ˚C and leaving them overnight allowed the stresses which arise from the difference in the coefficients of thermal expansion between the copolymer and support layer to be minimized. Once dried, the composite membrane was exposed to ultraviolet light (λ_{light} = 254 nm) for 20 min to improve the adhesion between the copolymer and microporous layers. This step was included because some films would delaminate during the etching process and compromise the mechanical stability. The UV exposure prevents this difficulty and also crosslinks the polystyrene block.[17] Following this procedure we could fabricate crack free membranes with areas greater than 100 cm^2.

The samples were then prepared either for inspection by SEM or for liquid flow and ultrafiltration experiments. Preparing a sample for SEM consisted of cutting a 1 cm by 1 cm piece from the larger sample, etching the polylactide block by submerging the sample in 0.5 M NaOH solution in 60:40 (v:v) methanol:water for 1 hour, and then transferring the sample to 60:40 (v:v) methanol:water for 30 min to rinse the base away. The samples were dried overnight and then coated with a 2-3 nm layer of gold prior to SEM to help prevent sample charging.

Sample preparation for transport measurements was more involved because the membranes were first checked for defects. A 2.5 cm diameter sample was punched out

from the 5 cm by 5 cm square using a hole punch. This disc was placed in an Amicon 8010 stirred cell and secured using a silicone O-ring. The cell was filled with 60:40 (v:v) methanol:water and a pressure drop of 25 psi was applied across the membrane using N_2 gas. If no flow was observed over a 3 hour period, the membrane was considered defect free and etching solution was put in the cell. The etching solution was left in the cell overnight to ensure all of the PLA was fully degraded. Water was then used to flush the membrane for 2 hours at a pressure drop of 25 psi, allowing the etching solution to be rinsed away before beginning liquid flow experiments. Because the etching solution contains methanol, the membranes are wet during the etching step and no pre-wetting steps are required. Liquid flow and solute rejection experiments were performed according to the procedures detailed in Chapter 2.

6.4 Results

The results of our experiments with cylinder forming PS-PLA copolymers will be discussed in three parts. First, our efforts to make large areas of membrane will be discussed. Producing large areas of membrane requires controlling the cylinder orientation. This is accomplished by selecting particular copolymers and solvents and then controlling the solvent evaporation rate. Second, we then turn to liquid water flow experiments. Liquid flow experiments allow the measurement of the pure water hydraulic permeability. We can compare our measured value with values predicted by Equation (6.2) and representative values for other UF membranes. Third, we conclude by probing

the practical value of the new block polymer templated composite membranes by measuring their ability to reject dissolved solutes.

Several research groups have been able to orient cylinders over large areas through the use of controlled solvent evaporation.[7, 18-21] This technique is particularly attractive for making UF membranes because controlling the solvent evaporation is already used for phase inversion casting techniques.[4-6] If successful on the lab scale, this method could be scaled up to produce square meters of membrane, instead of the square centimeters or smaller made in the lab.

6.4.1 Membrane Fabrication Results

Experiments attempting to orient the PLA cylinders begin by exploring the effects of solvent evaporation rate. Toluene and the 27k-26 sample were selected as the solvent-polymer pair with two evaporation rates, fast and slow. Fast evaporation was achieved by allowing the cast film to dry exposed to the ambient atmosphere. Such a sample took about 5 minutes to dry. To slow the evaporation rate, the sample was covered with a Petri dish directly after drawing the solution across the support. Drying such a sample took about 2 hours. Figure 6.2 shows representative SEM images of the membrane free surface for these two samples. The desired hexagonally packed perpendicular cylindrical structure is seen for the fast evaporation sample, while the slow evaporation rate produces a parallel cylinder structure. This suggests that the perpendicular cylinders which form are a kinetically trapped non-equilibrium structure. [7, 18-21] Further strengthening the argument that the perpendicular orientation is a non-equilibrium structure are SEM

images of a fast evaporation sample that has been dried and then annealed under a toluene atmosphere for 30 minutes. The resulting images look exactly like those of the slow evaporation samples, indicating that with enough time and mobility the polymer chains will rearrange to the thermodynamically favored parallel orientation.

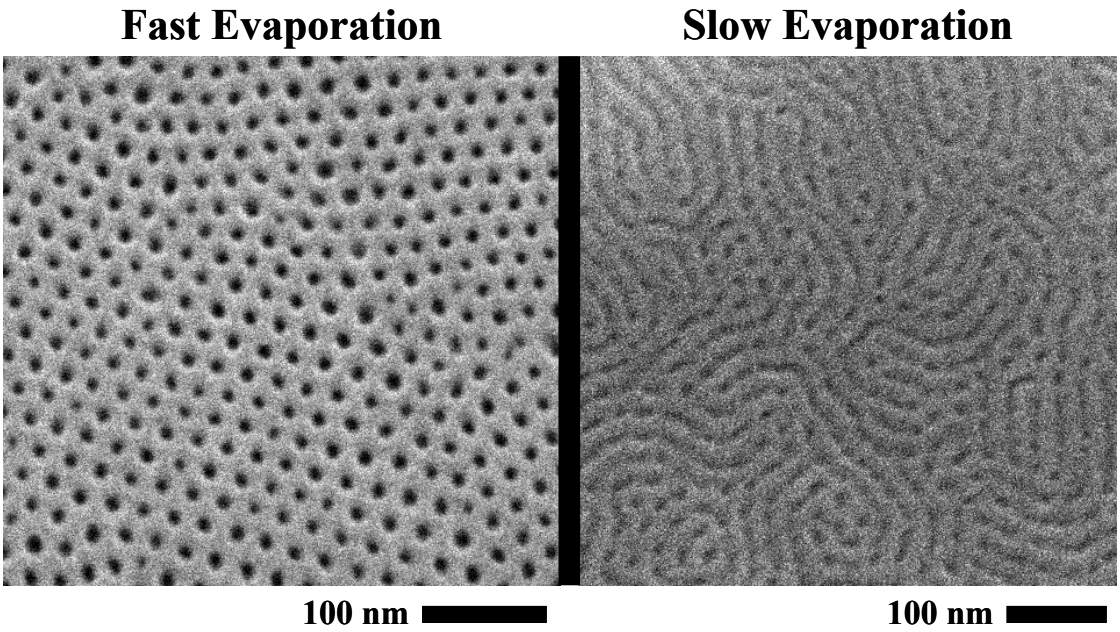

Figure 6.2: Fast Evaporation is Needed for Perpendicularly Oriented Cylinders. Evaporating toluene quickly kinetically traps the cylinders in a non-equilibrium perpendicular structure, while slow evaporation produces a parallel orientation.

Solvent selectivity has also been identified as a variable which influences the orientation of the cylinders.[7, 18] Motivated by this knowledge, we cast membranes with fast evaporation conditions using the 27k-26 copolymer sample and a variety of solvents with varying selectivity, assessed using the Hansen solubility parameters.[22] Figure 6.3 shows the volume dependent parameter δ_v, and hydrogen bonding parameter δ_h plotted for the different solvents as well as PS and PLA. This plot can be used to estimate

whether perpendicular cylinders will form.[22] Solvents which resulted in perpendicular cylinders, plotted as open circles, are PS selective because they are much further from the PLA point than the PS point. Membranes cast from the solvents represented by the filled squares had a mix of perpendicular and parallel orientations. Judging by their proximity to the PLA point these solvents are neutral. The difference between these two cases can be seen in Figure 6.4 where films cast from 1,1,2-tricholorethane and chloroform are shown.

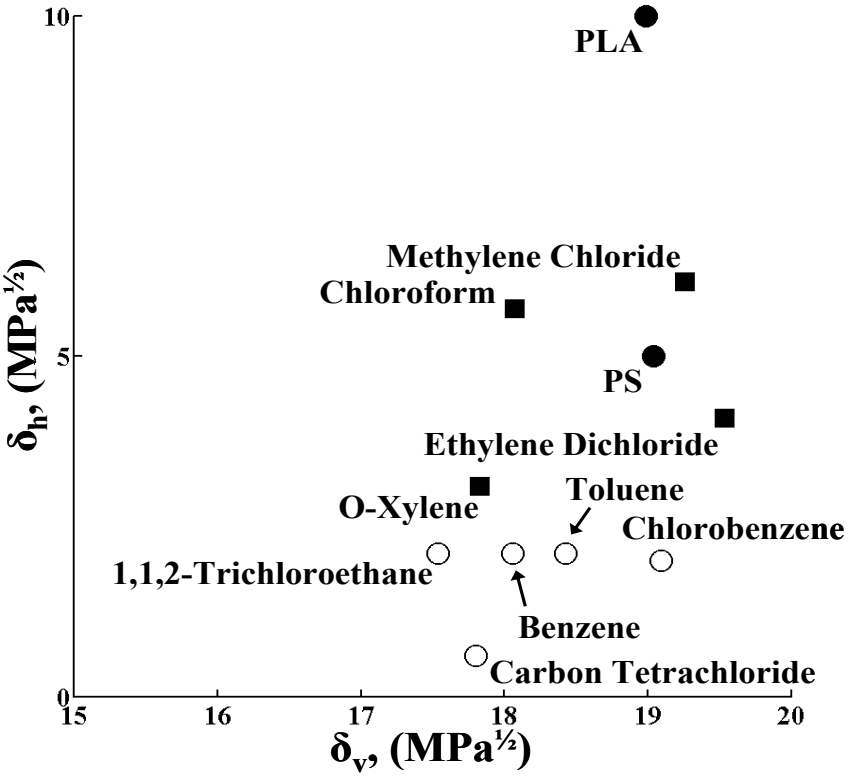

Figure 6.3: Hansen Solubility Parameters are Used to Determine Solvent Selectivity. The solvents which result in the formation of perpendicular cylinders are shown as open circles and the solvents that do not produce the desired orientation are shown as filled squares. The polymers which make up the block copolymer are shown as filled circles.

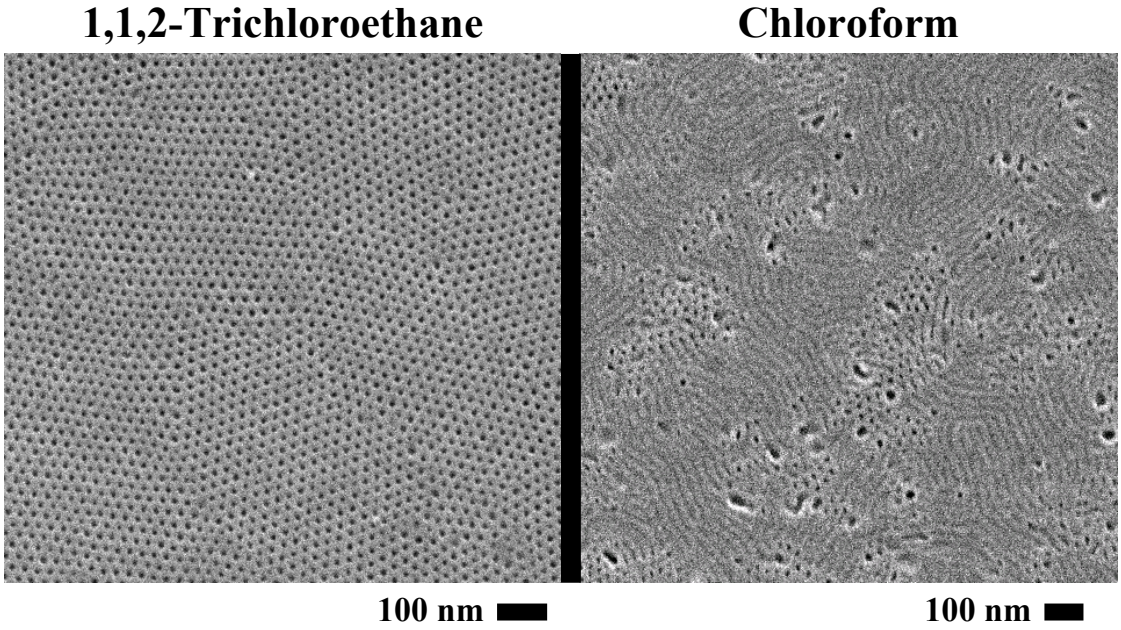

Figure 6.4: Perpendicular Cylinders Form From Polystyrene Selective Solvents. 1,1,2-trichloroethane a PS selective solvent allows perpendicular cylinders to be obtained, while a mixed orientation sample is produced when casting from the neutral solvent chloroform.

Another variable found to affect the orientation of cylinders is the volume fraction of polylactide.[23] To investigate this variable, PLA blocks of different molecular weight were grown from the same starting PS material. This process produced samples with nearly the same overall moleculer weight but with a PLA volume fraction ranging from 0.26 to 0.32. SAXS confirmed these samples all form the cylinder morphology in the bulk. Membranes cast using these different samples would exhibit a flip in orientation as the PLA volume fraction increased. The results for toluene, shown in Figure 6.5, are typical of what was observed. A small change in polylactide fraction from 0.26 to 0.28 results in a switch in the cylinder orientation. The same thing was observed for films cast from trichloroethane and chlorobenzene but the change in orientation occurred at the 0.28 to 0.30 and 0.30 to 0.32 change in PLA volume fraction, respectively. The influence of

the block volume fraction has been documented by researchers working with other systems, and while they use a different copolymer and alignment technique, their results also indicate the impact block volume fraction can have on orientation.[23]

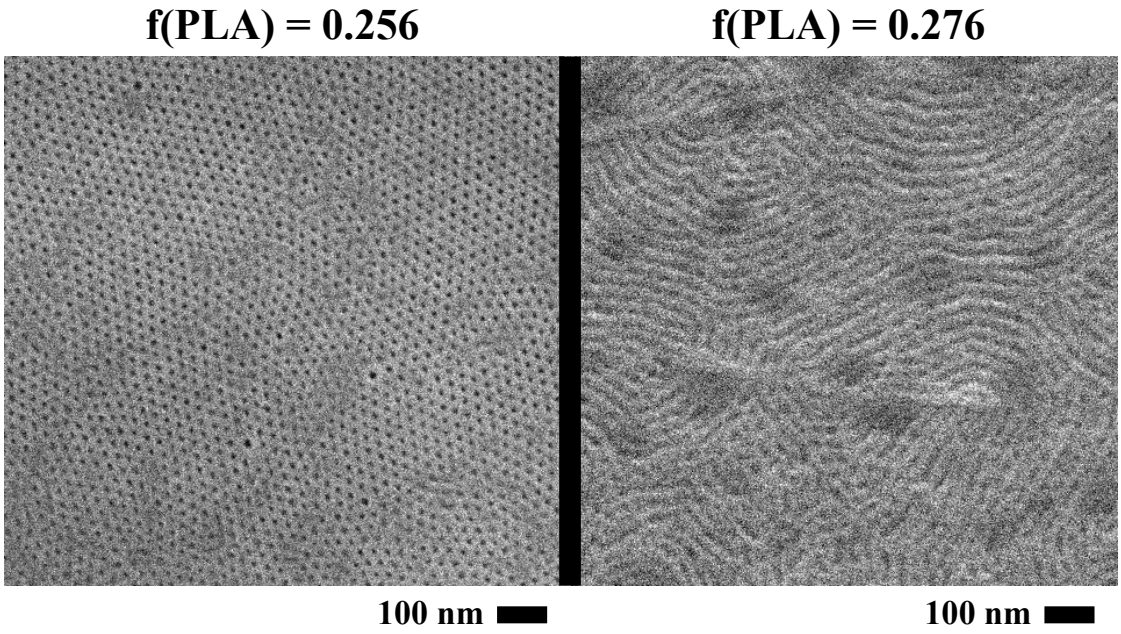

Figure 6.5: PLA Volume Fraction is Shown to Affect Orientation. Membranes were cast from toluene using two cylinder forming copolymer samples, but only the sample with the lower PLA volume fraction formed the perpendicular orientation.

The final copolymer property explored in this work is the effect the overall copolymer molecular weight has on the microstructure formed. Using fast evaporation conditions with 1,1,2-trichloroethane as the solvent, copolymer samples with PLA volume fractions between 0.25 and 0.27 but with different molecular weights were cast as membranes. Besides illuminating the effect molecular weight has on orientation, higher molecular weight samples were pursued in the hopes of increasing the mechanical stability of the final composite membranes. Sample 27k-26 and 42k-27 produce

hexagonally packed perpendicular cylinders as shown in the earlier SEM images. Figure 6.6 shows sample 52k-27 beginning to form what looks more like a dimpled structure. The sample does look like it has a hexagonally packed structure on the surface with some of the pores open and available for transport while others seem to be blocked by a continuous layer over the pore mouth. Sample 79k-25 also shown in Figure 6.6 makes this change to a dimpled structure more obvious with almost no pores being open.

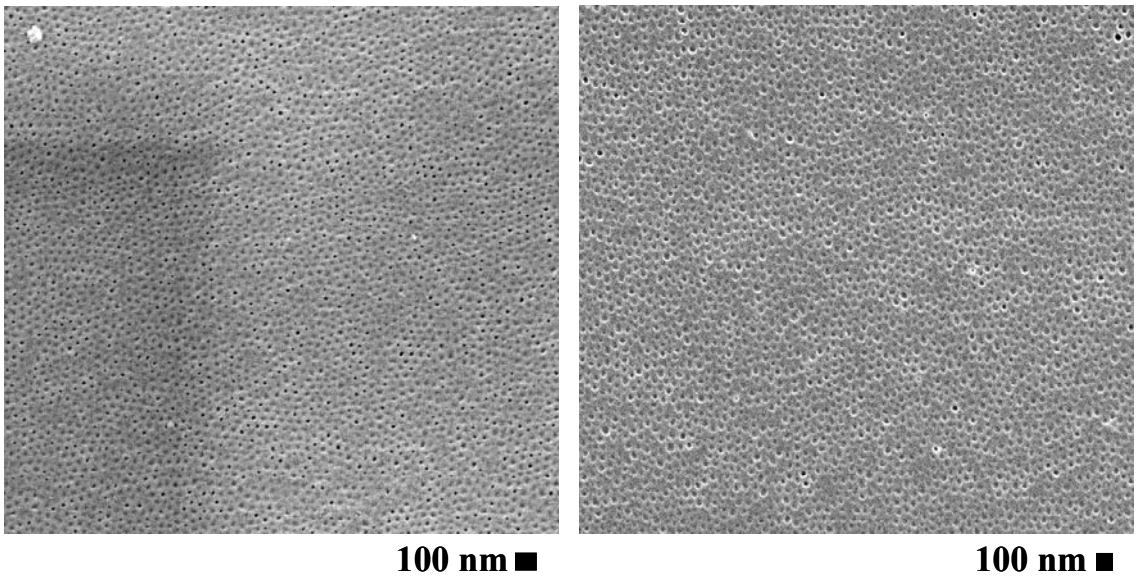

Figure 6.6: Higher Molecular Weight Samples Form "Pits" Not Pores. A small fraction of the cylinders form pores for the membrane cast from the 52k-27 sample, shown on the left. The number of pores formed for the membrane cast from the 71k-26 sample, on the right, is even smaller with most of the cylinders forming "pits".

6.4.2 Water Flow Experiments

Using the knowledge gained from exploring the effects of these different parameters, we were able to develop a technique to reproducibly make 100 cm^2 membrane areas that could be used for characterizing the transport properties of block

copolymer membranes. Specifically we measure liquid convection and solute rejection for a membrane made by casting the sample 42k-27 copolymer from the solvent 1,1,2-trichloroethane. The flux, in m^3 per m^2 sec, is plotted in Figure 6.7 vs. the pressure drop, in kPa. The linear relation expected from Equation (6.2) is observed. Using linear regression the pure water permeability (PWP) of the composite membrane is determined to be 1.15 liters/(m^2 hr bar) (LMH/bar).

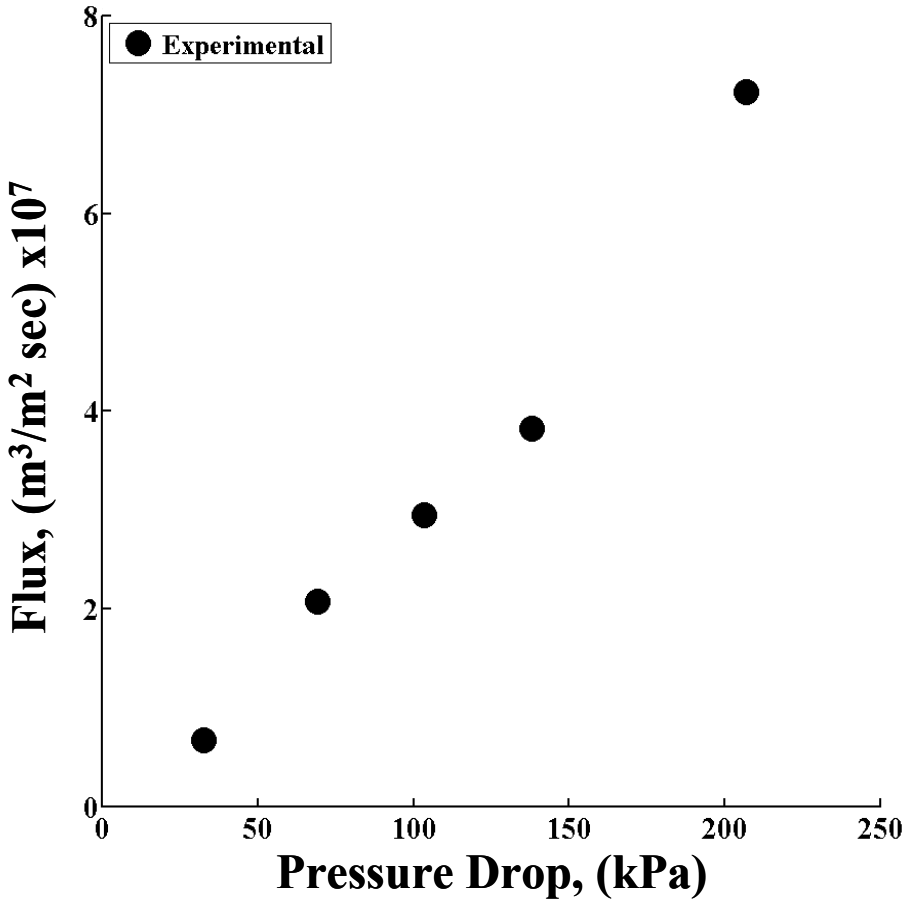

Figure 6.7: Pure Water Flux is Proportional to Pressure Drop. Experimentally observed fluxes for sample 42k-27 vary linearly with respect to pressure drop as predicted by Equation (6.2).

This experimentally determined PWP should be compared with several characteristic values. First, to ensure that the nanoporous polymer layer is the dominant resistance to mass transfer, we measured the PWP of the microporous support membrane. These experiments resulted in an average value of 3060 LMH/bar, over 3000 times that of the composite membrane. This indicates that flow through our nanopores is the dominant resistance to flow. Second, we compare our measured hydraulic permeability to that predicted by Equation (6.2). Assuming a pore diameter of 24.2 nm, a void fraction of 0.27 and a film thickness of 4 μm we predict a PWP of 450 LMH/bar, which is significantly higher than the experimental value.

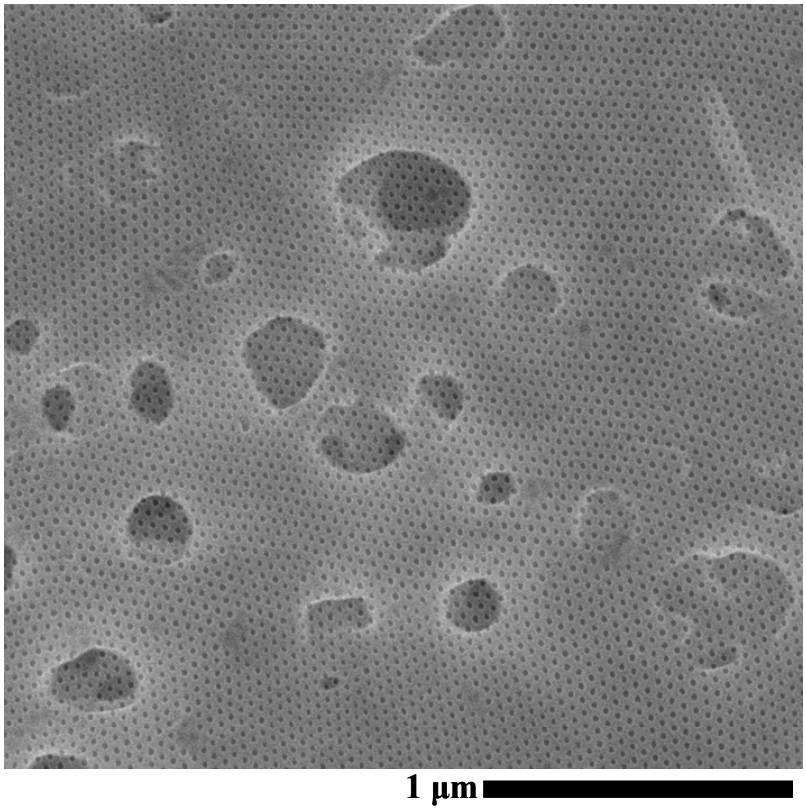

Figure 6.8: The Support Membrane Blocks The Nanopores. Pores in the selective layer must fall on top of a pore in the support membrane to be open for flow. This reduces the membrane's effective void fraction.

The structure of the composite membrane suggests several possible reasons for this observed difference. In Figure 6.8, we overlay the image on the right of Figure 6.1 onto the image from the left of Figure 6.1. By doing this, we can see that the structure of the support membrane results in a large number of nanopores being blocked. Only nanopores which fall on top of a pore in the support membrane will be available for flow.[6] This reduces the active void fraction from 0.27 to about 0.02.

Also, Equation (6.2) assumes right circular cylinders which span the entire membrane thickness. Although we assume perpendicular cylinders based on SEM images of the membrane top surface, the internal pore structure and bottom surface of the thin copolymer layer could be different. We explore both possibilities. Figure 6.9(a) shows an image where O_2 plasma reactive ion etching was used to expose a depth 100 nm into the copolymer layer. This image shows that the perpendicular cylinder orientation becomes a mixed perpendicular and parallel orientation somewhere in the bulk.[2] Using this technique to expose several different depths revealed that this transition occurred somewhere between 50 and 100 nm into the film. The change in orientation results in a tortuosity greater than 1 in Equation (6.2). Finally a film which delaminated during the etching step was flipped over so the bottom side morphology could be observed. Figure 6.9(b), a SEM image of this bottom surface, shows that not all the pores span the membrane's thickness.[7, 16] These factors suggest explanations for the difference between the experimentally measured PWP and the PWP anticipated from Equation (6.2).

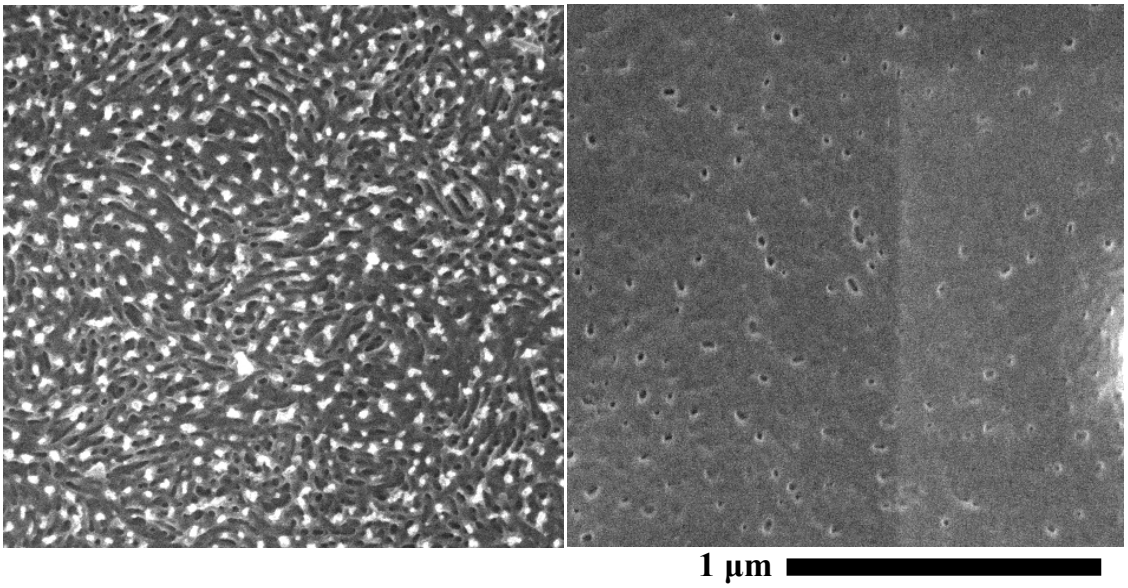

Figure 6.9: Flaws in the Membrane Reduce its Hydraulic Permeability. The SEM image on the left shows that the cylinders switch from a perpendicular to a mixed orientation 100 nm into the film. An image on the right, of the membrane backside, shows that not all the pores span the membrane thickness. These flaws explain the low flow rates observed.

6.4.3 Ultrafiltration Experiments

While the factors discussed in the previous paragraph may reduce the fluxes, neither the mixed morphology nor the reduced void fraction should inhibit the membranes' ability to selectively reject dissolved solutes. Because the dissolved solutes' sizes are on the same order of magnitude as the membrane pore size, the solutes should be at least partially retained. The membrane's ability to perform such a separation is described by the sieving coefficient S_a, defined as the concentration in the permeate $c_{1\ell}$ divided by that at the upstream membrane surface c_{10} (Equation (6.3)). In practical studies, the concentration at the membrane surface is replaced by the bulk upstream concentration, c_F. The bulk value is often lower than c_{10} due to concentration

polarization, where the ultrafiltration itself causes higher solute concentrations at the upstream membrane surface than in the bulk solution.[5, 13] By always making ultrafiltration experiments with rapid stirring, we avoid this complexity and measure the sieving coefficients of the membrane directly.

That the concentration polarization is negligible is supported by comparing the mass transfer coefficient of solute in the bulk solution, k, to the flux of the permeate, $\bar{v}$, across the membrane. The ratio of these values determines how closely the experimentally observed sieving coefficient reflects the membrane's actual sieving coefficient. Using the correlation given by Zeman and Zydney[5] for a stirred cell geometry at a stirring speed of 400 rpm, we calculate a mass transfer coefficient of 1.1 x 10^{-5} m/sec. This mass transfer coefficient and the filtrate flux at 150 kPa give a value for $\bar{v}/k$ of 0.05. At this flux and stirring speed, the system is not highly polarized and our experiments reflect the actual sieving coefficient.

These ultrafiltration experiments are summarized for a series of PEO solutes in Figure 6.10. The molecular weight of each solute is given next to each data point. The figure plots the percent rejected (1-S_a)x100 *vs* the solute diameter divided by the pore diameter, λ. The solute diameters, defined as two times the hydrodynamic radius are estimated as a function of molecular weight from tracer diffusion and intrinsic viscosity measurements given in the literature. The pore diameter is taken as a constant 24.2 nm, determined from the primary SAXS peak.[24, 25]

As expected, the rejection of the 14 kDa sample is small, around 15 percent; it increases with solute molecular weight until the rejection of the 100 kDa sample is near

complete, over 93 percent. Figure 6.10 also shows that the solute percent rejections of the microporous support alone are less than 5 percent, indicating that the block polymer layer is filtering the dissolved PEO solutes.

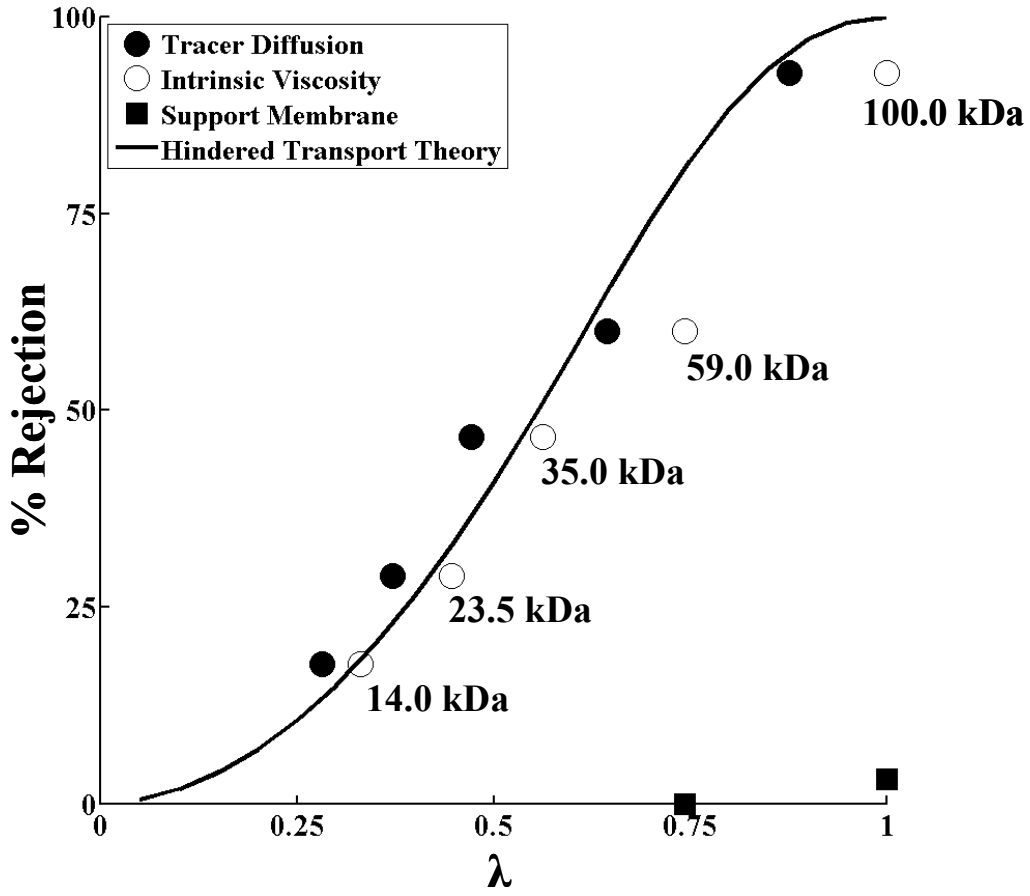

Figure 6.10: The Nanoporous Polystyrene Layer Rejects PEO Solutes as Expected. Single solute PEO solutions were used to challenge a composite membrane made using polymer sample 42k-27. The resulting rejection curve (filled and open circles) is compared with the predicted curve (solid line) using the hindrance coefficients of Brenner[11] for a 24.2 nm pore. The support membrane alone (filled squares) did not reject a significant percentage of the PEO molecules in this size range.

The curve shown in Figure 6.10 is not a best fit of the data, but a prediction without adjustable parameters based on Equation (6.3). This prediction depends on the

membrane thickness, on the fluid velocity, on the solute diffusion coefficient, and on the ratio of solute diameter to pore diameter λ, that is, on the values on the abscissa of Figure 6.10. From values of λ, we find the parameters K_c and K_d, using the equations developed by Bungay and Brenner[11] and then can calculate the curve in Figure 6.10. The agreement of this curve with the experimental results implies that the membrane pores are nearly monodisperse and reproducible across membranes made from the same polymer sample.

6.5 Discussion

Two features of our results warrant further discussion. First, based on the results from our work and that of other researchers who have used controlled solvent evaporation rates to align cylinders, we can develop a theory about how perpendicular cylinders form. Second, we discuss the potential block polymer thin films have as ultrafiltration membranes.

6.5.1 Perpendicular Cylinder Formation

In our attempts to produce large areas of membrane, several parameters affecting cylinder orientation in the PS-PLA system were explored. Varying the solvent evaporation rate suggested the perpendicular orientation is a kinetically trapped structure with the parallel orientation being the thermodynamically preferred equilibrium. This result is consistent with the findings of many other researchers. [7, 18-21] Another result common to our work and that done in other labs is that solvents selective for the majority PS block lead to perpendicular cylinders, whereas the use of neutral solvents leads to

mixed or parallel orientations.[7, 18] Also, SEM images show that above a certain molecular weight, the structure formed after PLA degradation still appears hexagonally close packed, like perpendicular cylinders, but resembles pits instead of pores. Similar results were seen in experiments using mixed solvents in the casting solution.[26] Another study which explicitly looked at molecular weight effects used SPM prior to PLLA degradation to examine the thin film's surface morphology and does not comment on a difference between pores and pits.[7] The final variable modified in this study was the volume fraction of the minority PLA block.[23] Interestingly, not all the samples which form cylinders in the bulk orient in the same direction when cast using the same procedure. In general, as the PLA volume fraction was increased, the cylinders transition from a perpendicular orientation to a parallel orientation.

These results lead us to speculate on the reason that perpendicular cylinders form. When dissolved in the casting solution, the PS-PLA copolymer is disordered because the solvent mediates the unfavorable interactions between the two blocks.[27-29] Once the solution is cast onto the microporous support and the solvent begins evaporating, the solvent concentration at the air-solution interface approaches zero because the atmospheric solvent concentration is zero. As the solvent concentration at the free surface decreases, one of two things can occur. First, the solvent concentration can decrease slowly such that the strength of the unfavorable interactions between the blocks increases until the copolymer reaches the order-disorder transition and a microphase separation occurs. Second, the loss of solvent can occur so quickly that the copolymer does not have time to rearrange and hence a disordered copolymer structure is trapped.

To understand which event occurs, we consider the rate constants which govern the two processes. First, for the microphase separation to occur, the polymer chains must rearrange. In the case of slightly entangled chains, this rearrangement occurs by the mechanism proposed in the Rouse model.[30] For this model, the rate constant for an ordering front moving into a disordered phase is the quotient R_g/τ, that is, the copolymer radius of gyration R_g divided by its longest relaxation time τ. In the second process, due to the decreased solvent concentration, the polymer mobility would be drastically reduced below the surface and within the film. The characteristic rate constant for this process is the solvent mass transfer rate out of the film. This rate constant is given by the sum of the gas phase resistance to mass transfer k_{gas}/H and the solution phase resistance to mass transfer D/ℓ where k_{gas} is the solvent mass transfer coefficient in the gas phase, H is the partition coefficient between the gas and solution phases, D is the diffusion coefficient in solution and ℓ is the thickness of the thin polymer skin that controls diffusion.[8, 9] This thickness will grow as a function of time t, given by $\ell = \sqrt{2Dt}$.[31] Writing these two rate constants as a second Damköhler number Da, the ratio of the ordering front velocity to the solvent mass transfer velocity, gives:

$$Da = \frac{\text{polymer ordering velocity}}{\text{solvent mass transfer velocity}} = \frac{R_g}{\tau}\left(\sqrt{\frac{2t}{D}} + \frac{H}{k_{gas}}\right) \tag{6.4}$$

When this number is greater than one, an ordered microphase will grow following a nucleation and growth mechanism into the film. When this number is smaller than one, the copolymer will be trapped as a disordered structure. For a system with no gas phase

resistance to mass transfer, using characteristic values of R_g = 10 nm, τ = 0.001 sec and D = $1x10^{-7}$ cm^2/sec and assuming that the transition between the two mechanisms occurs when the Damköhler number is one, we find that in the PS-PLA system all the solvent would need to evaporate in 5 seconds to trap a disordered structure. Because it isn't, we get the growth of an ordered microstructure. For polymers with longer relaxation times, such as triblock copolymers[32] or high molecular weight samples,[30] this limit would increase and a disordered structure could be observed. The disordered segregated phase seen by other researchers could be explained by this transition between mechanisms.[18, 33]

Thus we believe that perpendicular cylinders grow through a nucleation and growth mechanism that begins at the free surface. It is useful to consider the exact copolymer structure that nucleates when the order-disorder transition is reached. We suspect that, the phase separation first forms body centered cubic (BCC) spheres. The BCC spheres then grow through epitaxial relationships to form either perpendicular or parallel cylinders depending on the solvent evaporation rate. The need to use PS selective solvents, the transition from a perpendicular to a parallel orientation with increasing PLA volume fraction, and the SEM images obtained with higher molecular weight samples influence this suspicion.

With this basic picture, we now can consider how the mechanism will be affected by different chemistry. The phase transitions of block copolymers in the presence of solvents with varying selectivities have been studied extensively.[28, 34-37] We are interested in two cases: neutral solvents and solvents selective for the majority block. For a neutral solvent, increasing and decreasing the solvent concentration can be pictured as moving

up and down a vertical trajectory[28, 35] on the χN vs. f_{PLA} phase plot, because the solvent swells both blocks equally and dilutes the unfavorable interactions. Such a trajectory is shown in Figure 6.11. As the solvent begins to evaporate from a casting solution made using a neutral solvent, the copolymer will phase separate into a cylindrical structure once the spinodal is hit. When the cylinders precipitate, they do so with mixed orientation. The solvent concentration gradient is not strong enough to subsequently align the cylinders perpendicular to the membrane surface. Instead, the cylinders remain a mix of perpendicular and parallel orientations as seen for chloroform in Figure 6.4.

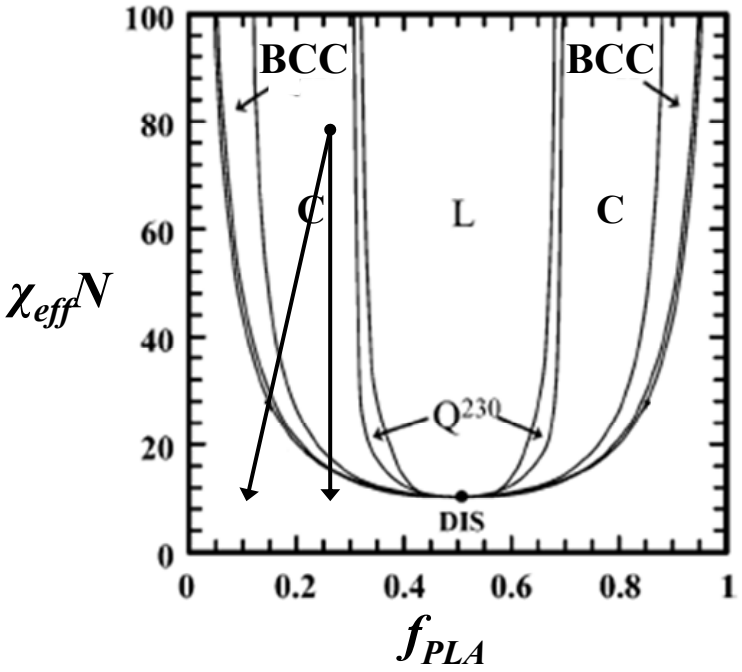

Figure 6.11: Trajectories for a Neutral and a PS Selective Solvent on the Copolymer Phase Plot. Using a neutral solvent dilutes the unfavorable interactions between the vertical trajectory shown, while a selective solvent dilutes the interactions and selectively swells one block, resulting in the diagonal trajectory. The diagonal trajectory passes through a larger window of the BCC sphere phase.

The situation is different for a selective solvent. Now the trajectory follows a diagonal path because along with diluting the unfavorable interactions, the solvent selectively swells one of the blocks thereby changing the effective volume fraction.[27-29, 35] For a plot of χN vs. f_{PLA} using a PS selective solvent to dissolve the PS-PLA copolymer is analogous to moving down and to the left on the phase plot, as is also shown in Figure 6.11. This moves the copolymer through a larger BCC spheres window. As solvent evaporates from this solution, once the spinodal is reached, BCC spheres form because of the modified volume fraction.[35, 38-40] These spheres do not have a preferred direction of

growth (i.e., they are 0-dimensional). If the polymer mobility is high enough when the transition from spheres to cylinders takes place, the spheres grow epitaxially along the solvent concentration gradient, into perpendicular cylinders. If the polymer does not have a high enough mobility to grow from spheres into cylinders, the BCC spheres would be the kinetically trapped phase. This may explain the dimpled structure we observe when casting membranes from the 52k-27 and 79k-25 samples.

That perpendicular cylinders grow through a spherical intermediate is also supported by the dependence of orientation on the volume fraction of the PLA block. As the size of the PLA block increases, the entropic penalty paid to form BCC spheres would become so great that the polymer would transition from a disordered phase directly to a cylindrical structure. This direct transition, similar to when using a neutral solvent, would result in non-perpendicular cylinders, as observed in Figure 6.5.

The final aspect related to cylinder orientation is how fast solvent evaporation leads to perpendicular cylinders and slow solvent evaporation produces parallel cylinders. To do this, we use the expression developed by Goveas and Milner,[41] which predicts the rate at which an ordered block copolymer phase will advance into a metastable disordered phase. This velocity, developed explicitly for a system with a single nucleation event that has already occurred, is given by

$$\frac{\partial \ell_{OD}}{\partial t} = \frac{R_g}{\tau}\left(\chi N - \chi N_{OD}\right) g\left(f_{PLA}\right) \tag{6.5}$$

where ℓ_{OD} is the thickness of the ordered phase and t is the time. The product of χ, the polymer-polymer Flory-Huggins interaction parameter, and N, the overall degree of

polymerization, is known as the segregation strength. This product has a value of χN_{OD} at the order disorder transition. The factor $g(f_{PLA})$, a constant of order one, depends on the copolymer composition. This expression should be valid for the PS-PLA system as long as $Da \gg 1$.

The experimental work done validating Equation (6.5) was based on a uniformly metastable disordered phase produced by a thermal quench.[41-44] In our case of solvent evaporation, the disordered phase forms as a result of the solvent concentration gradient that develops due to evaporation. This directional variation is what results in perpendicular cylinders forming.

We can see why directionality results in perpendicular cylinders by considering the variations with solvent of the terms in Equation (6.5). The quantity $g(f_{PLA})$ is an order one constant that has no effect on orientation. The other two groups of terms, R_g/τ and $(\chi N - \chi N_{OD})$, are what affect orientation. These terms can be regarded as a rate constant and the copolymer's degree of supersaturation, respectively. When the solvent concentration is high, R_g/τ is large and $(\chi N - \chi N_{OD})$ is small. When the solvent concentration is low, the reverse is true. How the product of these two groups varies as function of position (i.e., $\frac{\partial^2 \ell_{OD}}{\partial z \partial t}$) within the thin films dictates the direction in which the cylinders will grow. If $\frac{\partial^2 \ell_{OD}}{\partial z \partial t}$ is positive, growth of the cylinders into the film is faster, and perpendicular cylinders form. If $\frac{\partial^2 \ell_{OD}}{\partial z \partial t}$ is negative, the growth of cylinders is faster

in the plane of the ordering front, driving the cylinders to form parallel to the thin dimension.

For the case of an evaporating solvent, we can be more explicit about the variables which impact the sign of $\frac{\partial^2 \ell_{OD}}{\partial z \partial t}$ by expressing it in the form of Equation (6.6)

$$\frac{\partial^2 \ell_{OD}}{\partial z \partial t} = R_g g(f_{PLA}) \left(\frac{\partial \phi_1}{\partial z} \right) \left[\frac{\partial \left(1/\tau \left(\chi N - \chi N_{OD} \right) \right)}{\partial \phi_1} \right] \tag{6.6}$$

where ϕ_1 is the solvent volume fraction. Writing Equation (6.6) in this form ignores the weak depence of R_g on solvent concentration, and factors out $\frac{\partial \phi_1}{\partial z}$ because this term will always be positive and so has no effect on the sign of $\frac{\partial^2 \ell_{OD}}{\partial z \partial t}$. The term in the square bracket determines the sign of the whole expression and hence the resulting orientation. Using the chain rule, the term in the square bracket Δ can be written as

$$\Delta = \frac{1}{\tau} \frac{\partial \left(\left(\chi N - \chi N_{OD} \right) \right)}{\partial \phi_1} + \left(\chi N - \chi N_{OD} \right) \frac{\partial \left(1/\tau \right)}{\partial \phi_1} \tag{6.7}$$

To estimate the longest relaxation times as a function of solvent concentration, PS self diffusion data from Wesson[45] and the radius of gyration of a polymer chain[30] was used. These data were fit using an exponential function:

$$\tau = \frac{R_g^2}{D_s} = \tau_o \exp(-a\phi_1) \tag{6.8}$$

A modified version of the dilution approximation is used to estimate the segregation strength as a function of solvent concentration

$$\chi_{eff} N = \chi_{AB} N \left(1-\phi_1\right)^{1.3} \tag{6.9}$$

where the melt phase segregation strength is scaled with the polymer volume fraction. The exponent of 1.0 from the dilution approximation is replaced by 1.3 to account for the fact that the solvent is better at disrupting ordered structures than anticipated.[29, 46] These estimates are used in Equation (6.7) to produce the following expression where the common terms have been factored out because they do not affect the expression's sign.

$$\Delta = \left(-1.3\left(1-\phi_1\right)^{0.3}\right) + a\left(\left(1-\phi_1\right)^{1.3} - \left(1-\phi_{1,OD}\right)^{1.3}\right) \tag{6.10}$$

When *z* is positive, perpendicular cylinders will form.

We now look at the contributions to Δ. The first term, a result of the degree of polymer supersaturation varying with concentration, is always negative and so favors parallel cylinders. The second term, which results from the variation of the relaxation time with solvent concentration, can be positive, and so produces perpendicular cylinders. This makes physical sense. The degree of supersaturation decreases further into the film, favoring growth in the plane of the ordering front. The increase in polymer mobility in the regions of higher solvent concentration must be large enough to result in an increasing growth rate. We can estimate how large the variation of polymer relaxation time *a* needs to be to drive perpendicular cylinders by equating Equation (6.10) to zero, the value at which the transition from perpendicular to parallel cylinders occurs, and solving for *a*:

$$a \geq \frac{1.3\left(1-\phi_1\right)^{0.3}}{\left(1-\phi_1\right)^{1.3} - \left(1-\phi_{1,OD}\right)^{1.3}} \tag{6.11}$$

At a given location in the thin film, if the left side of Equation (6.11) is greater than the right side, the solvent concentration gradient will favor perpendicular cylinders.

6.5.2 The Potential of PS-PLA as Ultrafilters

The general framework presented above for understanding this phenomenon is encouraging because it suggests how the technique can be applied to other copolymer systems. In particular, more mechanically robust copolymers can be used to explore the potential for ultrafiltration (UF). Discussing this potential, it is helpful to remember UF membranes are judged by three criteria: selectivity, flux and resistance to fouling. The results in Figure 6.10 show the superior selectivity of PS-PLA templated membranes. Like the results in Chapter 4, the experimental data match existing theories for cylindrical pores. The nanoporous copolymer rejection curve is expected to be much sharper than the curve for traditional phase inversion membranes.[47] By controlling the PLA molecular weight, we can also control the pore size and hence selectivity.[47]

However, these positive results are accompanied by concerns with low fluxes, poor mechanical properties and possible fouling. Currently, the PS-PLA selective layer is cast onto a PES support membrane. The PES support, selected because its tight structure, provides the reinforcement required to keep the nanoporous PS intact. However, because of the tight structure, the PES support has a low void fraction blocking a large number of selective layer's pores. Combined with not all the pores spanning the selective layer thickness, this results in a significant decrease of the membrane's effective void fraction. The low fluxes observed are likely a direct consequence of this reduced void fraction.

Increasing the effective void fraction in order to realize the high fluxes promised by the cylindrical morphology is a high priority. Methods already exist for dealing with the void fraction reduction that results from the tight support layer.[5, 6, 33] Also, the understanding of why fast solvent evaporation rates lead to perpendicular cylinders suggests more pores can be forced to span the selective layer. Modifying the support membrane to access more of the selective layer pores should be attempted. One technique involves coating a gutter layer onto the existing PES support layer. The gutter layer, a 2-5 nm thick layer with a void fraction around 70-80 percent, serves as a manifold, rerouting flow from the pores in the selective layer to the pores of the support membrane. Using a gutter layer, already common practice when fabricating gas permeation membranes, could readily be done to our PS-PLA system. [5, 6, 33]

However, the fragility of PS-PLA is a concern regardless of how the support is modified. The nanoporous PS that remains after etching is only three to four times the entanglement molecular weight of PS,[30] so the selective layer is brittle. A higher order block polymer (e.g., polystyrene-b-polyisoprene-b-polystyrene-b-polylactide (PS-PI-PS-PLA) or polylactide-b-polystyrene-b-polyisoprene-b-polystyrene-b-polylactide (PLA-PS-PI-PS-PLA)) would leave a porous PS-PI-PS matrix after etching. This would have improved mechanical properties.[48] While we do not currently know how to align the cylinders in this material, we hope the framework proposed above can be extended to these systems. We could then access more pores in the selective layer by using an open porous support membrane without a gutter layer.

A more pressing concern is forcing all the copolymer templated pores to span from the top surface of the selective layer to the bottom surface. Presently, the four micron selective layer is too thick and the interaction energy between the support and copolymer dominates at the bottom surface. The theory proposed above implies that coating a thinner selective layer will result in more perpendicular cylinders spanning the selective layer. Moving deeper into the film decreases the driving force forming perpendicular cylinders, so they start to form a mixed orientation. This is observed for the PS-PLA system around 100 nm. This suggests coating a layer between 100 to 500 nm thick. A selective layer should be around 500 nm thick because films thinner than this result in the support layer being the dominant resistance to flow. In this situation, the support layer also influences the composite membrane's ability to perform a selective separation. [5, 6, 33] This should be avoided due to the superior selectivity of the nanoporous copolymer. Another technique that could potentially force pores to span the selective layer is to modify the surface energy of the substrate which the thin film is cast onto (i.e., the microporous support). This method has been used successfully by other research groups, but for nonporous supports.[2, 3, 23]

Finally, the superior selectivity and higher fluxes promised for these easily fabricated membranes may be lost if the membranes foul easily. There is some reason to expect that they will: the hydrophobic matrix which remains has been shown to foul easily when treating surface water. At the same time, the overall surface of the membranes appears on a micrometer scale to be much smoother than existing

ultrafiltration membranes[49] and the potential to modify the surface with PEO brushes exists.[50] Therefore it is critical to experimentally probe the fouling of these membranes.

6.6 References

(1) Phillip, W. A.; Rzayev, J.; Hillmyer, M. A.; Cussler, E. L. *Journal of Membrane Science,* **2006***, 286*, 144-152.

(2) Yang, S. Y.; Park, J.; Yoon, J.; Ree, M.; Jang, S. K.; Kim, J. K. *Adv.Funct.Mater.* **2008***, 18*, 1371-1377.

(3) Yang, S. Y.; Ryu, I.; Kim, H. Y.; Kim, J. K.; Jang, S. K.; Russell, T. P. *Adv.Mater.(Weinheim, Ger.)* **2006***, 18*, 709-712.

(4) Peinemann, K.; Abetz, V.; Simon, P. F. W. *Nat Mater* **2007***, 6*, 992-996.

(5) Zeman, L. J.; Zydney, A. L. In *Microfiltration and ultrafiltration : principles and applications;* M. Dekker: New York, 1996; , pp 618.

(6) Baker, R. W. In *Membrane technology and applications;* J. Wiley: Chichester ; New York, 2004; , pp 538.

(7) Ho, R.; Tseng, W.; Fan, H.; Chiang, Y.; Lin, C.; Ko, B.; Huang, B. *Polymer* **2005***, 46*, 9362-9377.

(8) Bird, R. B.; Stewart, W. E.; Lightfoot, E. N. In *Transport phenomena;* J. Wiley: New York, 2002; , pp 895.

(9) Cussler, E. L. In *Diffusion, mass transfer in fluid systems;* Cambridge University Press: New York, 2009; , pp 654.

(10) Dullien, F. A. L. In *Porous media : fluid transport and pore structure;* Academic Press: San Diego, 1992; , pp 574.

(11) Bungay, P. M.; Brenner, H. *Int. J. Multiphase Flow* **1973***, 1*, 25.

(12) Deen, W. M. *AICHE J.* **1987***, 33*, 1409-1425.

(13) Mehta, A.; Zydney, A. L. *J. Membr. Sci.* **2005***, 249*, 245-249.

(14) Zalusky, A. S.; Olayo-Valles, R.; Wolf, J. H.; Hillmyer, M. A. *J. Am. Chem. Soc.* **2002***, 124*, 12761-12773.

(15) Zalusky, A. S.; Olayo-Valles, R.; Taylor, C. J.; Hillmyer, M. A. *J. Am. Chem. Soc.* **2001***, 123*, 1519-1520.

(16) Olayo-Valles, R.; Guo, S.; Lund, M. S.; Leighton, C.; Hillmyer, M. A. *Macromolecules* **2005***, 38*, 10101-10108.

(17) Thurn-Albrecht, T.; Schotter, J.; Kastle, G. A.; Emley, N.; Shibauchi, T.; Krusin-Elbaum, L.; Guarini, K.; Black, C. T.; Tuominen, M. T.; Russell, T. P. *Science (Washington, D.C.); Science (Washington, D.C.)* **2000***, 290*, 2126-2129.

(18) Kim, G.; Libera, M. *Macromolecules* **1998***, 31*, 2569-2577.

(19) Kim, S.; Briber, R. M.; Karim, A.; Jones, R. L.; Kim, H. *Macromolecules (Washington, DC, U.S.); Macromolecules (Washington, DC, United States)* **2007***, 40*, 4102-4105.

(20) Kim, S. H.; Misner, M. J.; Xu, T.; Kimura, M.; Russell, T. P. *Adv.Mater.(Weinheim, Ger.); Advanced Materials (Weinheim, Germany)* **2004***, 16*, 226-231.

(21) Lin, Z.; Kim, D. H.; Wu, X.; Boosahda, L.; Stone, D.; LaRose, L.; Russell, T. P. *Adv.Mater.(Weinheim, Ger.); Advanced Materials (Weinheim, Germany)* **2002***, 14*, 1373-1376.

(22) Hansen, C. M. In *Hansen solubility parameters : a user's handbook;* CRC Press: Boca Raton, Fla., 2000; , pp 208.

(23) Ryu, D. Y.; Ham, S.; Kim, E.; Jeong, U.; Hawker, C. J.; Russell, T. P. *Macromolecules (Washington, DC, U.S.); Macromolecules (Washington, DC, United States)* , ACS ASAP.

(24) Koppi, K. A.; Tirrell, M.; Bates, F. S.; Almdal, K.; Mortensen, K. *J.Rheol.(N.Y.); Journal of Rheology (New York, NY, United States)* **1994***, 38*, 999-1027.

(25) Hamley, I. W.; Castelletto, V. *Prog.Polym.Sci.; Progress in Polymer Science* **2004***, 29*, 909-948.

(26) Park, S.; Wang, J.; Kim, B.; Chen, W.; Russell, T. P. *Macromolecules (Washington, DC, U.S.); Macromolecules (Washington, DC, United States)* **2007***, 40*, 9059-9063.

(27) Lodge, T. P.; Hamersky, M. W.; Hanley, K. J.; Huang, C. *Macromolecules* **1997***, 30*, 6139-6149.

(28) Lodge, T. P.; Hanley, K. J.; Pudil, B.; Alahapperuma, V. *Macromolecules* **2003***, 36*, 816-822.

(29) Naughton, J. R.; Matsen, M. W. *Macromolecules* **2002***, 35*, 5688-5696.

(30) Hiemenz, P. C., Lodge, T. In *Polymer chemistry;* CRC Press: Boca Raton, FL, 2007; pp 608.

(31) Crank, J. In *The mathematics of diffusion;* Clarendon Press: Oxford, Eng, 1975; , pp 414.

(32) Lodge, T. P.; Blazey, M. A.; Liu, Z.; Hamley, I. W. *Macromol.Chem.Phys.; Macromolecular Chemistry and Physics* **1997***, 198*, 983-995.

(33) Ho, W. S. W.; Sirkar, K. K. In *Membrane handbook;* Kluwer Academic Pub.: Boston, 2001; , pp 954.

(34) Lodge, T. P.; Hanley, K. J.; Huang, C.; Ryu, C. In *In Order-order and order-disorder transitions in block copolymer solutions and melts.* 1998; , pp PMSE-290.

(35) Lodge, T. P.; Pudil, B.; Hanley, K. J. *Macromolecules* **2002***, 35*, 4707-4717.

(36) Lodge, T. P.; Xu, X.; Ryu, C. Y.; Hamley, I. W.; Fairclough, J. P. A.; Ryan, A. J.; Pedersen, J. S. *Macromolecules* **1996***, 29*, 5955-5964.

(37) Lodge, T. P.; Hanley, K. J.; Huang, C.; Ryu, C. Y. *Polym.Mater.Sci.Eng.; Polymeric Materials Science and Engineering* **1998***, 79*, 377.

(38) Sota, N.; Sakamoto, N.; Saijo, K.; Hashimoto, T. *Polymer* **2006***, 47*, 3636-3649.

(39) Sota, N.; Sakamoto, N.; Saijo, K.; Hashimoto, T. *Macromolecules* **2003***, 36*, 4534-4543.

(40) Sakamoto, N.; Hashimoto, T. *Macromolecules* **1998***, 31*, 8493-8502.

(41) Balsara, N. P.; Garetz, B. A.; Chang, M. Y.; Dai, H. J.; Newstein, M. C.; Goveas, J. L.; Krishnamoorti, R.; Rai, S. *Macromolecules* **1998***, 31*, 5309-5315.

(42) Chastek, T. Q.; Lodge, T. P. *J. Polym. Sci. Part B* **2006***, 44*, 481-491.

(43) Chastek, T. Q.; Lodge, T. P. *Macromolecules* **2004***, 37*, 4891-4899.

(44) Kim, W. G.; Garetz, B. A.; Newstein, M. C.; Balsara, N. P. *J. Polym. Sci. Part B* **2001***, 39*, 2231-2242.

(45) Wesson, J. A.; Noh, I.; Kitano, T.; Yu, H. *Macromolecules* **1984***, 17*, 782-792.

(46) Lodge, T. P.; Blazey, M. A.; Liu, Z.; Hamley, I. W. *Macromol.Chem.Phys.; Macromolecular Chemistry and Physics* **1997***, 198*, 983-995.

(47) Phillip, W. A.; Amendt, M.; O'Neill, B.; Chen, L.; Hillmyer, M. A.; Cussler, E. L. *ACS Applied Materials & Interfaces* **2009***, 1*, 472-480.

(48) Meuler, A. J.; Fleury, G.; Hillmyer, M. A.; Bates, F. S. *Macromolecules (Washington, DC, U.S.); Macromolecules (Washington, DC, United States)* **2008***, 41*, 5809-5817.

(49) Zhu, X.; Elimelech, M. *Environ. Sci. Technol.* **1997***, 31*, 3654-3662.

(50) Asatekin, A.; Kang, S.; Elimelech, M.; Mayes, A. M. *J. Membr. Sci.* **2007***, 298*, 136-146.

Chapter 7: Strength and Weaknesses of and Challenges for Block Polymer Membranes

In this work we hoped to use our ability to control the chemistry and microstructure of block copolymer thin films to address issues facing current polymeric membranes. Chapter 3 reviewed an attempt to develop ammonia selective membranes that resist membrane conditioning. Chapters 4-6 focused on a variety of ways to improve ultrafiltration membranes by reducing the wide distribution of pore sizes. As a way to review the material in these chapters and highlight certain aspects of the research, we finally discuss the strengths and weaknesses of the new membranes produced. The weaknesses of these membranes present challenges for future researchers. These challenges offer opportunities for advancing the role of block copolymer membranes in separation systems, but represent threats if they cannot be addressed. The discussion begins with a review of ammonia selective membranes which are categorized as gas permeation membranes, and then the three nanoporous membranes for water purification are covered.

7.1 Ammonia Selective Membranes

Evaluating the potential of these membranes is aided by setting specifications for the membrane selectivity and permeance. By setting these specifications, we have benchmarks with which to compare our experimental data. The membrane must be

selective for ammonia over nitrogen and hydrogen; a selectivity of at least ten is needed to begin considering the design of an industrial process.[1, 2] Moreover, this selectivity should be for a mixed gas system. It is often the case that the high selectivity promised from pure gas experiments is lost during mixed gas experiments due to membrane conditioning.[3-5] Higher permeances are preferred for the design of membrane systems because this allows for smaller membrane surface areas to be used. To achieve a high permeance, the selective layer should be as thin as possible and materials with high ammonia permeabilities should be selected. Determining what constitutes a "thin" membrane is difficult because this definition will depend on both the type of membrane support selected and the permeability of the dense polymer layer. It is easier to set a specification for the ammonia permeability of the thin polymer film. If the permeability is at least 1 barrer, a membrane separation may be considered.

The ammonia selective membranes developed in this work were templated by a copolymer which self-assembles into a bicontinuous network structure with two interpenetrating nanoscopic domains. One domain is made from polystyrene-sulfonate (PSS) with a high ideal selectivity, while the other domain is made from crosslinked polycyclooctene (PCOE) or polydicyclopentadiene (PDCPD). The hope is that the rigid structure of the PCOE/PDCPD phase would prevent the PSS phase from swelling, allowing the membrane to remain selective for mixed gas feeds. At room temperature and an ammonia pressure of 2 bar, these membranes have an ammonia permeability over 600 barrers and a mixed gas selectivity greater than 100. Comparing these values to the

specifications set forth above, the high permeability and selectivity are definite strengths of the membranes.

Further experiments with the membranes explored the effects that varying the ammonia pressure, PSS domain size and the degree of crosslinking have on the membrane permeance and selectivity. The ammonia permeability was found to increase with increasing ammonia pressure, decreasing PSS domain size and decreasing degree of crosslinking. In general, the membranes were able to inhibit membrane conditioning at moderate pressure but would lose selectivity at industrially relevant pressure. Higher degrees of crosslinking and larger PSS domains (i.e., lower ammonia permeabilities) allowed higher ammonia pressures to be reached before a decrease in selectivity was observed. The ability to link nanoscale material properties such as the PSS domain size and degree of crosslinking to macroscale properties (i.e., the permeability) strengthens the value of the results of this project.

The research into ammonia selective membranes is not without its shortcomings. Currently these membranes are on the order of 100 microns thick, and decreasing the thickness to increase the membrane permeance should be a high priority. Based on balancing the support layer and selective layer contributions to the overall mass transfer resistance, Chapter 3 concluded that a 500 nm selective layer is ideal.

Reflecting on where this research has succeeded and fallen short suggests several ways to extend further into gas permeation membranes. The weaknesses tend to highlight future projects specific to improving the ammonia and nitrogen separation while the strengths indicate that the general principles used can be applied to other gas pairs (e.g.,

carbon dioxide and methane or ethane and ethylene). The Haber process reactor operates at 400 ˚C and a partial ammonia pressure of 30 atm, while our experiments were run at considerably milder conditions, 25 ˚C and 5 atm ammonia partial pressure. Experiments to probe the temperature and pressure space between the Haber process conditions and our current system limits are sensible. Experiments to test higher ammonia partial pressures can be attempted by modifying the current gas diffusion cell, described in Chapter 2. Our study stopped at 5 atm because this is the stability limit of the transducers presently on the diffusion cell; new transducers rated for higher operating pressures are available. Experiments that focused on membrane behavior at higher operating temperatures have been performed on similar cells up to 240 ˚C on Nafion thin films suggesting a way to probe the same behavior for our new membranes.[6] One concern is the thermal stability of the PSS and PDCPD domains. While published thermal gravimetric analysis data indicate that under a nitrogen atmosphere PDCPD is stable to 400 ˚C, PSS is stable to only 300 ˚C, suggesting the membrane would decompose if attached to a Haber process reactor.[7, 8] However, the insight gained from experimenting at temperatures up to 250 ˚C would inform future membrane designs.

Producing a thinner selective layer is another way to improve these membranes. Techniques which could potentially be used to coat a 500 nm thin layer onto a microporous support will be reviewed.

The overarching idea of using a block copolymer membrane, where one of the blocks is rigid and the other highly selective, can be extended to research other interesting gas pairs. In particular, the separation of carbon dioxide from methane would

benefit from CO_2 selective membranes that resist conditioning because the highly condensable carbon dioxide plasticizes glassy polymers in a similar fashion to ammonia.[5] Work has begun using a polycyclooctene-b-poly(N,N-dimethylaminoethyl methacrylate) (PCOE-PDMAEMA) block polymer membrane.[9, 10] Initial results shown in Figure 7.1 demonstrate its potential.[11] The figure shows the results of mixed gas experiments for carbon dioxide and methane in the presence of a 1 atm carbon dioxide atmosphere as well as the corresponding pure gas experiments. Like the ammonia system, the ideal selectivity promised from pure gas experiments is retained. The CO_2 permeability is over 50 barrers however the selectivity is low, around 10. Research into modifying the chemistry of the CO_2 selective block may improve the selectivity of these membranes.

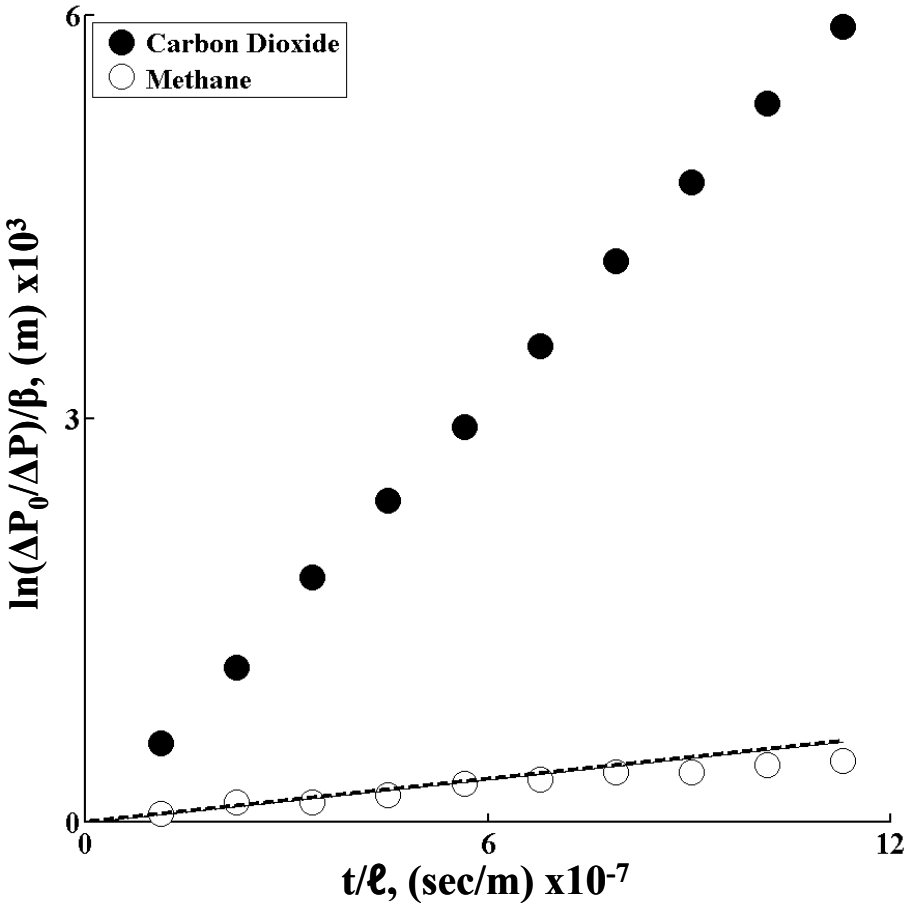

Figure 7.1: The Copolymer Membrane Remains Selective for CO_2 in Mixed Gas Experiments. The crosslinked PCOE phase prevents the PDMAEMA phase from swelling, so the membrane remains selective. The retention of selectivity can be seen graphically by comparing the methane single gas data (dashed lines) and mixed gas data (discrete points).

Although using block copolymers for gas permeation membranes appears promising, any emerging technology faces competition from both the established technologies and other new technologies. Considerations which guide whether to go with a new or established technology are beyond the scope of this work, but examples can be found in the literature. Here we focus instead inorganic membranes, mixed matrix

membranes and adsorption. Inorganic membranes, of which zeolites make up a large percentage, are attractive because of the high selectivity these materials provide. Because they are ceramic, they are unlikely to condition and they could withstand much higher operating temperatures. However, fabricating large membrane areas of these brittle materials has proven difficult. One way to circumvent this difficulty is to fabricate a mixed matrix membrane: an inorganic phase dispersed into a polymeric phase. In doing so researchers hope to use the inorganic phase to produce the selectivity while the polymer phase provides flexibility. These materials also face problems, for example, matching permeabilities of the organic and inorganic phase, and producing good adhesion at the interface between the zeolites and the polymer phase. Adsorption especially pressure swing adsorption is another technology that may be able to produce some of the same gas separations currently being pursued. Keeping up with these alternatives provides benchmarks for polymeric membrane design.

7.2 Pores Aligned by Shear

Having discussed our attempt to use block copolymer membranes for a gas phase separation, we turn our attention to the different ways we investigated the use of copolymers as a template for ultrafiltration membranes. These efforts are discussed in Chapters 4-6. Here we will discuss the work in Chapter 5 first and then cover the topics presented in Chapters 4 and 6 in tandem.

Using a cylinder forming copolymer sample requires aligning the cylinders in the direction of mass transport. The work in Chapter 5 accomplished this by using an applied

shear force, creating 2-5 cm thick monoliths that were used to make membranes for studying gas diffusion and liquid flow across nanoporous copolymers. While research done with these monoliths does not have practical value, this work did motivate continued efforts into producing ultrafiltration membranes using self-assembled copolymers. At the time the research with polystyrene-b-polydimethylacrylamide-b-polylactide (PS-PDMA-PLA) monoliths began, no experimental measurements had established the transport properties of such porous block polymer materials; SEM images and SAXS patterns were used to infer how gas and liquid would move across these membranes. Through experiments, our work established that these inferred properties closely matched measured values. These results conclude that shear alignment followed by PLA etching produces monodisperse nanoscopic pores which span the membrane thickness. These pores do have the simple right circular cylindrical structure inferred from SEM and SAXS with few defects.

Although these monolithic samples will not find any applications as new UF membranes, the monodisperse pore size and ability to tailor pore chemistry could be beneficial in chromatography operations. The PDMA brush which coats the pore wall provides an opportunity for further chemical modification. Tailoring the pore chemistry such that it selectively interacts with heavy metal ions or proteins would open the possibility to design columns around these materials. The monodispersed nanometer scale pores would reduce Taylor-Aris dispersion i.e., coupled radial diffusion and axial convection, resulting in a more effective, well defined chromatographic separation.[12, 13]

This may motivate self-assembled block copolymer materials being implemented as a chromatography column.

7.3 Ultrafiltration Membranes

Using the knowledge gained in Chapter 5, we continued pursuing the goal of producing ultrafiltration membranes with narrow pore size distributions looking to avoid the use of an applied external force to orient the cylinders. We used the concentration gradient from an evaporating solvent to align the pores or generated a bicontinuous network structure which does not require alignment. The strengths, weaknesses and challenges for these two projects have enough similarities that we will discuss them together.

The research using a network structure was presented in Chapter 4. Because the morphology of these materials is different than the cylinders previously explored, we examined the connection between the pore diameter determined using techniques such as SEM, SAXS and BET with the pore diameter found from gas diffusion and liquid flow experiments. These experiments were pursued in particular because the network structure has pores with a diameter which oscillates along its length. This variation has interesting implications on how the pore diameter should be averaged to appropriately reflect transport properties. As in Chapter 5, the pore diameters found from transport experiments and from BET and SAXS characterization techniques were in excellent agreement. Currently, UF membrane nominal pore diameters are estimated by more involved experimental techniques such as bubble point or solute rejection measurements.

The ability to use SAXS to accurately estimate the membrane pore diameters is valuable.[1, 2, 14]

After establishing the relationship between the pore diameters measured using different techniques, the focus of the research was shifted to measuring the ability of the PDCPD membranes to reject dissolved solutes. These rejection experiments are more practically interesting and allow the potential of the membranes to be evaluated. Single solute polyethylene oxide (PEO) and mixed solute dextrans techniques were used to measure the molecular weight cut-off (MWCO) curves. The single solute experiments allow checks with theory, while the significantly faster mixed solute experiments mimic industrial quality control techniques. Comparing the data collected for the PEO solutes with the theory for hindered diffusion showed the membrane behaved as expected for a membrane with pores 14.2 nm in diameter. Without adjustable parameters, the theory and experiments were in agreement, further strengthening our confidence in the pore diameter measured from transport experiments. The mixed dextrans experiments showed that UF membranes made using copolymer self-assembly provide a sharper cut-off than traditional phase inversion membranes. The other interesting finding using the mixed dextrans was the finer control over pore size which copolymer self-assembly offers. By increasing or decreasing the molecular weight of the etchable PLA block, the MWCO could be shifted to higher or lower molecular weights. Combined, these results suggest an understanding of transport through the monodisperse nanopores, as well as the potential of UF membranes made from block polymers.

The relation between the pore size measured from transport experiments and that found from SAXS and SEM was established for the cylinder morphology in Chapter 5. Therefore, Chapter 6 begins with single solute PEO MWCO experiments on composite membranes where the thin selective layer is made from a cylinder forming PS-PLA. Reassuringly, the selective layer rejects solute as predicted by the hindered diffusion theory for monodisperse 23.3 nm pores. Showing the full MWCO curve for a nanoporous copolymer membrane has only been done by one other research group. Obtaining similar results using a different starting material suggests a variety of copolymers can be used as long as the cylinders can be aligned and subsequently etched. The ability to extend the idea to other copolymer systems is critical for advancing this research.

Demonstrating the ability to reject dissolved solutes is important for establishing the practical value of these membranes. Equally important to testing the membranes is the ability to reproducibly make the membranes using a simple technique. Prior attempts to make a selective layer from a self-assembled copolymer have been scientifically interesting but not commercially attractive. Some involved etching the cylinders using harsh chemical treatments; others involved multiple steps often with several hours of annealing; and some used the expensive copolymers to create both the selective layer and underlying microporous support.[15-19] The technique developed here produces a composite membrane structure using a two step process: a casting step, where solvent evaporation is controlled to orient the cylinders; and an etching step, where the PLA is etched using a dilute base. The resulting structure uses all of the copolymer in the selective layer. This fabrication technique is an attractive feature of the work. Another strong point was our

ability to develop an understanding of how the solvent evaporation rate, solvent selectivity and copolymer structure affected the cylinder orientation, which means this framework can be extended to other copolymer systems.

However, both the bicontinuous network and cylindrical structures have shortcomings which must be addressed. The PDCPD and PS matrices which remain after PLA degradation are hydrophobic. Such hydrophobic membranes foul more easily than hydrophilic membranes when being used to treat surface water. Fouling can occur by a variety of mechanisms, leading to a decrease in the permeate flux over time. This point merits more research.[1, 14, 20, 21]

In addition, both of these membrane structures have unattractively low hydraulic permeabilties. Compared to the fluxes observed across typical phase inversion membranes, those of the copolymer membranes fabricated in this work are about 100 times lower. The chance to close this gap is real. For the bicontinuous PDCPD membranes, this difference is a result of the membranes being about 100 microns thick. Because the resistance to flow is inversely proportional to the thickness, a 500 nm selective layer onto a support membrane will result in a 200 time increase in flux. This increase would make the flux across the bicontinuous structure competitive with phase inversion membranes. The low fluxes in the cylindrical PS-PLA system result from the membrane pores being blocked by the tight structure of the current polyethersulfone (PES) support membrane and by not all of the nanopores spanning the selective layer thickness. We are working to overcome this.

There are other weaknesses of the nanoporous thin films we have investigated. During the production of the PDCPD membranes, a dense skin about 1 μm thick forms on the top surface. Why this skin forms is not understood, without its removal, flow across the film is significantly retarded. Removing the dense layer during the lab scale membrane preparation is achieved through the use of O_2 plasma reactive ion etching (RIE). This technique is acceptable for producing small membrane areas for testing transport properties, but it is not reasonable when trying to produce thousands of square meters. Understanding the skin formation mechanism so that the RIE step can be eliminated would help address this weak point of using a bicontinuous network structure.

The mechanical strength of the continuous PS matrix which remains after PLA degradation in the cylinder forming samples is also a serious concern. High molecular weight copolymer samples do not quickly form a well ordered porous structure because the rearrangement of the polymer chains is slow. To avoid this, lower molecular weight samples are used during the fabrication of the composite membranes. The highest molecular weight copolymer sample had a PS block molecular weight near 30 kDa, only 2-3 times the entanglement molecular weight. This low degree of entanglement compromises the mechanical integrity of the membranes. If block polymer self-assembly is going to be used to produce UF membranes, more mechanically robust polymers which do not crack during membrane production and operation are needed.

7.4 Research Priorities

Even with the long list of areas where porous copolymer thin films need to be improved, their great potential suggests undertaking the challenges. Several preexisting techniques for addressing these challenges already exist.

For both of the systems studied, the low fluxes should be addressed first. The best start for addressing the problem of a low flux for the composite membrane will be the use of a different block polymer. Likely candidates are either asymmetric polystyrene-b-polyisoprene-b-polystyrene-b-polylactide (PS-PI-PS-PLA) or symmetric polylactide-b-polystyrene-b-polyisoprene-b-polystyrene-b-polylactide (PLA-PS-PI-PS-PLA) polymers. Both would leave a continuous matrix consisting of PS-PI-PS after PLA degradation resulting in an increase in mechanical stability.[22] Samples of both of these materials which form the cylinder morphology have already been synthesized.

Increasing the number of nanopores which span the thin selective layer thickness would also increase the permeability of these membranes. Based on the theory developed in Chapter 6, the pores should span the entire thickness of thinner films. With the more robust matrix material, it should be easier to make thin films on the order of 500 nm. If going to thinner films alone does not result in the pores spanning the membranes thickness, treating the support membrane to balance the interaction energies between the support and the different blocks has been successful in forcing pores to span the film thickness for other copolymer systems.[15, 16, 23]

The PDCPD membranes are made from a mechanically robust thermosetting polymer. At present, these membranes, cast without a support, have a thickness of 100

μm. Casting membranes which are around 0.5 μm on a non-woven support in order to increase the flux is obviously a high priority. Casting membranes which are dramatically thinner than 0.5 μm is less important because the resistance to flow of the support becomes dominant.[1, 14] Several techniques exist for casting a thin selective layer onto a support layer. We are confident these methods can be tailored to the constraints our system presents. Because the microstructure of these thin films forms due to a polymerization induced phase separation, the possibility of using an interfacial polymerization technique similar to that used when making reverse osmosis membranes seems interesting. Another possibility would be to cast a PDCPD onto the non-woven support using a technique similar to that used in making the composite films. In the end, the technique developed for the nanoporous PDCPD material should also be applicable to the ammonia selective membranes because of the similarities between the underlying chemistry.

If the flux across these thin films can be increased, the next opportunity for membranes templated by block polymer self-assembly would be in the ability to tailor the pore chemistry. Chapter 5 demonstrated that a PDMA brush could be used to coat the pore wall. Using this idea the pore walls can be made hydrophilic, hopefully eliminating the need to pre-wet the membranes. Work which uses chemistries similar to that of the bicontinuous porous structure chemistry has made membranes with PDMA and poly(*ter* butylacrylic acid) coated pores.[24] These membranes wet without pretreatments.

While pore walls chemically modified to avoid the use of pre wetting solutions are attractive, the real opportunity for tailored pore chemistry is fouling prevention. By

modifying the pore walls with a PEO brush, researchers have eliminated irreversible fouling in phase inversion membranes.[21] Block copolymer monodisperse pores coated with a PEO brush should also resist fouling. To judge success, we must be capable of evaluating membrane fouling. With this goal in mind, experiments have begun using two sets of standard fouling solutions. In the first set, PDCPD membranes are being challenged by a solution containing minute virus of mice (size 18 nm) and bovine serum albumin. Figure 7.2 shows the normalized flux as a function of permeate volume collected.[25] The normalized flux stays near one during the whole experiment, indicating these membranes do not foul easily. Additionally, the ability of the PDCPD membrane to reject the virus particles during the whole experiments was a strong point as greater than log 7 reduction was achieved for each permeate sample collected. In the second set, Suwannee River organic matter is being tested as representative of the foulants found in surface water samples. The expertise in making these measurements will be needed as future membranes are chemically tailored using different types of polymer brushes.

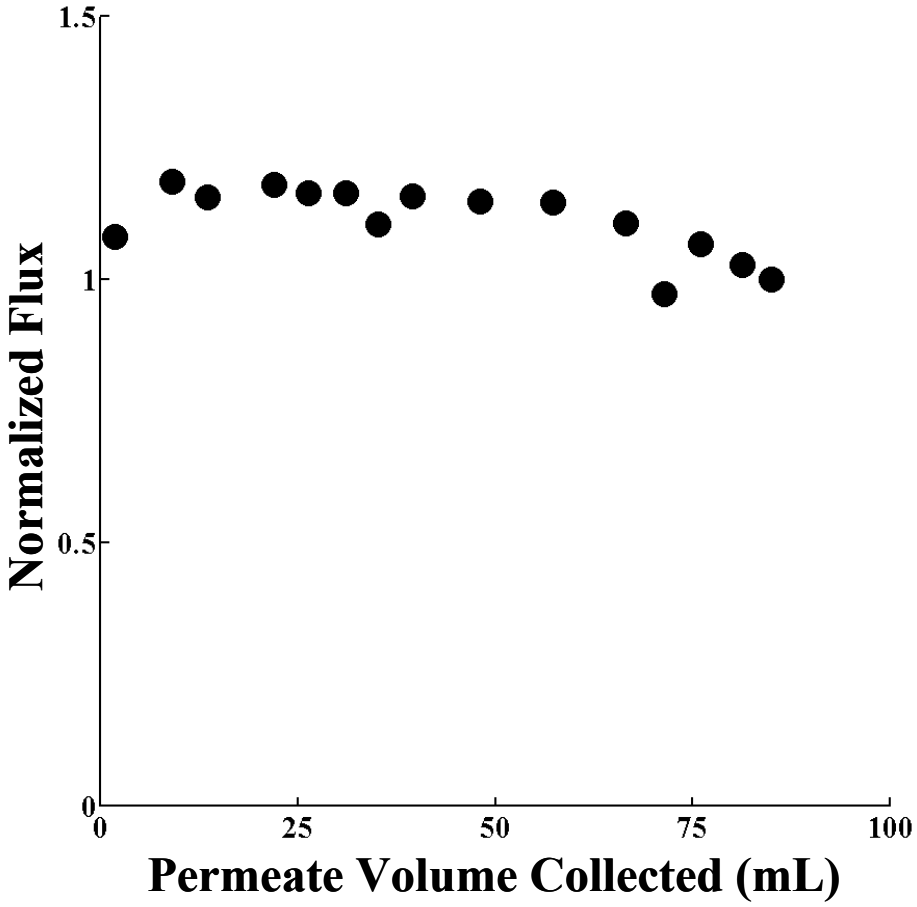

Figure 7.2: A PDCPD Membrane Resists Fouling. The permeate flux remains nearly constant while the nanoporous polymer membrane is challenged by a solution containing bovine serum albumin indicating its ability to resist fouling.

Finally, while membranes templated by block copolymers seem promising, other technologies may produce similar monodisperse pore size distributions. Lithographic techniques using PDMS are able to produce monodisperse pores on the order of 100 nm,[26, 27] slightly larger than desired for UF applications. New specialized lithographic tehniques using a very hydrophobic fluorinated polymer are able to produce monodisperse pores in the right size range but the resulting matrix is highly hydrophobic.[28, 29] Very small samples of aligned carbon nanotubes have demonstrated

extremely high fluxes due to a new transport mechanism occurring in these molecularly smooth channels.[30-33] Even more than our cylinder forming samples, the alignment of the nanotubes is difficult. Bicontinuous microemulsions[34, 35] and alumina nanoparticles can produce monodisperse pore size distributions. However, none of these other membrane systems are developed as far as copolymer membranes. Research should continue in hopes of improving our current copolymer systems and realizing more of their strong potential.

7.5 References

(1) Baker, R. W. In *Membrane technology and applications;* J. Wiley: Chichester ; New York, 2004; , pp 538.

(2) Ho, W. S. W.; Sirkar, K. K. In *Membrane handbook;* Kluwer Academic Pub.: Boston, 2001; , pp 954.

(3) Visser, T.; Masetto, N.; Wessling, M. *J. Membr. Sci.* **2007**, *306*, 16-28.

(4) Visser, T.; Wessling, M. *Macromolecules* **2007**, *40*, 4992-5000.

(5) Baker, R. W.; Lokhandwala, K. *Ind Eng Chem Res* **2008**, *47*, 2109-2121.

(6) He, Y.; Cussler, E. L. *J. Membr. Sci.* **1992**, *68*, 43-52.

(7) Chen, L.; Phillip, W. A.; Cussler, E. L.; Hillmyer, M. A. *J. Am. Chem. Soc.* **2007**, *129*, 13786-13787.

(8) Park, K. R.; Kang, P. H.; Nho, Y. C. *React Funct Polym* **2005**, *65*, 47-56.

(9) Du, R.; Feng, X.; Chakma, A. *J. Membr. Sci.* **2006**, *279*, 76-85.

(10) Zhao, H.; Cao, Y.; Ding, X.; Zhou, M.; Yuan, Q. *J. Membr. Sci.* **2008**, *310*, 365-373.

(11) Work done by Dr. Sarah Querelle.

(12) Bird, R. B.; Stewart, W. E.; Lightfoot, E. N. In *Transport phenomena;* J. Wiley: New York, 2002; , pp 895.

(13) Cussler, E. L. In *Diffusion, mass transfer in fluid systems;* Cambridge University Press: New York, 2009; , pp 654.

(14) Zeman, L. J.; Zydney, A. L. In *Microfiltration and ultrafiltration : principles and applications;* M. Dekker: New York, 1996; , pp 618.

(15) Yang, S. Y.; Park, J.; Yoon, J.; Ree, M.; Jang, S. K.; Kim, J. K. *Adv.Funct.Mater.* **2008**, *18*, 1371-1377.

(16) Yang, S. Y.; Ryu, I.; Kim, H. Y.; Kim, J. K.; Jang, S. K.; Russell, T. P. *Adv.Mater.(Weinheim, Ger.)* **2006**, *18*, 709-712.

(17) Kim, S. H.; Misner, M. J.; Xu, T.; Kimura, M.; Russell, T. P. *Adv.Mater.(Weinheim, Ger.); Advanced Materials (Weinheim, Germany)* **2004**, *16*, 226-231.

(18) Lin, Z.; Kim, D. H.; Wu, X.; Boosahda, L.; Stone, D.; LaRose, L.; Russell, T. P. *Adv.Mater.(Weinheim, Ger.); Advanced Materials (Weinheim, Germany)* **2002**, *14*, 1373-1376.

(19) Peinemann, K.; Abetz, V.; Simon, P. F. W. *Nat Mater* **2007**, *6*, 992-996.

(20) Zhu, X.; Elimelech, M. *Environ. Sci. Technol.* **1997**, *31*, 3654-3662.

(21) Asatekin, A.; Kang, S.; Elimelech, M.; Mayes, A. M. *J. Membr. Sci.* **2007**, *298*, 136-146.

(22) Meuler, A. J.; Fleury, G.; Hillmyer, M. A.; Bates, F. S. *Macromolecules (Washington, DC, U.S.); Macromolecules (Washington, DC, United States)* **2008**, *41*, 5809-5817.

(23) Ryu, D. Y.; Ham, S.; Kim, E.; Jeong, U.; Hawker, C. J.; Russell, T. P. *Macromolecules (Washington, DC, U.S.); Macromolecules (Washington, DC, United States)* , ACS ASAP.

(24) Work done by Dr. Monique Roerdink.

(25) Work done by Dr. Ranil Wickramsinghe and Justin Weaver.

(26) Girones, M.; Akbarsyah, I. J.; Nijdam, W.; van Rijn, C. J. M.; Jansen, H. V.; Lammertink, R. G. H.; Wessling, M. *J. Membr. Sci.* **2006**, *283*, 411-424.

(27) Vogelaar, L.; Lammertink, R. G. H.; Barsema, J. N.; Nijdam, W.; Bolhuis-Versteeg, L. A. M.; van Rijn, C. J. M.; Wessling, M. *Small; Small* **2005**, *1*, 645-655.

(28) Rolland, J. P.; Hagberg, E. C.; Denison, G. M.; Carter, K. R.; De Simone, J. M. *Angew. Chem. Int. Ed Engl.* **2004**, *43*, 5796-5799.

(29) Rolland, J. P.; Maynor, B. W.; Euliss, L. E.; Exner, A. E.; Denison, G. M.; DeSimone, J. M. *J. Am. Chem. Soc.* **2005**, *127*, 10096-10100.

(30) Mauter, M. S.; Elimelech, M. *Environ. Sci. Technol.* **2008**, *42*, 5843-5859.

(31) Holt, J. K.; Park, H. G.; Wang, Y.; Stadermann, M.; Artyukhin, A. B.; Grigoropoulos, C. P.; Noy, A.; Bakajin, O. *Science (Washington, DC, U.S.); Science (Washington, DC, United States)* **2006**, *312*, 1034-1037.

(32) Sholl, D. S.; Johnson, J. K. *Science (Washington, DC, U.S.); Science (Washington, DC, United States)* **2006**, *312*, 1003-1004.

(33) Skoulidas, A. I.; Ackerman, D. M.; Johnson, J. K.; Sholl, D. S. *Phys. Rev. Lett.* **2002**, *89*, 185901/1-185901/4.

(34) Zhou, N.; Bates, F. S.; Lodge, T. P. *Polym.Prepr.(Am.Chem.Soc., Div.Polym.Chem.); Polymer Preprints (American Chemical Society, Division of Polymer Chemistry)* **2007**, *48*, 868.

(35) Jones, B. H.; Lodge, T. P. *J. Am. Chem. Soc.* **2009**, *131*, 1676-1677.

Bibliography

(1) Anderson, C. J.; Pas, S. J.; Arora, G.; Kentish, S. E.; Hill, A. J.; Sandler, S. I.; Stevens, G. W. *J. Membr. Sci.* **2008**, *322*, 19-27.

(2) Anderson, J. L.; Quinn, J. A. *Biophys. J.* **1974**, *14*, 130-150.

(3) Anderson, J. L.; Quinn, J. A. *J.Chem.Soc., Faraday Trans.1* **1972**, *68*, 744-748.

(4) Angelescu, D. E.; Waller, J. H.; Adamson, D. H.; Deshpande, P.; Chou, S. Y.; Register, R. A.; Chaikin, P. M. *Adv.Mater.(Weinheim, Ger.); Advanced Materials (Weinheim, Germany)* **2004**, *16*, 1736-1740.

(5) Asatekin, A.; Kang, S.; Elimelech, M.; Mayes, A. M. *J. Membr. Sci.* **2007**, *298*, 136-146.

(6) ASTM - ASTM International In *Standard Test Method for Molecular Weight Cutoff Evaluation of Flat Sheet Ultrafiltration Membranes;* 2001; Vol. ASTM E 1343 - 90 (reapproved 2001).

(7) Baker, R. W. In *Membrane technology and applications;* J. Wiley: Chichester ; New York, 2004; , pp 538.

(8) Baker, R. W.; Lokhandwala, K. *Ind Eng Chem Res* **2008**, *47*, 2109-2121.

(9) Balsara, N. P.; Eastman, C. E.; Foster, M. D.; Lodge, T. P.; Tirrell, M. *Makromol.Chem., Macromol.Symp.; Makromolekulare Chemie, Macromolecular Symposia* **1991**, *45*, 213-235.

(10) Balsara, N. P.; Garetz, B. A.; Chang, M. Y.; Dai, H. J.; Newstein, M. C.; Goveas, J. L.; Krishnamoorti, R.; Rai, S. *Macromolecules* **1998**, *31*, 5309-5315.

(11) Barrett, E. P.; Joyner, L. G.; Halenda, P. P. *J. Am. Chem. Soc.* **1951**, *73*, 373-380.

(12) Bates, F. S. *Science (Washington, D.C., 1883-)* **1991**, *251*, 898-905.

(13) Bates, F. S.; Fredrickson, G. H. *Annu. Rev. Phys. Chem.* **1990**, *41*, 525-557.

(14) Beck, R. E.; Schultz, J. S. *Biochim.Biophys.Acta, Biomembr.; Biochimica et Biophysica Acta, Biomembranes* **1972**, *255*, 273-303.

(15) Bhown, A.; Cussler, E. L. *J. Am. Chem. Soc.* **1991**, *113*, 742-749.

(16) Bikson, B.; Nelson, J. K.; Perrin, J. E. Patent Application Country: Application: US; Patent Country: US Patent 5009678, 1991.

(17) Bird, R. B.; Stewart, W. E.; Lightfoot, E. N. In *Transport phenomena;* J. Wiley: New York, 2002; , pp 895.

(18) Brenner, H.; Gaydos, L. J. *J. Colloid Interface Sci.* **1977**, *58*, 312-356.

(19) Bungay, P. M.; Brenner, H. *Int. J. Multiphase Flow* **1973**, *1*, 25.

(20) Car, A.; Stropnik, C.; Yave, W.; Peinemann, K. *J. Membr. Sci.* **2008**, *307*, 88-95.

(21) Cavicchi, K. A.; Berthiaume, K. J.; Russell, T. P. *Polymer* **2005**, *46*, 11635-11639.

(22) Chastek, T. Q.; Lodge, T. P. *J. Polym. Sci. Part B* **2006**, *44*, 481-491.

(23) Chastek, T. Q.; Lodge, T. P. *Macromolecules* **2004**, *37*, 4891-4899.

(24) Chen, L.; Phillip, W. A.; Cussler, E. L.; Hillmyer, M. A. *J. Am. Chem. Soc.* **2007**, *129*, 13786-13787.

(25) Chen, Z.; Kornfield, J. A. *Polymer* **1998**, *39*, 4679-4699.

(26) Chen, Z.; Kornfield, J. A.; Smith, S. D.; Grothaus, J. T.; Satkowski, M. M. *Science (Washington, D.C.); Science (Washington, D.C.)* **1997**, *277*, 1248-1253.

(27) Connolly, D. J.; Gresham, W. F. Patent Country: GB; Priority Application Country: US Patent 1034197, 1966.

(28) Cooney, D. T.; Hillmyer, M. A.; Cussler, E. L.; Moggridge, G. D. *Crystallogr.Rev.; Crystallography Reviews* **2006**, *12*, 13-24.

(29) Crank, J. In *The mathematics of diffusion;* Clarendon Press: Oxford, Eng, 1975; , pp 414.

(30) Cussler, E. L. In *Diffusion, mass transfer in fluid systems;* Cambridge University Press: New York, 2009; , pp 654.

(31) Cussler, E. L. In *Diffusion, mass transfer in fluid systems;* Cambridge University Press: New York, 1997; , pp 580.

(32) de Gennes, P. G.; Prost, J. In *The physics of liquid crystals;* The International series of monographs on physics; Clarendon Press; Oxford University Press: Oxford; New York, 1993; Vol. 83, pp 597.

(33) Deen, W. M. *AICHE J.* **1987**, *33*, 1409-1425.

(34) DeRocher, J. P.; Gettelfinger, B. T.; Wang, J.; Nuxoll, E. E.; Cussler, E. L. *J. Membr. Sci.* **2005**, *254*, 21-30.

(35) DeRouchey, J.; Thurn-Albrecht, T.; Russell, T. P.; Kolb, R. *Macromolecules* **2004**, *37*, 2538-2543.

(36) Du, R.; Feng, X.; Chakma, A. *J. Membr. Sci.* **2006**, *279*, 76-85.

(37) Dullien, F. A. L. In *Porous media : fluid transport and pore structure;* Academic Press: San Diego, 1992; , pp 574.

(38) Eggeman, T. In *Kirk-Othmer encyclopedia of chemical technology;* Kirk, R. E. (. E., Othmer, D. F. (. F., Eds.; Encyclopedia of chemical technology; Wiley: New York, 2000; .

(39) Faraone, A.; Magazu, S.; Maisano, G.; Migliardo, P.; Tettamanti, E.; Villari, V. *J. Chem. Phys.* **1999**, *110*, 1801-1806.

(40) Fasolka, M. J.; Harris, D. J.; Mayes, A. M.; Yoon, M.; Mochrie, S. G. J. *Phys. Rev. Lett.* **1997**, *79*, 3018-3021.

(41) Flory, P. J. In *Principles of polymer chemistry;* Cornell University Press: Ithaca, 1953; .

(42) Freeman, B. D. *Macromolecules* **1999**, *32*, 375-380.

(43) Freger, V. *Polymer* **2002**, *43*, 71-76.

(44) Giddings, J. C.; Kucera, E.; Russell, C. P.; Myers, M. N. *J. Phys. Chem.* **1968**, *72*, 4397-4408.

(45) Girones, M.; Akbarsyah, I. J.; Nijdam, W.; van Rijn, C. J. M.; Jansen, H. V.; Lammertink, R. G. H.; Wessling, M. *J. Membr. Sci.* **2006**, *283*, 411-424.

(46) Green, P. F.; Limary, R. *Adv. Colloid Interface Sci.* **2001**, *94*, 53-81.

(47) Gunkel, I.; Stepanow, S.; Thurn-Albrecht, T.; Trimper, S. *Macromolecules (Washington, DC, U.S.); Macromolecules (Washington, DC, United States)* **2007**, *40*, 2186-2191.

(48) Guo, S.; Rzayev, J.; Bailey, T. S.; Zalusky, A. S.; Olayo-Valles, R.; Hillmyer, M. A. *Chem.Mater.; Chemistry of Materials* **2006**, *18*, 1719-1721.

(49) Gusler, G. M.; Cohen, Y. *Ind Eng Chem Res* **1994**, *33*, 2345-2357.

(50) Hamley, I. W. *Dev.Block Copolym.Sci.Technol.; Developments in Block Copolymer Science and Technology* **2004**, 1-29.

(51) Hamley, I. W. *Curr.Opin.Colloid Interface Sci.; Current Opinion in Colloid & Interface Science* **2000**, *5*, 342-350.

(52) Hamley, I. W.; Castelletto, V. *Prog.Polym.Sci.; Progress in Polymer Science* **2004**, *29*, 909-948.

(53) Hanioka, S.; Maruyama, T.; Sotani, T.; Teramoto, M.; Matsuyama, H.; Nakashima, K.; Hanaki, M.; Kubota, F.; Goto, M. *J. Membr. Sci.* **2008**, *314*, 1-4.

(54) Hanley, K. J.; Lodge, T. P. *J. Polym. Sci. Part B* **1998**, *36*, 3101-3113.

(55) Hansen, C. M. In *Hansen solubility parameters : a user's handbook;* CRC Press: Boca Raton, Fla., 2000; , pp 208.

(56) He, Y.; Cussler, E. L. *J. Membr. Sci.* **1992**, *68*, 43-52.

(57) Hiemenz, P. C., Lodge, T. In *Polymer chemistry;* CRC Press: Boca Raton, FL, 2007; pp 608.

(58) Hillock, A. M. W.; Miller, S. J.; Koros, W. J. *J. Membr. Sci.* **2008**, *314*, 193-199.

(59) Ho, R.; Tseng, W.; Fan, H.; Chiang, Y.; Lin, C.; Ko, B.; Huang, B. *Polymer* **2005**, *46*, 9362-9377.

(60) Ho, W. S. W.; Sirkar, K. K. In *Membrane handbook;* Kluwer Academic Pub.: Boston, 2001; , pp 954.

(61) Holt, J. K.; Park, H. G.; Wang, Y.; Stadermann, M.; Artyukhin, A. B.; Grigoropoulos, C. P.; Noy, A.; Bakajin, O. *Science (Washington, DC, U.S.); Science (Washington, DC, United States)* **2006**, *312*, 1034-1037.

(62) Horvat, A.; Lyakhova, K. S.; Sevink, G. J. A.; Zvelindovsky, A. V.; Magerle, R. *J. Chem. Phys.* **2004**, *120*, 1117-1126.

(63) Huizenga, D. G.; Smith, D. M. *AICHE J.* **1986**, *32*, 1-6.

(64) Hwang, J.; Huh, J.; Jung, B.; Hong, J.; Park, M.; Park, C. *Polymer* **2005**, *46*, 9133-9143.

(65) Imaizumi, K.; Ono, T.; Kota, T.; Okamoto, S.; Sakurai, S. *J.Appl.Crystallogr.; Journal of Applied Crystallography* **2003**, *36*, 976-981.

(66) Jeong, U.; Ryu, D. Y.; Kho, D. H.; Kim, J. K.; Goldbach, J. T.; Kim, D. H.; Russell, T. P. *Adv.Mater.(Weinheim, Ger.); Advanced Materials (Weinheim, Germany)* **2004**, *16*, 533-536.

(67) Jones, B. H.; Lodge, T. P. *J. Am. Chem. Soc.* **2009**, *131*, 1676-1677.

(68) Karim, A.; Singh, N.; Sikka, M.; Bates, F. S.; Dozier, W. D.; Felcher, G. P. *J. Chem. Phys.* **1994**, *100*, 1620-1629.

(69) Kim, G.; Libera, M. *Macromolecules* **1998**, *31*, 2569-2577.

(70) Kim, J.; Hwang, J. R.; Kim, U. Y.; Kim, S. S. *J. Membr. Sci.* **1995**, *108*, 25-36.

(71) Kim, S. O.; Solak, H. H.; Stoykovich, M. P.; Ferrier, N. J.; de Pablo, J. J.; Nealey, P. F. *Nature (London, U.K.); Nature (London, United Kingdom)* **2003**, *424*, 411-414.

(72) Kim, S.; Briber, R. M.; Karim, A.; Jones, R. L.; Kim, H. *Macromolecules (Washington, DC, U.S.); Macromolecules (Washington, DC, United States)* **2007**, *40*, 4102-4105.

(73) Kim, S. H.; Misner, M. J.; Xu, T.; Kimura, M.; Russell, T. P. *Adv.Mater.(Weinheim, Ger.); Advanced Materials (Weinheim, Germany)* **2004**, *16*, 226-231.

(74) Kim, W. G.; Garetz, B. A.; Newstein, M. C.; Balsara, N. P. *J. Polym. Sci. Part B* **2001**, *39*, 2231-2242.

(75) Knoll, A.; Horvat, A.; Lyakhova, K. S.; Krausch, G.; Sevink, G. J. A.; Zvelindovsky, A. V.; Magerle, R. *Phys. Rev. Lett.* **2002**, *89*, 035501.

(76) Knoll, A.; Magerle, R.; Krausch, G. *J. Chem. Phys.* **2004**, *120*, 1105-1116.

(77) Koonaphapdeelert, S.; Li, K. *J. Membr. Sci.* **2007**, *291*, 70-76.

(78) Koppi, K. A.; Tirrell, M.; Bates, F. S.; Almdal, K.; Mortensen, K. *J.Rheol.(N.Y.); Journal of Rheology (New York, NY, United States)* **1994**, *38*, 999-1027.

(79) Koros, W. J.; Coleman, M. R.; Walker, D. R. B. *Annu.Rev.Mater.Sci.* **1992**, *22*, 47-89.

(80) Kreuer, K. D. *J. Membr. Sci.* **2001**, *185*, 29-39.

(81) Laciak, D. V.; Pez, G. P. Patent Application Country: Application: US; Patent Country: US Patent 4758250, 1988.

(82) Laciak, D. V.; Quinn, R.; Pez, G. P.; Appleby, J. B.; Puri, P. S. *Separation Science and Technology* **1990**, *25*, 1295.

(83) Lai, J. T.; Filla, D.; Shea, R. *Macromolecules* **2002**, *35*, 6754-6756.

(84) Lape, N. K.; Nuxoll, E. E.; Cussler, E. L. *J. Membr. Sci.* **2004**, *236*, 29-37.

(85) Lape, N. K.; Yang, C.; Cussler, E. L. *J. Membr. Sci.* **2002**, *209*, 271-282.

(86) Lee, S. B.; Mitchell, D. T.; Trofin, L.; Nevanen, T. K.; Soederlund, H.; Martin, C. R. *Science (Washington, DC, U.S.); Science (Washington, DC, United States)* **2002**, *296*, 2198-2200.

(87) Lin, H.; Freeman, B. D. *Journal of Molecular Structure* **2005**, *739*, 57-74.

(88) Lin, Z.; Kim, D. H.; Wu, X.; Boosahda, L.; Stone, D.; LaRose, L.; Russell, T. P. *Adv.Mater.(Weinheim, Ger.); Advanced Materials (Weinheim, Germany)* **2002**, *14*, 1373-1376.

(89) Liu, G.; Ding, J.; Hashimoto, T.; Kimishima, K.; Winnik, F. M.; Nigam, S. *Chem.Mater.; Chemistry of Materials* **1999**, *11*, 2233-2240.

(90) Liu, G.; Ding, J.; Stewart, S. *Angew.Chem., Int.Ed.; Angewandte Chemie, International Edition* **1999**, *38*, 835-838.

(91) Lodge, T. P.; Hanley, K. J.; Huang, C.; Ryu, C. Y. *Polym.Mater.Sci.Eng.; Polymeric Materials Science and Engineering* **1998**, *79*, 377.

(92) Lodge, T. P.; Xu, X.; Ryu, C. Y.; Hamley, I. W.; Fairclough, J. P. A.; Ryan, A. J.; Pedersen, J. S. *Macromolecules* **1996**, *29*, 5955-5964.

(93) Lodge, T. P.; Blazey, M. A.; Liu, Z.; Hamley, I. W. *Macromol.Chem.Phys.; Macromolecular Chemistry and Physics* **1997**, *198*, 983-995.

(94) Lodge, T. P.; Hamersky, M. W.; Hanley, K. J.; Huang, C. *Macromolecules* **1997**, *30*, 6139-6149.

(95) Lodge, T. P.; Hanley, K. J.; Huang, C.; Ryu, C. In *In Order-order and order-disorder transitions in block copolymer solutions and melts.* 1998; , pp PMSE-290.

(96) Lodge, T. P.; Hanley, K. J.; Pudil, B.; Alahapperuma, V. *Macromolecules* **2003**, *36*, 816-822.

(97) Lodge, T. P.; Pudil, B.; Hanley, K. J. *Macromolecules* **2002**, *35*, 4707-4717.

(98) Loeb, S.; Sourirajan, S. Patent Application Country: Application: US; Patent Country: US; Priority Application Country: US Patent 3133132, 1964.

(99) Loeb, S.; Sourirajan, S.; Weaver, D. E. Patent Application Country: Application: US; Patent Country: US; Priority Application Country: US Patent 3133137, 1964.

(100) Majumder, M.; Chopra, N.; Andrews, R.; Hinds, B. *Nature (London, U.K.); Nature (London, United Kingdom)* **2005**, *438*, 930.

(101) Malek, K.; Coppens, M. *J. Chem. Phys.* **2003**, *119*, 2801-2811.

(102) Mauritz, K. A.; Moore, R. B. *Chem.Rev.(Washington, DC, U.S.)* **2004**, *104*, 4535-4585.

(103) Mauter, M. S.; Elimelech, M. *Environ. Sci. Technol.* **2008**, *42*, 5843-5859.

(104) Mavrovouniotis, G. M.; Brenner, H. *J. Colloid Interface Sci.* **1988**, *124*, 269-283.

(105) Mehta, A.; Zydney, A. L. *J. Membr. Sci.* **2005**, *249*, 245-249.

(106) Meireles, M.; Bessieres, A.; Rogissart, I.; Aimar, P.; Sanchez, V. *J. Membr. Sci.* **1995**, *103*, 105-115.

(107) Meuler, A. J.; Fleury, G.; Hillmyer, M. A.; Bates, F. S. *Macromolecules (Washington, DC, U.S.); Macromolecules (Washington, DC, United States)* **2008**, *41*, 5809-5817.

(108) Mills, R.; Woolf, L. A.; Watts, R. O. *AICHE J.* **1968**, *14*, 671-673.

(109) Mochizuki, S.; Zydney, A. L. *J. Membr. Sci.* **1993**, *82*, 211-227.

(110) Moggridge, G. D.; Lape, N. K.; Yang, C.; Cussler, E. L. *Prog.Org.Coat.; Progress in Organic Coatings* **2003**, *46*, 231-240.

(111) Morkved, T. L.; Lu, M.; Urbas, A. M.; Ehrichs, E. E.; Jaeger, H. M.; Mansky, P.; Russell, T. P. *Science (Washington, D.C.); Science (Washington, D.C.)* **1996**, *273*, 931-933.

(112) Munoz, D. M.; Maya, E. M.; de Abajo, J.; de la Campa, J. G.; Lozano, A. E. *J. Membr. Sci.* **2008**, *323*, 53-59.

(113) Naughton, J. R.; Matsen, M. W. *Macromolecules* **2002**, *35*, 5688-5696.

(114) Nuxoll, E. E.; Cussler, E. L. *AICHE J.* **2005**, *51*, 456-463.

(115) Oki, T.; Kanae, S. *Science (Washington, DC, U.S.); Science (Washington, DC, United States)* **2006**, *313*, 1068-1072.

(116) Olayo-Valles, R.; Guo, S.; Lund, M. S.; Leighton, C.; Hillmyer, M. A. *Macromolecules* **2005**, *38*, 10101-10108.

(117) Olayo-Valles, R.; Guo, S.; Lund, M. S.; Leighton, C.; Hillmyer, M. A. *Macromolecules* **2005**, *38*, 10101-10108.

(118) Park, C.; Simmons, S.; Fetters, L. J.; Hsiao, B.; Yeh, F.; Thomas, E. L. *Polymer* **2000**, *41*, 2971-2977.

(119) Park, H. B.; Lee, C. H.; Sohn, J. Y.; Lee, Y. M.; Freeman, B. D.; Kim, H. J. *Journal of Membrane Science* **2006**, *285*, 432-443.

(120) Park, K. R.; Kang, P. H.; Nho, Y. C. *React Funct Polym* **2005**, *65*, 47-56.

(121) Park, S.; Wang, J.; Kim, B.; Chen, W.; Russell, T. P. *Macromolecules (Washington, DC, U.S.); Macromolecules (Washington, DC, United States)* **2007**, *40*, 9059-9063.

(122) Peinemann, K.; Abetz, V.; Simon, P. F. W. *Nat Mater* **2007**, *6*, 992-996.

(123) Peng, J.; Xuan, Y.; Wang, H.; Yang, Y.; Li, B.; Han, Y. *J. Chem. Phys.* **2004**, *120*, 11163-11170.

(124) Pez, G. P.; Carlin, R. T.; Laciak, D. V.; Sorensen, J. C. United States Patent 4761164, 1988.

(125) Pez, G. P.; Laciak, D. V. Patent Application Country: Application: US; Patent Country: US Patent 4762535, 1988.

(126) Phillip, W. A.; Amendt, M.; O'Neill, B.; Chen, L.; Hillmyer, M. A.; Cussler, E. L. *ACS Applied Materials & Interfaces* **2009**, *1*, 472-480.

(127) Phillip, W. A.; Martono, E.; Chen, L.; Hillmyer, M. A.; Cussler, E. L. *J. Membr. Sci.* **2009**, *337*, 39-46.

(128) Phillip, W. A.; Rzayev, J.; Hillmyer, M. A.; Cussler, E. L. *Journal of Membrane Science*, **2006**, *286*, 144-152.

(129) Rafiqul, I.; Weber, C.; Lehmann, B.; Voss, A. *Energy (Amsterdam, Neth.)* **2005**, *30*, 2487-2504.

(130) Renkin, E. M. *J. Gen. Physiol.* **1954**, *38*, 225-243.

(131) Rolland, J. P.; Hagberg, E. C.; Denison, G. M.; Carter, K. R.; De Simone, J. M. *Angew. Chem. Int. Ed Engl.* **2004**, *43*, 5796-5799.

(132) Rolland, J. P.; Maynor, B. W.; Euliss, L. E.; Exner, A. E.; Denison, G. M.; DeSimone, J. M. *J. Am. Chem. Soc.* **2005**, *127*, 10096-10100.

(133) Ryu, D. Y.; Ham, S.; Kim, E.; Jeong, U.; Hawker, C. J.; Russell, T. P. *Macromolecules (Washington, DC, U.S.); Macromolecules (Washington, DC, United States)* , ACS ASAP.

(134) Rzayev, J.; Hillmyer, M. A. *Macromolecules* **2005**, *38*, 3-5.

(135) Rzayev, J.; Hillmyer, M. A. *J. Am. Chem. Soc.* **2005**, *127*, 13373-13379.

(136) Sakai, T.; Takenaka, H.; Torikai, E. *J. Electrochem. Soc.* **1986**, *133*, 88-92.

(137) Sakai, T.; Takenaka, H.; Wakabayashi, N.; Kawami, Y.; Torikai, E. *J. Electrochem. Soc.* **1985**, *132*, 1328-1332.

(138) Sakamoto, N.; Hashimoto, T. *Macromolecules* **1998**, *31*, 8493-8502.

(139) Sakurai, S. *Polymer* **2008**, *49*, 2781-2796.

(140) Sakurai, S.; Aida, S.; Okamoto, S.; Ono, T.; Imaizumi, K.; Nomura, S. *Macromolecules* **2001**, *34*, 3672-3678.

(141) Sakurai, S.; Okamoto, S.; Sakurai, K. *Dev.Block Copolym.Sci.Technol.; Developments in Block Copolymer Science and Technology* **2004**, 127-158.

(142) Scholl, M.; Ding, S.; Lee, C. W.; Grubbs, R. H. *Org. Lett.* **1999**, *1*, 953-956.

(143) Scholl, M.; Ding, S.; Lee, C. W.; Grubbs, R. H. *Org. Lett.* **1999**, *1*, 953-956.

(144) Schwarzenbach, R. P.; Escher, B. I.; Fenner, K.; Hofstetter, T. B.; Johnson, C. A.; von Gunten, U.; Wehrli, B. *Science (Washington, DC, U.S.); Science (Washington, DC, United States)* **2006**, *313*, 1072-1077.

(145) Shannon, M. A.; Bohn, P. W.; Elimelech, M.; Georgiadis, J. G.; Marinas, B. J.; Mayes, A. M. *Nature* **2008**, *452*, 301-310.

(146) Shao, J.; Baltus, R. E. *AICHE J.* **2000**, *46*, 1149-1156.

(147) Shimotori, T.; Nuxoll, E. E.; Cussler, E. L.; Arnold, W. A. *Environ. Sci. Technol.* **2004**, *38*, 2264-2270.

(148) Sholl, D. S.; Johnson, J. K. *Science (Washington, DC, U.S.); Science (Washington, DC, United States)* **2006**, *312*, 1003-1004.

(149) Skoulidas, A. I.; Ackerman, D. M.; Johnson, J. K.; Sholl, D. S. *Phys. Rev. Lett.* **2002**, *89*, 185901/1-185901/4.

(150) Sota, N.; Sakamoto, N.; Saijo, K.; Hashimoto, T. *Polymer* **2006**, *47*, 3636-3649.

(151) Sota, N.; Sakamoto, N.; Saijo, K.; Hashimoto, T. *Macromolecules* **2003**, *36*, 4534-4543.

(152) Staudt-Bickel, C.; Koros, W. J. *J. Membr. Sci.* **1999**, *155*, 145-154.

(153) Staudt-Bickel, C.; Koros, W. J. *J. Membr. Sci.* **1999**, *155*, 145-154.

(154) Taniguchi, I.; Duan, S.; Kazama, S.; Fujioka, Y. *J. Membr. Sci.* **2008**, *322*, 277-280.

(155) Tassopoulos, M.; Rosner, D. E. *Chem. Eng. Sci.* **1992**, *47*, 421-443.

(156) Teubner, M.; Strey, R. *J. Chem. Phys.* **1987**, *87*, 3195-3200.

(157) Thurn-Albrecht, T.; DeRouchey, J.; Russell, T. P.; Jaeger, H. M. *Macromolecules* **2000**, *33*, 3250-3253.

(158) Thurn-Albrecht, T.; Schotter, J.; Kastle, G. A.; Emley, N.; Shibauchi, T.; Krusin-Elbaum, L.; Guarini, K.; Black, C. T.; Tuominen, M. T.; Russell, T. P. *Science (Washington, D.C.); Science (Washington, D.C.)* **2000**, *290*, 2126-2129.

(159) Timashev, S. F.; Vorobiev, A. V.; Kirichenko, V. I.; Popkov, Y. M.; Volkov, V. I.; Shifrina, R. R.; Lyapunov, A. Y.; Bondarenko, A. G.; Bobrova, L. P. *Journal of Membrane Science* **1991**, *59*, 117-131.

(160) Vigild, M. E.; Chu, C.; Sugiyama, M.; Chaffin, K. A.; Bates, F. S. *Macromolecules* **2001**, *34*, 951-964.

(161) Visser, T.; Masetto, N.; Wessling, M. *J. Membr. Sci.* **2007**, *306*, 16-28.

(162) Visser, T.; Wessling, M. *Macromolecules* **2007**, *40*, 4992-5000.

(163) Vogelaar, L.; Lammertink, R. G. H.; Barsema, J. N.; Nijdam, W.; Bolhuis-Versteeg, L. A. M.; van Rijn, C. J. M.; Wessling, M. *Small; Small* **2005**, *1*, 645-655.

(164) Warta, A. M.; Arnold, W. A.; Cussler, E. L. *Environ. Sci. Technol.* **2005**, *39*, 9738-9743.

(165) Wesson, J. A.; Noh, I.; Kitano, T.; Yu, H. *Macromolecules* **1984**, *17*, 782-792.

(166) Wirtz, M.; Martin, C. R. *Adv.Mater.(Weinheim, Ger.); Advanced Materials (Weinheim, Germany)* **2003**, *15*, 455-458.

(167) Wu, L.; Lodge, T. P.; Bates, F. S. *J.Rheol.(N.Y., NY, U.S.); Journal of Rheology (New York, NY, United States)* **2005**, *49*, 1231-1252.

(168) Xu, Z.; Wang, J.; Shen, L.; Men, D.; Xu, Y. *J. Membr. Sci.* **2002**, *196*, 221-229.

(169) Yang, C.; Cussler, E. L. *AICHE J.* **2001**, *47*, 2725-2732.

(170) Yang, C.; Nuxoll, E. E.; Cussler, E. L. *AICHE J.* **2001**, *47*, 295-302.

(171) Yang, R. T. In *Gas separation by adsorption processes;* Series on chemical engineering; Imperial College Press ;$aSingapore; Distributed by World Scientific: London; River Edge, NJ, 1997; Vol. ol. 1, pp 352.

(172) Yang, S. Y.; Ryu, I.; Kim, H. Y.; Kim, J. K.; Jang, S. K.; Russell, T. P. *Adv.Mater.(Weinheim, Ger.)* **2006**, *18*, 709-712.

(173) Yang, S. Y.; Park, J.; Yoon, J.; Ree, M.; Jang, S. K.; Kim, J. K. *Adv.Funct.Mater.* **2008**, *18*, 1371-1377.

(174) Zalusky, A. S.; Olayo-Valles, R.; Taylor, C. J.; Hillmyer, M. A. *J. Am. Chem. Soc.* **2001**, *123*, 1519-1520.

(175) Zalusky, A. S.; Olayo-Valles, R.; Wolf, J. H.; Hillmyer, M. A. *J. Am. Chem. Soc.* **2002**, *124*, 12761-12773.

(176) Zeman, L. J.; Zydney, A. L. In *Microfiltration and ultrafiltration : principles and applications;* M. Dekker: New York, 1996; , pp 618.

(177) Zeman, L.; Wales, M. *ACS Symp. Ser.* **1981**, *154*, 411-434.

(178) Zhang, M.; Yang, L.; Yurt, S.; Misner, M. J.; Chen, J.; Coughlin, E. B.; Venkataraman, D.; Russell, T. P. *Adv.Mater.(Weinheim, Ger.); Advanced Materials (Weinheim, Germany)* **2007**, *19*, 1571-1576.

(179) Zhang, Y.; Musselman, I. H.; Ferraris, J. P.; Balkus, K. J. *J. Membr. Sci.* **2008**, *313*, 170-181.

(180) Zhao, H.; Cao, Y.; Ding, X.; Zhou, M.; Liu, J.; Yuan, Q. *J. Membr. Sci.* **2008**, *320*, 179-184.

(181) Zhao, H.; Cao, Y.; Ding, X.; Zhou, M.; Yuan, Q. *J. Membr. Sci.* **2008**, *310*, 365-373.

(182) Zhou, N.; Bates, F. S.; Lodge, T. P. *Polym.Prepr.(Am.Chem.Soc., Div.Polym.Chem.); Polymer Preprints (American Chemical Society, Division of Polymer Chemistry)* **2007**, *48*, 868.

(183) Zhu, X.; Elimelech, M. *Environ. Sci. Technol.* **1997**, *31*, 3654-3662.